

# **Mechanics of Dry Granular Flow through an Opening**

by

Mohsen Ostadi

A thesis submitted in partial fulfillment of the requirements for the degree of

Master of Science

in

Geotechnical Engineering

Department of Civil and Environmental Engineering

University of Alberta

© Mohsen Ostadi, 2019

## Abstract

Granular flow is a historical study which has been widely investigated experimentally, analytically and numerically in last decades. This topic has been discussed in several disciplines, e.g., in Chemical engineering to study granular discharge rate in silos and hoppers or in Geotechnical engineering to study soil erosion. Hourglass as a time-keeping machine can be mentioned as a familiar granular flow application.

In most studies grains have been assumed to be uniform sized particles and most analytical and numerical models are about this assumption. In nature, dealing with semi sized grains seems not to be factual, and particle size distribution is believed to play an essential role in granular flow, which has been ignored in most studies. This study aims at investigating the effect of particle size distribution (PSD) on the granular flow by experiments.

This research studies the behavior of granular flow for non-uniform particle size conditions and free fall arch (FFA) formation. Some experiments were carried out with different particle size distributions to examine previously presented correlations. An attempt was made to identify and introduce the characteristic particle size based on experimentation on non-uniform particle size distributions for better prediction of granular flow rate with current correlations, although this attempt was not successful.

For this study, two-dimensional granular flow was investigated through experimentation with granular flow through long-enough slots. A specific apparatus with variable and adjustable slot width was designed to be able to experimentally model and investigate the 2-D flow in different conditions. Sub-angular sand has been used as the granular material.

For this thesis, the particle size, particle size distribution and slot width are the critical parameters in granular flow rate. It was confirmed that under non-uniform sized grain condition the independence of flow rate to granular height over the slot is still valid and in different size grain condition existence of free fall arch (FFA) is justifiable. Also, the granular flow rate is dominated by the finer portion of the PSD rather than the coarser grains. In the investigation of two correlations, one did not show any meaningful results whereas the other one showed an overestimation in comparison with experiments due to some simplifications in this formula, i.e., not considering the shape factor or simplifying the parameter of flowing density with minimum density.

## Acknowledgement

I would like to express my sincere appreciation to my supervisors Prof. Dave Chan and Prof. Alireza Nouri for their support and invaluable supervision. Dr. Chan provided me with this topic and helped me to understand the crucial aspects of granular flow. He spent much time discussing the problem and solving them during this research. He taught me how to see and think about problems, analyze them and find a solution for them. Dr. Nouri also advised me in different aspects and allowed me to use and benefit from his laboratory facilities. Also, he supported me by assigning funding and his research group staff for my research purpose.

I appreciate Dr. Mahmood Salimi for designing and preparing the apparatus which was designed precisely according to my research requirements. I could complete all my experiments without any issue with this laboratory apparatus which saved time and improved efficiency. Without his design ideas and help, this research in this quality was impossible. He also brought me very helpful and valuable ideas during the design and actual tests and helped me a lot in any issue which I had in the lab.

I would like to appreciate the funding from RGL Resources Management and NSERC to provide the opportunity to complete this research.

I wish to thank my friends Xin Xu, Rahman Miri, Arian Velayati, Chenxi Wang, Jesus Montero, Omar Kotb for all their ideas and assistance in the laboratory and the research group office. Also, Yao Tang, who graduated recently and worked on granular flow research, helped me a lot to understand the topic at the beginning and provided me with all the resources and information he had about this topic. I appreciate the opportunity to see him and discuss many concepts of granular flow.

I would like to express my sincere gratitude to my mother, Sona. She was here far from her home to help my wife and me as we both were students and supported us being with my little son when we were out of the house with little time to spend with him. Also, I appreciate times when my wife, Hasti supported me to be able to spend more time focused on my research. She always helped me and put on her shoulder most of my responsibilities as a father and husband to be able to focus on my research duties.

# Table of Contents

1	Introduction.....	1
	1.1 Background .....	1
	1.2 Problem Statement .....	1
	1.3 Scope of Research .....	2
	1.4 Thesis Outline .....	2
2	Literature Review.....	4
	2.1 Granular Discharge Rate through an Opening .....	4
	2.2 Critical Aperture Size and Jamming .....	14
	2.3 Dynamic Arching – Free Fall Arch (FFA).....	16
	2.4 Hourglass Theory .....	18
	2.5 Review of Tang’s Formula in Granular Flow .....	19
3	Experimental Design and Test Matrix .....	23
	3.1 Material used in the experiment.....	23
	3.2 Sample Preparation .....	23
	3.3 Experimental Apparatus.....	25
	3.4 Experimental Procedure .....	27
4	Experimental Results and Observation.....	31
	4.1 U-I Uniform Sized Sand Ranged 1.19 mm to 1.68 mm.....	31
	4.2 U-II Uniform Sized Sand Ranged 2.38 mm to 2.83 mm .....	32
	4.3 S-I Fine Sand Ranged 0.5 mm to 2.38 mm.....	33
	4.4 S-II Coarse Sand Ranged 2.38 mm to 4.75 mm.....	35
	4.5 S-III Size Range from 0.5 mm to 4.75 mm.....	37
	4.6 Analysis and Discussion.....	39

4.7	Determination of the Characteristic Particle Size .....	66
5	Conclusion and Recommendations .....	71
5.1	Summary of findings .....	71
5.2	Limitations .....	72
5.3	Recommendations for future work.....	72
	References.....	73
Appendix A	All Experimental Results in Graphs.....	78
Appendix B	Apparatus Shop Drawings .....	129

## List of Figures

Figure 2-1 Vena Contracta (Brown and Richards, 1965) .....	5
Figure 2-2 Schematic view of FFA (Tang, 2017).....	8
Figure 2-3 Schematic view of the analytical model (Tang, 2017).....	8
Figure 2-4 Mixture of coarse and fine particles.....	11
Figure 2-5 Coordinate systems in the analysis of granular flow (Barletta et al., 2003) .....	12
Figure 2-6 Nondimensionalized velocity profile with and without gas drag effects (Hilton and Cleary, 2011).....	13
Figure 2-7 Hemispherical region modeling for flow rate with considering gas drag effects (Hilton and Cleary, 2011).....	14
Figure 2-8 Shapes of Silos: (a): bin, (b): hoppers, and (c): bunker (Rao and Nott, 2008) .....	15
Figure 2-9 Profile of spherical grain's velocity and defined free fall arch structure (Lin et al., 2015) .....	17
Figure 2-10 Schematic view of an hourglass with dimensional parameters (Le Penneec et al., 1996).....	19
Figure 2-11 (Re) Schematic view of FFA (Tang, 2017).....	20
Figure 2-12 (Re) Schematic view of the analytical model (Tang, 2017).....	21
Figure 3-1 Schematic view of the apparatus with a sliding part.....	26
Figure 3-2 Granular flow apparatus (85 cm height × 50 cm width × 10 cm depth) .....	26
Figure 3-3 Right triangle plate for adjusting slot width (left) and control gate with lock below the slot (right).....	27
Figure 3-4: Apparatus filled with the material before the beginning of the test.....	28
Figure 3-5: Stagnant zones after sand flow was completed.....	29
Figure 4-1 Particle size distribution of S-I sand group .....	34
Figure 4-2 Particle size distribution of S-II samples .....	36
Figure 4-3 PSD of S-III samples.....	38
Figure 4-4: Granular flow rate vs. time for (U-I) sand group.....	42
Figure 4-5 granular flow rate vs. time for (U-II) sand group.....	42
Figure 4-6 granular flow rate vs. time for (S-I) sand group.....	43
Figure 4-7 granular flow rate vs. time for (S-II) sand group .....	43

Figure 4-8 granular flow rate vs. time for (S-III) sand group.....	44
Figure 4-9 Cumulative discharged mass vs. time for (U-I) sand group.....	44
Figure 4-10 Cumulative discharged mass vs. time for (U-II) sand group.....	45
Figure 4-11 Cumulative discharged mass vs. time for (S-I) sand group.....	45
Figure 4-12 Cumulative discharged mass vs. time for (S-II) sand group.....	46
Figure 4-13 Cumulative discharged mass vs. time for (S-III) sand group.....	46
Figure 4-14 Granular flow vs. D/d50 for (U-I) sand group.....	51
Figure 4-15 Granular flow vs. D/d50 for (S-I) sand group.....	51
Figure 4-16 Granular flow vs. D/d50 for (U-II) sand group.....	52
Figure 4-17 Granular flow vs. D/d50 for (S-III) sand group.....	52
Figure 4-18 Granular flow vs. D/d50 for (S-II) sand group.....	53
Figure 4-19 Schematic view of arch and calculation parameters (Tang, 2017).....	54
Figure 4-20 Comparison between experiment and Tang’s correlation in (U-I).....	58
Figure 4-21 Comparison between experiment and Tang’s correlation in (U-II).....	58
Figure 4-22 Comparison between experiment and Tang’s correlation in (S-I).....	59
Figure 4-23 Comparison between experiment and Tang’s correlation in (S-II).....	59
Figure 4-24 Comparison between experiment and Tang’s correlation in (S-III).....	60
Figure 4-25 Comparison between experiments and modified Beverloo’s correlation in (U-I)...	64
Figure 4-26 Comparison between experiments and modified Beverloo’s correlation in (U-II)..	64
Figure 4-27 Comparison between experiments and modified Beverloo’s correlation in (S-I)....	65
Figure 4-28 Comparison between experiments and modified Beverloo’s correlation in (S-II) ..	65
Figure 4-29 Comparison between experiments and modified Beverloo’s correlation in (S-III).	66
Figure A-1 a Experiment # 1 Granular flow rate vs. time.....	79
Figure A-1 b Experiment # 1 Cumulative discharge mass vs. time.....	79
Figure B-1 Apparatus walls – all are made of transparent polycarbonate- dimensions are in inches.....	130
Figure B-2 Parts of apparatus bottom side consisting of movable triangle for slot width adjustment – These elements are made of Aluminum 6061 – dimensions are all in inches.....	131

## List of Tables

Table 4-1 Sieves specifications used in the experiment .....	24
Table 4-2 Initial test matrix.....	30
Table 5-1 (U-I) group experiment results .....	32
Table 5-2 (U-II) group experiment results.....	33
Table 5-3 (S-I) group experiments results .....	34
Table 5-4 (S-II) group experiments results.....	36
Table 5-5 (S-III) group experiments results.....	38
Table 5-6 Comparison of results with different sand heights over the slot .....	40
Table 5-7 Comparison of results with different particle size distributions.....	47
Table 5-8 Comparison of results with different PSDs and same $d_{50}$ with same opening size .....	49
Table 5-9 Comparison between experiments and Tang's presented correlation (2017) .....	55
Table 5-10 Comparison between experiments and modified Beverloo's equation (Mayers and Sellers, 1978) .....	61
Table 6-1 Equivalent particle size based on modified Beverloo to provide the same results as experiments.....	67

# **1 Introduction**

## **1.1 Background**

A collection of grains is called granular material. Common granular materials are sand, gravel, cement, seeds and food grains. This study focuses on the flow of sand as a granular material through a single slot opening (two-dimensional flow).

Granular flow through an opening is a fundamental topic in many real-life problems such as sinkhole and ground surface collapse (Hermosilla, 2012), soil loss into defective sewer pipe (Guo and Zhu, 2017), sand control in petroleum oil wells (Meza-Diaz et al., 2003), granular flow in hoppers and silos (Hilton and Cleary, 2011) and (Rao and Nott, 2008), and also hourglass (Le Pennec et al., 1996). The underlying mechanism of granular flow is focused on the idea of a free-fall arch formation which produces specific characteristics in granular flow, i.e., the flow rate is independent of material height over the orifice, unlike fluid flow.

A wide range of studies has been conducted to investigate the mechanism of granular flow through an opening from different aspects. The assumption in almost all studies is based on uniform grains size which seems to be unreasonable in many real-life problems.

This study can help to develop a better understanding of granular flow through silos, hoppers, defective sewer pipes and karsts. Flow conditions and rates in non-uniform sized grains, which is more realistic, can be estimated and modeled. Settlement due to karsts in coastal areas is one of the important Geotechnical concerns to be addressed.

## **1.2 Problem Statement**

Many current studies on granular flow through an opening or slot are based on uniform grains. In almost all experimental or numerical relationships for calculating granular flow rate, grain size distribution or the effect of grain size is ignored. In nature, all phenomena related to granular discharge such as soil erosion due to defective pipe or sinkhole and ground surface collapse are encountered in sands with non-uniform grain size distribution.

This research is focused on the effects of grain size distribution on the flow characteristics of the granular material. It is believed that grain size has an essential role in forming the free-fall

arch in the granular flow process. Moreover, the effective grain size which is used in calculating the discharge rate is defined and investigated through experimental work.

The experimental study in this research investigates the effects of slot opening size, the height of granular material over the opening and the particle size distribution on the granular flow rate.

### **1.3 Scope of Research**

This thesis presents the results of an investigation into the granular flow and improves the theory presented by Tang (2017) which estimates the granular flow rate based on one single grain size. It is also the objective of this study to clarify the effect of grain size distribution on granular flow rate by suggesting a characteristic grain size in estimating the flow rate. This correlation is explained in the next chapter.

This characteristic grain size will be used in the correlation mentioned above and other published relationships, which may not be the average grain size ( $d_{50}$ ), to more accurately estimate the granular flow rate. This study also aims to clarify the role of characteristic grain size in the formation of the free fall arch.

### **1.4 Thesis Outline**

This thesis is composed of seven chapters on granular flow through a slot. Below is a summary of each chapter.

Chapter two explains the definitions of arching and dynamic arching and provides the literature review on granular discharge rate. The effect of critical aperture size and gas pressure will also be discussed. In the end, the hourglass theory, as one of the classical granular flow phenomena, will be explained.

Chapter three discusses the work of Tang (2017) on the analytical estimation of granular flow rate and modeling of free flow arch.

Chapter four starts with the criteria and assumption for the experimental design. The chapter continues with the design parameters and characteristics of the designed apparatus and ends with the test procedure and test matrix.

Chapter five presents the experimental observations and the results from 52 experiments. The chapter compares between the experimental results and analytical calculations for 2D granular discharge based on Tang's formula, and other equations.

Chapter six presents the determination of characteristic particle size for non-uniform particle size materials. The chapter presents the feasibility/practicability based on the comparison between Tang and modified Beverloo's equation and experiments.

Chapter seven provides the conclusions of this study and some recommendations for further research work in this area.

## 2 Literature Review

### 2.1 Granular Discharge Rate through an Opening

#### 2.1.1 General flow rate equations

##### a. Circular orifice

A well-known characteristic of granular flow through an opening compared with fluid flow is that the rate of granular flow is independent of grains height over an orifice. This phenomenon is noted and presented as Janssen effect (Janssen, 1895). The widely accepted expression to estimate the flow rate of grains through a circular orifice, called “Beverloo’s law”, was presented by Beverloo et al. (1961) as below:

$$W = C\rho_b\sqrt{g}(D_0 - kd_p)^{2.5} \quad (2.1)$$

where  $W$  is mass discharge rate through the orifice,  $D_0$  is orifice diameter,  $d_p$  is grains diameter,  $C$  and  $k$  are empirical dimensionless discharge and shape coefficients, respectively,  $\rho_b$  is the apparent density and  $g$  is gravitational acceleration. The parameter  $k$  depends on particle and orifice properties with value lying between 1 and 3 (Nedderman and Laohakul, 1980). The parameter  $C$  is found to lie between 0.55 and 0.65 (Nedderman, 1992). Other experimental results have supported Eq. (2.1) (Brown and Richards, 1965).

As can be seen in the above correlation, when the material height is high enough in comparison with the opening size, the discharge rate is related to the opening size with a power of about 2.5 (Beverloo et al., 1961; Al-Din and Gunn, 1984; Nedderman, 1992). Also, Franklin and Johnson (1955) claimed that this relationship has a power of 2.95.

The Beverloo’s law has been tested and approved for uniform-size granular assembly with diameters larger than  $d_p=0.5$  mm and orifice size  $D_0$  big enough to prevent jamming around the opening (Zuriguél et al., 2005a). Different correlations have been presented to estimate granular flow rate under different situations based on experimental and analytical results which all have a similar form to Beverloo’s correlation (Khanam and Nanda, 2005; Ahn et al., 2008). On the applicability of Beverloo’s law, Nedderman (1992), Mankoc et al. (2007), and Mankoc et al. (2009) have stated that this correlation can be used when the range of particle size lies between

0.4 mm and  $D_0/6$ . For smaller size grains, the effect of air is significant which cannot be neglected. For larger particles, there is a possibility of interlocking between particles.

Beverloo assumed that there is a zone at the corners of the orifice which is not mobile (vena contracta). They explained that this zone is proportional to  $d_p$  and for this reason the equation with  $kd_p$  is valid. They stated the average value for  $k$  could be assumed to be  $k=1.4$ . They also claimed that the influence of the particle shape could be implicitly incorporated in the  $\rho_b$  and  $d_p$  parameters. They found deviations of 5% in most of the materials with bulk density  $\rho_b$  of about 0.7 (Beverloo et al., 1961). Flowing density,  $\rho_b$ , is defined as the ratio of mass flow rate to volumetric flow rate.

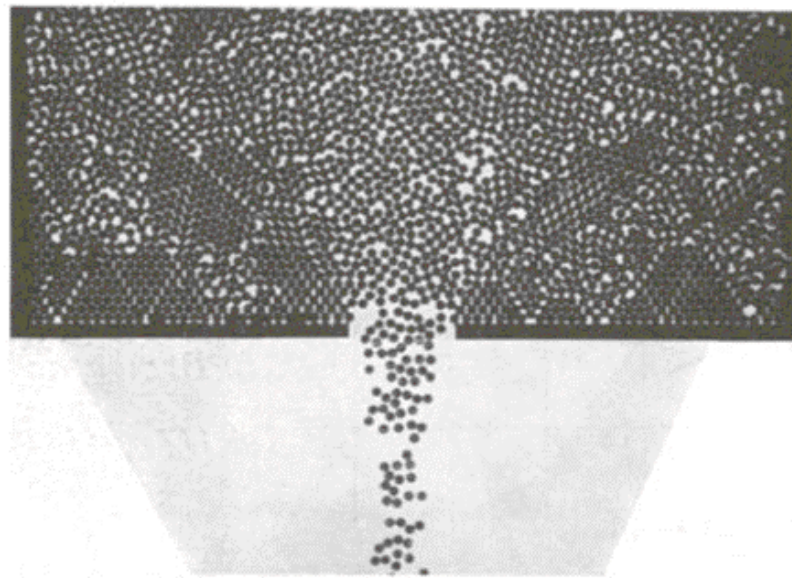


Figure 2-1 Vena Contracta (Brown and Richards, 1965)

Brown and Richard (1965) were able to confirm the existence of an FFA (Free Fall Arch) using ball bearing and cutting away small strips of supporting plane above the aperture (Figure 2-1). They also found that the flow becomes radial near the aperture. They statistically observed the empty space adjacent to the edge of aperture (vena contracta) and claimed that particles could not approach within a distance of  $kd_p/2$  from the edge of the orifice, resulting in an effective orifice diameter of  $D_0 - kd_p$ . It is concluded from these experiments that while there is a tendency for flow to be radial near the aperture, the radial velocity may vary asymmetrically (Brown and Richards, 1965).

Mankoc et al. (2007) found that the flow rate is independent of the diameter of the silo (L) if:

- 1- L is greater than 2.5 times the diameter of the outlet orifice ( $D_0$ )
- 2- L is greater than  $D_0 + 30 d_p$  ( $d_p$  is the diameter of the particle)

As mentioned before, Beverloo's law is valid for particles larger than 0.5 mm. Also, it has been seen that Beverloo's law underestimates the flow rate by about 10% in  $R=10$  ( $R=D_0/d_p$ ). For small R, this law is acceptable, but for  $R \leq 10$ , it overestimates the flow rate. For particles smaller than 0.5 mm, a modification has been made to consider the effect of pressure gradient generated by air passing through the interfaces between grains. Mankoc et al. (2007) by implementing experimental work on the 2D silo and numerical simulations showed that this equation better fits the actual flow rate and also fits the data neatly for a large range of values of R including very small orifices in 2D and 3D:

$$W_b = C' \left(1 - \frac{1}{2} e^{-b \cdot (R-1)}\right) (R - 1)^{2.5} \quad (2.2)$$

where  $C' = C \rho_b \sqrt{g}$ ,  $R = D_0/d_p$  and  $b = 0.051$ . As can be seen, the parameter k has been omitted. Apart from demonstrating that the concept of "empty annulus" (vena contracta) is wrong and unable to describe the experimental results, they explained the correction by introducing local density variations near the outlet (Mankoc et al., 2007).

Janda et al. (2012) studied the grain flow through an aperture placed at the bottom of a 2D silo. In this study, they presented an equation for grains flow rate through an opening in determining the velocity and density profiles:

$$v(x) = \sqrt{2gR} \sqrt{1 - \left(\frac{x}{R}\right)^2} \quad (2.3)$$

$$\phi(x) = \phi_\infty [1 - \alpha_1 e^{-R/\alpha_2}] (1 - (x/R)^2)^{1/\nu} \quad (2.4)$$

where  $v$  and  $\phi$  are velocity and density profiles respectively,  $\phi_\infty$  is the asymptotic value of the volume fraction of big openings,  $\alpha_1$  and  $\alpha_2$  are curve fitting parameters ( $\phi_\infty = 0.83 \pm 0.01$ ,  $\alpha_1 =$

$0.50 \pm 0.01$  and  $\alpha_2 = 3.3 \pm 0.05$ ). Both profiles are self-similar demonstrating the generality of the mechanism for controlling the flow rate passing through the orifice. These two profiles do not show any meaningful difference between small orifices with clogging potential and large apertures with continuous flow. The final expression for mass flow rate is:

$$W = C'' \sqrt{g} \phi_\infty [1 - \alpha_1 e^{-R/\alpha_2}] R^{3/2} \quad (2.5)$$

where  $C'' = 4\beta(\frac{v+2}{2v}, \frac{1}{2})/\pi d^2$ . The functionality of both profiles reveals that the empty annulus (vena contracta) concept is not necessary for justifying the k parameter (Janda et al., 2012).

Vivanco et al. (2012) studied granular flow in a 2D hopper using particle tracking and photo-elastic methods. They saw an intermittent network of forces consisting of arches and force chains. They found that this network is the leading cause of any fluctuations in the vertical velocity, but it does not have any role in controlling the outflow. They obtained the mass flow rate through average vertical velocity.

Lin et al. (2015) carried out numerical simulations of granular flow. They found that the granular flow is not related to the filling height. Moreover, if the height and width of the hopper are more than 2.5 times the orifice diameter, the flow rate is independent of the height and width of the hopper. They also observed that unlike an ideal FFA assumption, the vertical velocity on the arch surface is not zero.

### **b. Rectangular orifice**

Beverloo's law was modified by Mayers and Sellers (1978) for the specific situation of a flat-bottomed hopper with the rectangular orifice (slot) to predict the granular discharge rate:

$$W = 1.03 \rho_f \sqrt{g} (L - kd)(W_0 - kd)^{1.5} \quad (2.6)$$

where  $L$  and  $W_0$  are the length and width of the orifice respectively, and  $\rho_f$  is the flowing bulk density (ratio of mass flow rate to volumetric flow rate).

Tang (2017) developed an analytical model to estimate the granular discharge rate through a two-dimensional opening. Tang calculated the granular flow rate by determining the size of the

free fall arch (FFA). Figures 2-2 and 2-3 illustrate the schematic of an FFA and the analytical models. Experimental and numerical results were used to verify the model.

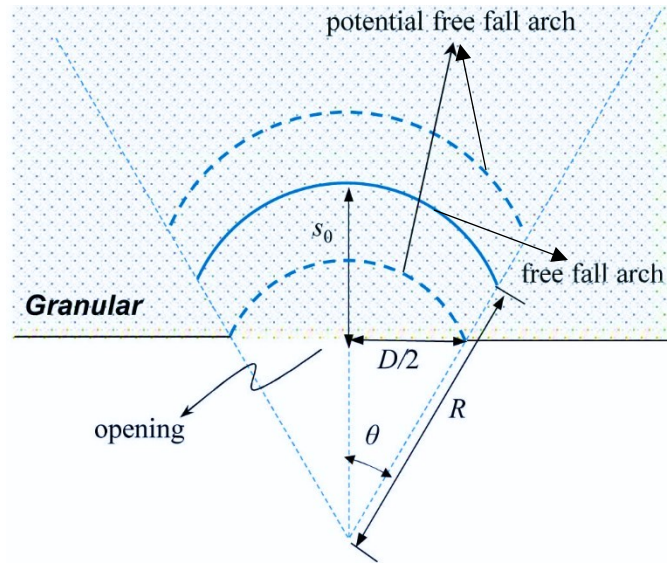


Figure 2-2 Schematic view of FFA (Tang, 2017)

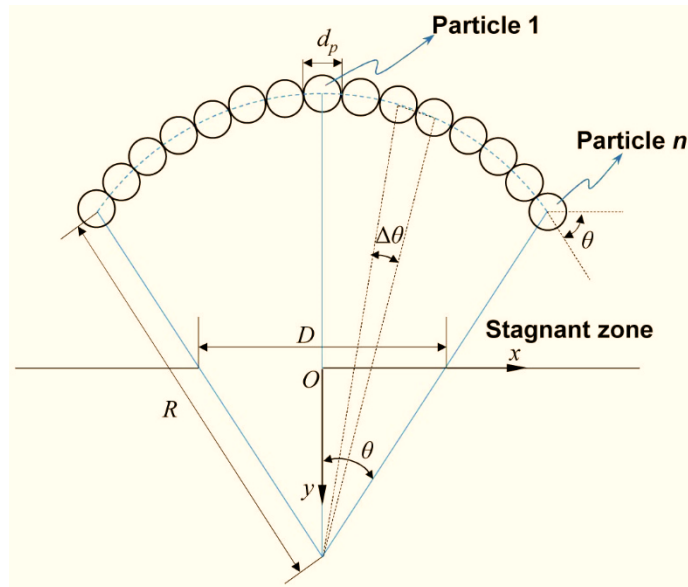


Figure 2-3 Schematic view of the analytical model (Tang, 2017)

Tang's (2017) proposed the following equation to calculate the flow rate:

$$Q = (1 - \varepsilon)D_0\sqrt{2gS_0} \quad (2.7)$$

where  $Q$  is the volumetric discharge rate per unit length  $\left(\frac{m^3}{s/m}\right)$ ,  $\varepsilon$  is the porosity of the granular assembly,  $D_0 = D - K_p d_p$  as in Beverloo's equation,  $g$  is the gravitational acceleration  $\left(\frac{m}{s^2}\right)$ ,  $S_0 = R - \frac{D_0}{2 \tan \theta}$ ,  $R$  is the radius of the FFA (m), and  $\theta$  is half of the central angle of the FFA.

### 2.1.2 The wall effects

For the first time, Franklin and Johanson (1955) studied the granular discharge rate through an opening with an inclination angle. They found a linear relationship between the discharge rate and the cosine of the inclination angle. A correlation considering wall effect and another correlation for the slot openings (noncircular) were proposed by Nedderman (1992). Another experimental work on the investigation of the wall inclination was carried out by Sheldon and Durian (2010). They presented an empirical correlation for glass beads of different sizes and a circular opening with a variety of inclination angles. Liu (2014) developed the theoretical and analytical correlations for discharge rate for an inclined opening.

### 2.1.3 Effect of particle shapes

It is clear that the shape of particles in a granular assembly plays a crucial role in the discharge rate. It is believed that particle shape affects grain interlocking and intergranular friction and eventually affects the granular flow rate. Most simplified analytical models assume spherical particles. In reality, granular particles are not perfectly spherical.

Zuriguél et al. (2005b) claimed that the particle shape has a significant effect on the discharge rate although it has a negligible effect on the material properties. Li et al. (2004) studied the discharge of sphere-disc shape particles. Wu et al. (2008) and Tao et al. (2010) investigated the flow pattern and discharge behavior of particles with three different shapes and four different granular materials with a mixture of hexahedron and sphere shapes. Cleary and Sawley (2002) studied the particles angularity numerically using discrete element method and found that angular particles have about 30% lower discharge rate than spherical particles. Sukumaran and Ashmawy (2003) investigated sands and glass beads with the particle size in the range of 0.30 to 0.50 mm and found that with the increasing angularity of the particles, the discharge rate decreases.

Regarding particle shapes and its effect on the hopper discharge rate, Mamtani (2011) presented a new equation to estimate the flow rate for various spherical and non-spherical particles. He found that the results from this newly proposed equation deviated by less than 20% for all tested materials. He proposed the following equation to calculate the mass discharge rate:

$$\frac{W}{\rho_b D_h^{2.5} g^{0.5}} = \left(\frac{D_h}{d_p}\right)^{0.094} \left(\frac{1}{\lambda}\right)^{0.289} \left(\frac{1}{\mu}\right)^{0.098} \quad (2.8)$$

where  $D_h$  is the hydraulic diameter and is defined as  $D_h = \frac{4A_0}{P_0}$ ,  $A_0$  and  $P_0$  are area and perimeter of the orifice respectively,  $\mu$  is the coefficient of friction and  $\lambda$  is a shape factor which is defined as the ratio of spherical diameter to the average screen size of the particles. The flow rate of different materials was also investigated in an experiment on the hopper with a cone angle of 55°. The results were compared with a common flat-bottom hopper. The difference between these two hoppers for spherical particles was less than 5% and less than 15% for non-spherical particles (Mamtani, 2011).

#### 2.1.4 Effect of the particle size distribution

Ahn et al. (2008) investigated the effect of grain size experimentally and found that finer particles have higher discharge rates than coarser ones and claimed that this is due to the empty annulus in an orifice. Other investigations have shown higher flow rates for finer particles in comparison with coarser ones.

Another important aspect of the grain size effect is particle size distribution (PSD) when different sizes of particles are mixed to form the material. Anand et al. (2008) studied the effect of PSD on granular flow numerically in 3D condition and found that the granular flow rate increases due to the rise in the mass percentage of finer particles. Dias et al. (2004) explained when the fine fraction of granular material increases, the voids between coarse particles are filled resulting an increase in flowing density and eventually increase in discharge rate as shown in Figure 2-4.

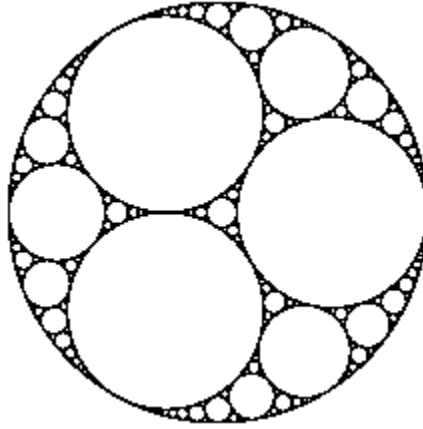


Figure 2-4 Mixture of coarse and fine particles

### 2.1.5 Effect of air pressure gradient

Other studies on granular flow have incorporated the effect of air resistance. Air resistance is important particularly for finer particles in which the air causes a reduction in outflow rate (Hilton and Cleary, 2011). The theoretical and empirical equations proposed without considering air/gas pressure tend to overestimate the granular flow rate for fine-grain materials ( $<500\mu\text{m}$ ) by as much as a factor of 10.

Donsi et al. (1997) used glass, polymer and Fluid Catalytic Cracking (FCC) particles of different sizes in their experiment. They proposed two models based on the prevailing hypothesis that there is a zone or arch over the orifice in which solid motion switches from a form of the granular flow to a form of the suspension, or in other words, discontinuous change in the void ratio of flowing grains. This suspension zone is the main reason for having the pressure gradient near the hopper orifice. They measured this transition zone along the hopper axis to be equal to half the orifice diameter above the orifice. In their second model with conical shape (hoper), they considered a relative solid-gas velocity which can cause a higher pressure gradient than the first model which has a cylindrical geometry. The increase in grain velocity approaching the orifice introduces a significant dilation of the material. Different flow velocity between the grains and interstitial fluid causing friction between the two phases generates the pressure gradient. Therefore equations such as the Beverloo's law, which do not consider gas pressure, are not accurate in calculating the flow rate for fine grains material (Donsi et al., 1997).

Barletta et al. (2003) developed an equation to calculate discharge flow rate by considering the minimum energy theorem presented by Brown (Brown, 1961) and total energy conservation

below the arch based on an extension of the Brown and Richards model (1970) and solids dilation during the flow process. As Figure (2-5) illustrates, the spherical coordinate system is used in modeling the two-phase conical hoppers.

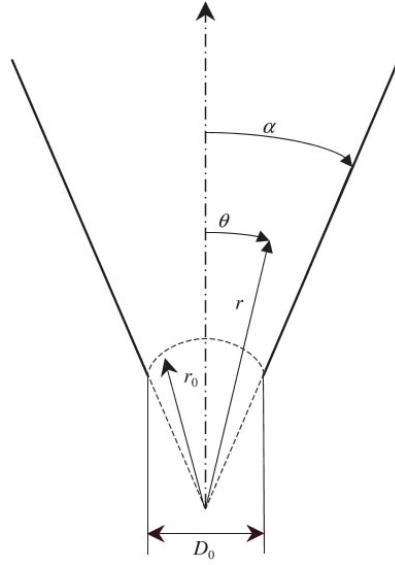


Figure 2-5 Coordinate systems in the analysis of granular flow (Barletta et al., 2003)

The granular flow rate in the presence of gas pressure gradient can be determined from the following equation (Barletta et al., 2003):

$$W_s = \frac{\pi}{4} \rho_s (1 - \epsilon_0) (D_0 - kd_p)^{2.5} \left[ \frac{2}{3} g^{\frac{1}{2}} \frac{1 - \cos \alpha^{\frac{3}{2}}}{\sin \alpha^{\frac{5}{2}}} + \left( \frac{1}{\rho_s (1 - \epsilon_0)} \frac{dp}{dr} \Big|_{r=r_0} \right)^{0.5} \frac{1 - \cos \alpha}{\sin \alpha^{\frac{5}{2}}} \right] \quad (2.9)$$

where  $\rho_s$  is the solid particle density,  $p$  is the interstitial gas pressure, and  $\epsilon_0$  is void ratio at the hopper outlet. Barletta et al. (2003) also presented the equation below to evaluate the interstitial fluid pressure gradient at the ideal surface:

$$\frac{dp}{dr} \Big|_{r=r_0} = \frac{150 \mu_f (1 - \epsilon_0)^2}{d_p^2 \epsilon_0^2} \frac{4W_s}{\rho_s (1 - \epsilon_0) \pi D_0^2} \times \left( \frac{1 - \epsilon_0}{\epsilon_0} \frac{\epsilon_b}{1 - \epsilon_b} - 1 \right) \quad (2.10)$$

where  $\varepsilon_b$  is solids bulk void ratio and  $\mu_f$  is the gas viscosity. They compared their models with previous experimental results to validate their model. It was observed that using the pressure gradient corresponding to the grain suspension would lead to an underestimation of the flow rate. In fact, the pressure gradient is larger than that used in Eq. (2.10). Barletta et al. (2003) also observed that a minimal solid expansion or dilation is enough to produce a measurable gas pressure gradient which affects the granular flow rate.

Hilton and Cleary (2011) studied the effect of gas drag on discharge rate in a cylindrical flat-based hopper. They modeled the granular flow with and without gas drag. They found that in the situation without gas drag, their correlation is the same as Beverloo's law. As seen in Figure 2-6, the critical Stokes' number, at which transition between inertial and viscous dominated grains motion occurs, is  $St \sim 10$ .

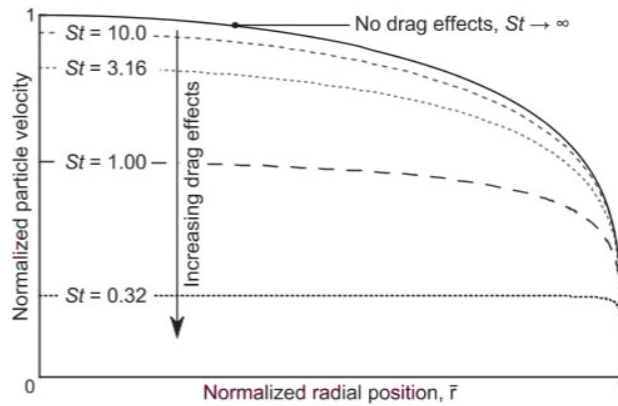


Figure 2-6 Nondimensionalized velocity profile with and without gas drag effects (Hilton and Cleary, 2011)

When  $St \rightarrow \infty$ , the interstitial gas has a negligible effect and when  $St \rightarrow 0$ , the granular flow is dominated by viscous drag effect. By incorporating gas drag effects, the flow rate is given by:

$$Q = \pi \rho_b R_B^2 \tau_\eta g \left[ 1 + 2 \int_0^1 \bar{r} W(-e^{-k\bar{h}-1}) d\bar{r} \right] \quad (2.11)$$

where  $\tau_\eta$  is the viscous timescale,  $W$  is the Lambert-W function, and  $k$  is the empirical parameter in Beverloo's law. Other parameters are shown in Figure 2-7. They compared their expressions to numerical results and previous empirical results and found good agreement.

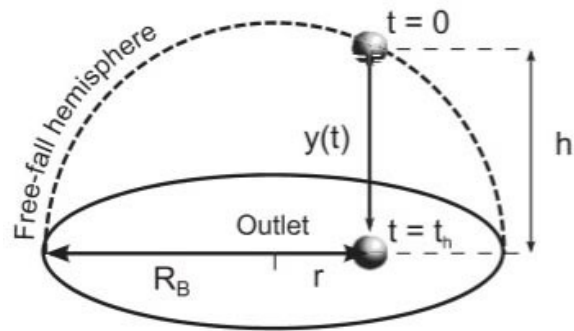


Figure 2-7 Hemispherical region modeling for flow rate with considering gas drag effects (Hilton and Cleary, 2011)

## 2.2 Critical Aperture Size and Jamming

When particle size becomes large compared to the size of the orifice, flow stops as a result of the formation of a stable arch (Le Penne et al., 1996). Particle jamming may happen when a compressed solids flow directly through an opening. The channeling of particles through the opening may cause the impromptu formation of an arch-shape adjustment of particles directly over the orifice (Lafond, 2014).

Le Penne et al. (1996) stated that the plug is a composite structure and its equilibrium is under the influence of gravity, friction (between grains and grains and wall), and hydrodynamic forces. Drescher et al. (1995a) discussed the theories related to stable arching in symmetrical hoppers considering the bulk material flow properties. In other words, the relationship between the flow condition and immediate and effective yield situations was discussed. This analysis investigated and compared the result of direct shear tests on coal, bentonite, limestone, gypsum, and taconite which led to some modifications on the theories of arching.

Arch forming can be a function of opening, hopper geometry and size. Previous literature assumed stacking of isolated structural members for the hopper bulk material. If the member's strength is more than the stresses caused by weight, an arch is formed. This approach is called structural mechanics (SM). If the material inside the hopper is considered as a mass and arching is treated as a phenomenon of global equilibrium, this theory is based on continuum mechanics (CM) and is called Enstad theory (Drescher et al., 1995a).

In determining the flow properties of bulk materials in terms of effective yield conditions, some approximations are required. Drescher et al. (1995a) determined the requirements in the direct shear test that result in the reduction procedure to be valid and comparable with the arching theory. These requirements relate to the bulk unit weight, interface friction angle, instantaneous yield loci (EYL) and effective yield loci (EYL).

Zuriguel et al. (2003) and To et al. (2001) described jamming as the formation of the arch-shape structure immediately over the point of particle discharge. To et al. (2001) investigated and modeled the jamming phenomenon experimentally and explained that jamming depends on the opening size and gains size ratio. Zuriguel et al. (2005a) and Zuriguel et al. (2003) introduced a border between two different regimes of continuous outflow and the onset of orifice jamming. In this article, the parameter  $R$  is introduced as the ratio between the diameter of the aperture and diameter of the beads. It is claimed that the critical value of  $R$ , which was called  $R_c$ , is equal to 5. For jamming to occur, according to this criterion, the maximum ratio of the aperture to particle size should be equal to  $R_c=5$ , or less.

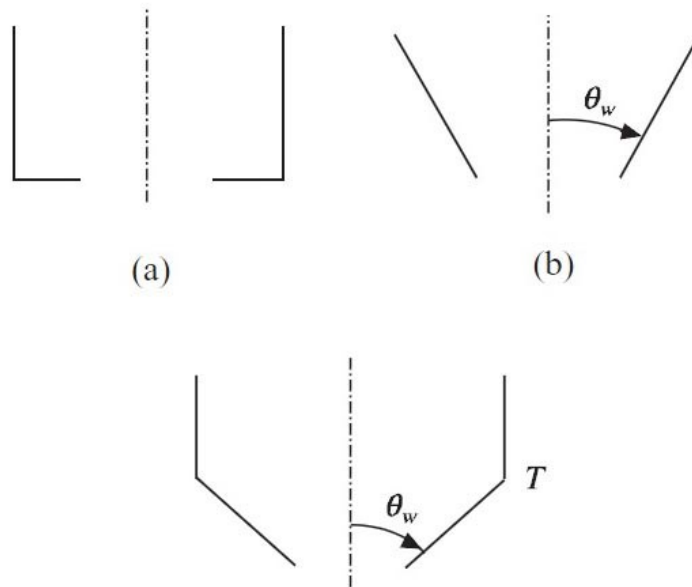


Figure 2-8 Shapes of Silos: (a): bin, (b): hoppers, and (c): bunker (Rao and Nott, 2008)

Vivanco et al. (2012) studied grains flow in a two-dimensional hopper and mentioned that the critical aperture size depends on the inclination of the hopper walls ( $\alpha$ ) which can be expressed

as  $D_c = 3.3d \sin \alpha$ . In this equation  $D_c$  is the critical aperture size,  $d$  is the particle size, and  $\alpha$  is the inclination of the hopper. The definition of silos are illustrated in Figure (2-8).

Drescher et al. (1995b) studied the critical outlet size theories and compared them with experiments on medium scale symmetrical, plane (wedge-type) and conical hoppers. They aimed to find the critical opening size to prevent the formation of arches during discharge. They used gypsum, coal, limestone, taconite, and cement as their testing materials. They observed that most of the existing theories on arching overestimate the aperture size by a factor of 2 to 4. They also discussed the probable source of errors and some possible modifications to existing arching theories. They claimed that in the SM-based arching theories, the reaction of the weight of the particles over the assumed arch was omitted, which has caused an overestimation of the aperture size.

### **2.3 Dynamic Arching – Free Fall Arch (FFA)**

Terzaghi (1943) explains that if a soil loses part of its support, that portion of soil stress which was on [now failed] support would move between adjoining soils which is still standing. This transfer of stress from the failed soil mass onto the adjacent section is called arching. He stated that stresses in the sand normal to the failed part of the soil for a distance of two or three times of the width of the failed part do not have any effect on the stresses in the yielded (failed) part. Drescher et al. (1995a) state “arching” is the formation of an arch-shape supported dormant bulk material mass over an outlet such as a hopper, bin, aperture or slot.

Generally, the stable form of arching in granular materials can be classified into two different categories. The first category of flow occurs in wet conditions such as arching in the slot openings of screens in oil production wells to control sand production (called sand arching) (Drescher et al., 1995a). The second category occurs under dry conditions in bins, hoppers or silos (Fig. 2-8) in which particle jamming may occur during discharge. In the second category, the dynamic form of the arching or “free fall arch” (FFA) phenomenon allows continuous and constant granular flow.

Granular material falling under self-weight from a hopper is one of the research topics being studied widely. It is believed that dynamic arch formation, or in other words free fall arch (FFA), is the reason for a constant rate of flow. FFA is a concept or hypothesis that considers forming and breaking of an arch in a fraction of a second. Although Beverloo’s equation can

predict the granular discharge rate with reasonable accuracy, a theoretical explanation is needed to study and investigate the mechanism of granular flow through an orifice. For the first time, Brown (1961) claimed that energy of grains in approaching process to the orifice reaches a minimum above and close to the orifice and after that boundary particles fall freely under own weight. Brown and Richards (1965) called this boundary a Free Fall Arch (FFA).

The assumption of an FFA in studying the process of granular discharge is very beneficial. However, direct observation and visualization of the FFA are difficult and complicated (Figure 2-9). Tian et al. (2015) studied the free fall surfaces with a 3D simulation model assuming mono-size steel spherical particles. They found that after forming the FFA, discharge flow becomes constant and free fall surfaces are in parabolic shape rather than the traditional assumption of a circular shape.

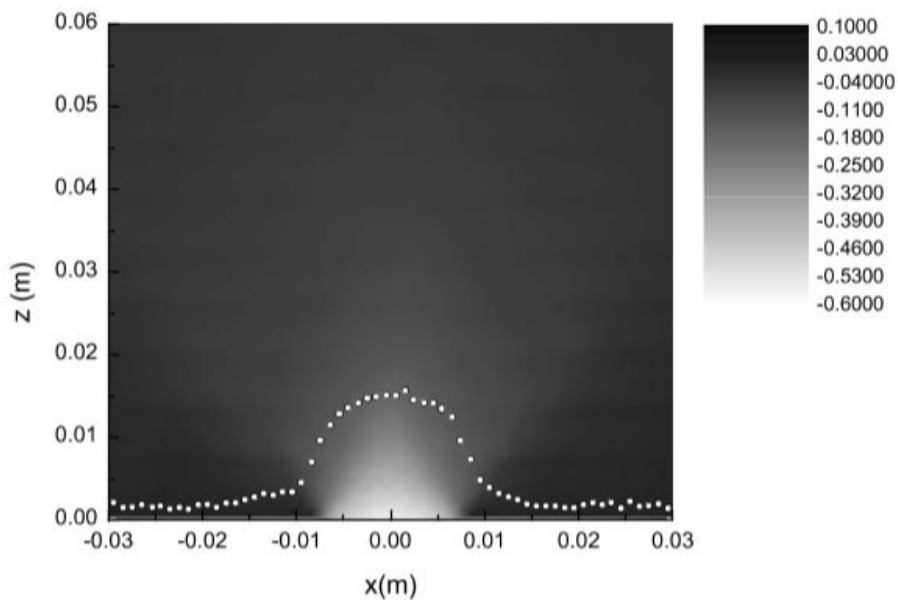


Figure 2-9 Profile of spherical grain's velocity and defined free fall arch structure (Lin et al., 2015)

Vivanco et al. (2012) used the FFA concept for theoretical estimations of discharge rate in hoppers. They explained that the FFA is defined as the lower surface of the granular material in a hopper. The lower surface is usually spherical and is a boundary between a zone where grains move freely under their weight and the other zone where grains are under some finite stress.

Le Pennec et al. (1996) claimed that they have been able to identify structures in the sand, such as FFA and plug, using the laser technology. They also defined the FFA as a boundary separating regions where grains are in contact and regions where grains are not in contact and fall freely. They explained that the forces acting on the particles in the first region are stress from other particles in addition to gravity and hydrodynamic forces. In the second region, only gravity and hydrodynamic forces are acting. They explained that the existence of a well-defined sharp interface (theoretical ideas of the free-fall arch) is unclear. They could prove rapid density variation in intermittent sand flow. They used a CCD (Charge Coupled Device) camera to capture the FFA.

Rubio-Largo et al. (2015) performed 3D numerical modeling (DEM) to model granular flow in a silo. They observed that there is a distinct transition zone where the flow of grains changed. In this zone, movement of grains is associated with the macroscopic flow. They also found that the shape of the arch followed a parabola.

Janda et al. (2012) also considered the existence of an FFA in their investigations per the FFA hypothesis and their results showed that this boundary should be parabolic instead of commonly assumed circular. The existence of an FFA was also confirmed by Brown and Richards (1965).

## **2.4 Hourglass Theory**

The hourglass is one of the earliest and simplest applications of the granular flow phenomenon, which has been investigated and studied widely. This device (Figure 2-10) is based on the steady flow of sand at a constant rate from the upper chamber to the lower chamber (Le Pennec et al., 1996). The hourglass device is the case of granular flow with no interstitial fluid effects (Nedderman, 1992). The hourglass theory is based on the FFA theory and the lack of material head effect over a slot on the flow rate (Davidson and Nedderman, 1973).

It is believed that interstitial air effect in hourglass happens when the sizes of sand particles fall in the range  $0.04 \text{ mm} < d < 0.3 \text{ mm}$  in a 1 mm orifice size. For  $d < 0.04 \text{ mm}$ , there is no flow due to cohesion between particles (inter-granular interactions). The particle size should be greater than 0.3 mm to prevent intermittency in an hourglass (Wu et al., 1993).

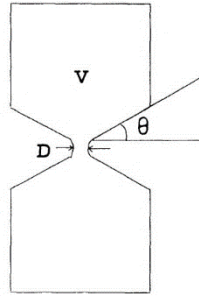


Figure 2-10 Schematic view of an hourglass with dimensional parameters (Le Penne et al., 1996)

The intermittent flow in hourglass has been investigated by measuring pressure fluctuations inside the device. It has been shown that small fluctuations, e.g.,  $10^{-3}$  atm, may cause particle jamming in the upper chamber of the hourglass and stop the granular flow (Le Penne et al., 1996).

## 2.5 Review of Tang's Formula in Granular Flow

### 2.5.1 Overview

Tang (2017) studied the mechanism of soil erosion in the formation of sinkholes. In his research, Tang discussed the mechanism of soil erosion due to defective sewer pipes. His dissertation presents the development of an analytical model to predict the granular flow of uniform-sized sand through a two-dimensional orifice (slot) based on the free-fall assumption.

He adopted the FFA theory as the basis of his analytical work. Before Tang's work, no analytical model had been developed for granular flow through an orifice. In this model, the location of the free-fall arch above a two-dimensional slot is calculated, which is used to calculate the granular flow rate of uniform particles. Unlike fluid flow, friction between grains has an essential effect on granular flow. It has been discussed that a stagnant zone is formed in granular flow through an orifice in a flat-bottom bin, which does not contribute to the granular flow rate. Based on these assumptions, Tang (2017) developed the basic model as shown in Figure 2-11.

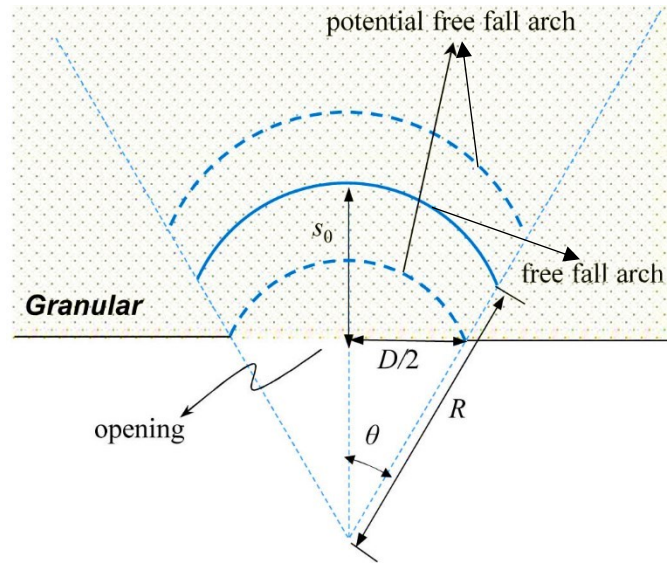


Figure 2-11 (Re) Schematic view of FFA (Tang, 2017)

### 2.5.2 Tang's model formulation

The arch size can be calculated assuming a perfect circle over a two-dimensional opening, according to the location of the FFA and the angle of the stagnant zone. Figure 2-12 shows a schematic view of an analytical model. The size of the arch is a function the slot size, particle size and friction between particles. Once the arch is established, the granular flow rate can be calculated since it is assumed that particles will fall freely under self-weight below the arch.

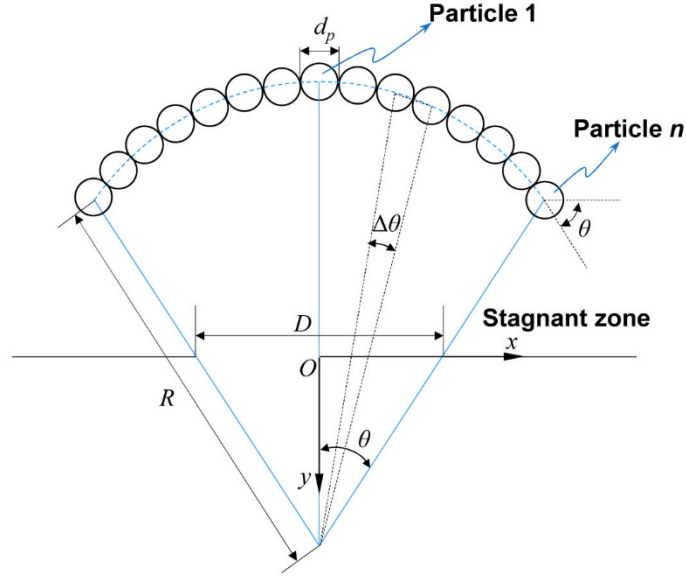


Figure 2-12 (Re) Schematic view of the analytical model (Tang, 2017)

Tang (2017) derived the radius  $R$  of the arch to be equal to:

$$R = \frac{d_p}{2 \sin(\Delta\theta/2)} \quad (3.1)$$

where  $R$  is the radius of free fall arch,  $d_p$  is particle diameter, and  $\Delta\theta$  is the angle between any two adjacent particles. The granular flow rate then can be estimated from:

$$Q = (1 - \varepsilon) D_0 \sqrt{2gS_0} \quad (3.2)$$

where  $Q$  is the volumetric granular flow rate,  $\varepsilon$  is porosity,  $D_0$  is the corrected slot width,  $g$  is gravity acceleration,  $S_0$  is the distance from the apex of the arch to the opening ( $S_0 = R - \frac{D_0}{2 \tan \theta}$ ), and  $\theta$  is half of the central angle of the arch.

Since this equation is based on uniform-sized sand, and therefore the effect of different particle sizes is omitted, experiments have been designed in this work to investigate the role of PSD on granular flow. To this end, different particle size sands with different slot sizes are chosen to study the PSD effect experimentally. The results are also compared with analytical calculations. Another objective of this study is to find the characteristic particle size for use in Eq. (3.2), as a

single particle size ( $d_p$ ) is required to calculate the flow rate. Also, the effect of other parameters such as the height of material over the slot, the ratio of particle size to the slot width, the stagnant zone angle, particle size alone and slot width alone on granular flow are investigated.

## **3 Experimental Design and Test Matrix**

### **3.1 Material Used in the Experiments**

Only clean sands were used in the current experiments as per the Unified Soil Classification System (USCS) (ASTM D2487). The sands were chosen to be greater than 0.5 mm and smaller than 4.76 mm to minimize the effect of air flow on granular flow. To compare the results of the experiments with available correlations which assume the particles are spherical, sands with the maximum sphericity from the available commercial sands were chosen for the tests. Based on the information provided by the commercial supplier, the sand particles contained around 92% silicon dioxide ( $\text{SiO}_2$ ) with a particle density of  $2.65 \text{ g/cm}^3$  (confirmed in the lab according to ASTM C-128). Although the particle density was confirmed in the lab (ASTM D854), the mineralogy of the sand was not considered as it is believed that mineralogy is not an influential parameter in this study at dry condition. Based on existing charts and visual analysis, sand particles were sub-angular and were sieved in the laboratory to provide the desired PSD for the tests. Characterization of the shape factors was not a focus in this research. This factor is aimed to be investigated further in another study by using real spherical particles such as glass beads.

### **3.2 Sample Preparation**

About 200 kg of commercial sands in 4 different size groups (I- 0.43 to 0.85 mm, II- 0.85 to 2.0 mm, III- 1.18 to 2.36 mm and IV- 2.5 mm to 4.75 mm) were sieved with an electrical sieve shaker to produce sand batches in different size categories. The mineralogy and shape characteristic of sands are described in (3.1). Table 3-1 summarizes the particle and sieve sizes used in the tests. The sand batches were then mixed with a hand shovel to provide the required materials with the desired PSD. Sands were mixed in three different size combinations for the experiments. According to USCS, the sizes are: 1- fine sand (S-I) with the particle size between 0.5 mm and 2.38 mm (Figure 5-1), 2- coarse sand (S-II) with the particle size between 2.38 mm and 4.75 mm (Figure 5-2) and 3- full ranged sand (S-III) with the particle size between 0.5 mm and 4.75 mm (Figure 5-3). Also, two uniform PSD's were tested: U-I with the particle size between 1.19 mm to 1.68 mm, and U-II with the particle size between 2.38 mm and 2.83 mm.

Table 3-1 Sieves specifications used in the experiment

No	Sieve size (U.S. Mesh)	Opening (Inches)	Opening (Microns)	Opening (Millimeters)
1	4	0.187	4760	4.76
2	5	0.157	4000	4
3	6	0.132	3360	3.36
4	7	0.111	2830	2.83
5	8	0.0937	2380	2.38
6	10	0.0787	2000	2
7	12	0.0661	1680	1.68
8	16	0.0469	1190	1.19
9	18	0.0394	1000	1
10	20	0.0331	840	0.84
11	30	0.0232	590	0.59
12	35	0.0197	500	0.5

Bulk densities of the sands were measured based on ASTM D4253 and D4254 since soils with different PSD's have different maximum and minimum bulk densities. For particle sizes ranging from 0.5 mm to 4.76 mm, static electricity has no significant effect, and the materials could be air-dried at room temperature, and the capillary effect was negligible under the low relative humidity in the laboratory. The particle size is uniformly distributed within the defined range for different PSD's. In other words, nearly the same amount of weight in each sand size has been chosen.

After mixing, the sands were poured and packed in the apparatus in 5-cm-thick layers. For consistency in all experiments, each layer was compacted using a 5-mm-diameter steel rod to reach 90% of the maximum bulk density based on the Standard Proctor Test. The reason for choosing 90% compaction is this amount is easily reachable for all sand groups in the lab. After filling the apparatus to the desired height, the overall bulk density can be measured, by knowing the total mass and the volume. Table 3-2 shows the average densities and porosities for each group. The maximum deviation from these averages is about 1% (0.02 g/cm<sup>3</sup>). Porosity has been calculated

from bulk and grain densities. After filling and compacting of the material, the test was started by opening the slot at the base of the apparatus to allow the flow of sand.

Table 3-2 Bulk density and porosity of all sand groups

Group	Size Range (mm)	Description	Bulk Density (g/cm <sup>3</sup> )	Porosity
U-I	1.19-1.68	Uniform	1.65	0.38
U-II	2.38-2.83	Uniform	1.64	0.38
S-I	0.5-2.38	Fine	1.64	0.38
S-II	2.38-4.75	Coarse	1.69	0.36
S-III	0.5-4.75	Full	1.84	0.31

### 3.3 Experimental Apparatus

#### 3.3.1 Setup design

The experimental apparatus is a cuboid hopper (85 cm high × 50 cm wide × 10 cm deep) with a flat bottom (50 cm × 10 cm) and adjustable rectangular orifice (slot) with a maximum width of 2.5 cm (10 cm × 2.5 cm). Figures 3-1 and 3-2 show the schematic and two views of the apparatus. This apparatus is made of metal frame and transparent polycarbonate plates to allow visual examination of the flow process. The shop drawings of the apparatus are shown in Appendix B.

In designing the experimental apparatus, it was necessary to have an estimate of the granular flow rate to determine the size of the apparatus. The modified Beverloo's equation was used to estimate the rate of flow for rectangular openings (Eq. 2.2). The purpose is to provide sufficient material for continuous flow for at least 30 seconds to allow the investigation of the flow characteristics. The capacity of the apparatus to sustain continuous flow for at least 30 seconds was determined based on the flow density ( $\rho_f$ ) of 2 g/cm<sup>3</sup>. The depth of the apparatus is equal to  $L = 10$  cm to minimize side boundary effects (Figure 3.1). With these assumptions and considering the modified Beverloo's equation for slot and  $k=1.4$ , the flow rate is calculated to be 2,427 g/s or 72.8 kg based on a total experiment time of 30 seconds. Assuming a density ( $\rho_f$ ) of 2 g/cm<sup>3</sup>, this is equal to a volume of 36,404 cm<sup>3</sup>. There are stagnant (non-flowing) zones on both sides of the slot. Based on a stagnant zone angle of 35°, the stagnant zone volume is calculated to be about 4,500 cm<sup>3</sup>. Therefore, the total volume required is about 41,000 cm<sup>3</sup> or 82 kg of granular material.

The minimum width of the slot to prevent jamming of particles should be five times the maximum grain size. Therefore, the minimum slot width is calculated to be 25 mm and the width of the apparatus ( $W$ ) is designed to be 50 cm (Figure 3.1). Based on these dimensions and the calculated total volume of material, the apparatus height ( $H$ ) should be higher than 82 cm.

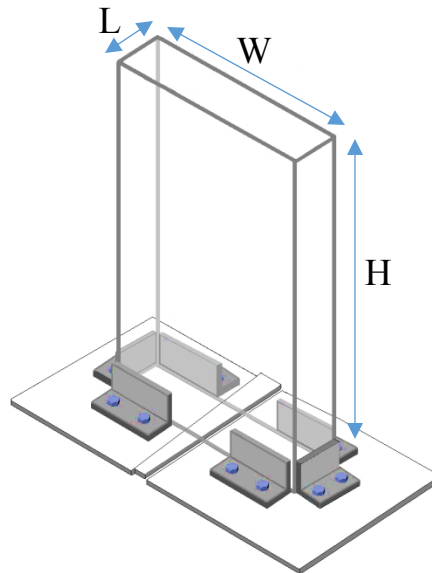


Figure 3-1 Schematic view of the apparatus with a sliding part



Figure 3-2 Granular flow apparatus (85 cm height  $\times$  50 cm width  $\times$  10 cm depth)

Part of the base of the apparatus was designed to accommodate a movable right triangle plate to adjust the slot size. The plate can move forward and backward to provide the desired slot width. A rectangular plate is used as a gate below the bottom section connected with a hinge which can be locked at the other side to stop the material flow during the filling of the apparatus (Figure 3-3). Once unlocked, the gate opens quickly to initiate the material flow.



Figure 3-3 Right triangle plate for adjusting slot width (left) and control gate with lock below the slot (right)

### 3.4 Experimental Procedure

This part describes the experimental procedure for measuring the granular discharge rate for different PSD's. The test matrix is designed to include different PSD, material height over the slot, slot size and the ratio of slot (opening) size to the average particle size.

At the beginning of each test, the hopper was thoroughly cleaned, and all sand particles from the previous experiment or any other contamination were removed. A digital scale with the accuracy of 0.9 g (0.002 lb.) was placed on the floor below the hopper with a container on it to collect the outflow material, and the scale was connected to a computer to record the mass rate. Then the slot size was adjusted to a specific width controlled by a caliper. After adjusting the opening size, the gate was closed to prevent material flow during placement and compaction of the material. A camera with the capability of capturing 24 frames per second was set up in front of the apparatus to monitor the discharge process and the formation of a stagnant zone.

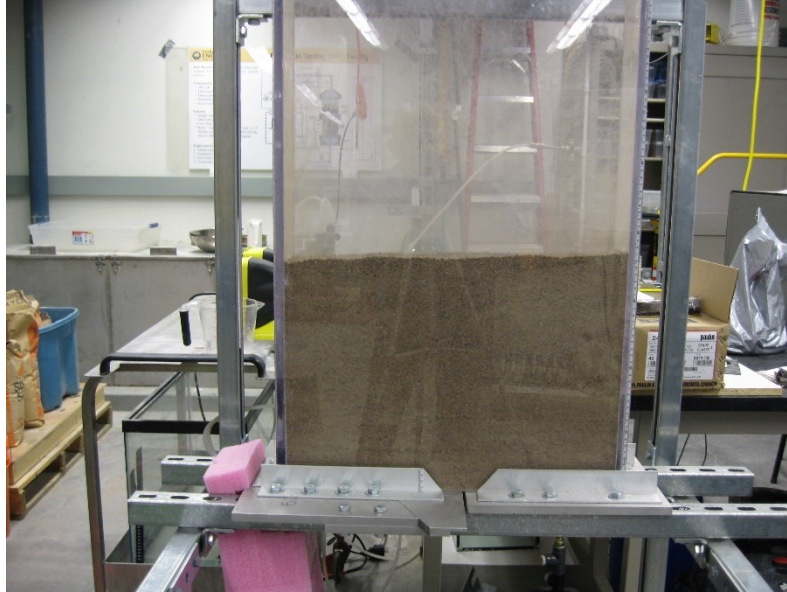


Figure 3-4: Apparatus filled with the material before the beginning of the test

Sample preparation started with pouring the mix into the apparatus chamber by using a 1.5-lit cylindrical plastic container in 5-cm layers to a specific height (Figure 3-4). Each layer was compacted with a steel rod. In pouring and compacting the sand, extra care was required to prevent material segregation. After placing all the materials required based on the known volume and mass, the bulk density and relative compaction could be determined. As explained in (3.2), the target density was equal to 90% of the optimum density of the Standard Proctor Maximum Dry Density.

The test was initiated by opening the gate to allow the granular discharge. A computer was used to record the mass rate from the scale every 0.1 seconds. The first and last 25% of flow duration were neglected in the granular flow assessment to obtain a steady state granular flow after forming the FFA. At the end of the flow process, the stagnant zones inside the hopper (Figure 3-5) were measured. During the discharge, regions of granular movement could be traced visually through the transparent hopper wall, and the free fall zone could be estimated and marked on the wall for each test.



Figure 3-5: Stagnant zones after sand flow was completed.

The initial plan was to perform two tests for each set of parameters to prove repetition of test results. The test matrix consisted of variable opening size/particle size ratio, different material heights and five PSD's (including two uniform-sized sands). Table 3-3 shows the initial test matrix. In this matrix, three groups of material were tested with the slot width/particle size ratio of 3, 5 and 7 with two different material heights of 500 and 800 mm.

Table 3-3 Initial test matrix

Material	Group	Description	Size Range	d50	Ratio	Slot Opening	Height of material over slot	Number of Experiments / Measurements														
								Sieve and Mix Design	Repose & stagnant zone Angle	Bulk Density	Grain Density	Porosity	Loose density (After discharge)	Mass Flow Rate								
Sand	S-I	Fine	0.5 - 2.5	1.5	3	4.5	500	1	2	1	2	1	2	2								
							800		2													
							500	1	2						1	2	2	2				
							800		2													
							500	1	2										1	2	2	2
							800		2													
	S-II	Coarse	2.5 - 4.75	3.6	3	11	500	1	2	1	2	1	2	2								
							800		2													
							500	1	2						1	2	2	2				
							800		2													
							500	1	2										1	2	2	2
							800		2													
S-III	Full	0.5 - 4.75	2.6	3	8	500	1	2	1	2	1	2	2									
						800		2														
						500	1	2						1	2	2	2					
						800		2														
						500	1	2										1	2	2	2	
						800		2														

## 4 Experimental Results and Observation

This chapter presents the testing procedure, observations, results, and findings. The testing started with two uniform PSD's (U-I & U-II) and then proceeded with three additional non-uniform PSD's (S-I, S-II, SIII).

### 4.1 U-I Uniform Sized Sand Ranged 1.19 mm to 1.68 mm

For comparing the uniform sand with uniformly distributed one, this uniform size range has been chosen to have same  $d_{50}$  as the  $d_{50}$  for S-I equal to 1.4 mm.

#### 4.1.1 Test procedures

*About 55 kg sand between 1.19 mm and 1.68 mm (Sieve # 12 and 16) was used to prepare the materials for this test. The tests were carried out with 4.3-, 4.8-, 8- and 11.2-mm slot opening sizes, and 310- and 570-mm sand height. Some tests were repeated for test accuracy and repeatability confirmation. Due to limited size range for U-I, only 55 kg sand could be obtained from sieving of all available materials. Other experiments proved the independence of the flow rate from the material height; hence, a greater amount of materials (above 55 kg) was not necessary.*

About 55 kg sand between 1.19 mm and 1.68 mm (Sieve # 12 and 16) was used to prepare the materials for this test. The tests were carried out with 4.3-, 4.8-, 8 and 11.2- mm slot opening sizes and 310- and 570-mm sand height. Some tests were repeated to examine the testing repeatability and reproducibility of results. Due to limited size range for U-I, only 55 kg sand could be obtained from sieving of all available materials. Other experiments proved the independence of the flow rate from the material height; hence, a greater amount of materials (above 55 kg) was not necessary.

#### 4.1.2 Test results

Seven tests were conducted in this size range. The test results are provided in Table 4-1. These measured flow rate results are the average of flow rates shown in Appendix A.

Table 4-1 Test results for U-I samples

No	Sand Group	Size Range	Range Description	d <sub>50</sub> (mm)	(D) Slot Opening (mm)	R=D/d <sub>50</sub>	Observed Arch Height (mm)	Sand Height (mm)	Stagnant Angle (°)	Measured Flow Rate (g/s)
1	U-I	1.19-1.68	uniform	1.4	4.3	3.1	9	315	42	21.74
2	U-I	1.19-1.68	uniform	1.4	4.8	3.4	9	570	40	26.88
3	U-I	1.19-1.68	uniform	1.4	4.8	3.4	9	310	41	27.20
4	U-I	1.19-1.68	uniform	1.4	8	5.7	15	570	38	79.03
5	U-I	1.19-1.68	uniform	1.4	8	5.7	15	310	36	83.00
6	U-I	1.19-1.68	uniform	1.4	11.2	8	20	570	37	159.17
7	U-I	1.19-1.68	uniform	1.4	11.2	8	27	310	33	161.94

## 4.2 U-II Uniform Sized Sand Ranged 2.38 mm to 2.83 mm

For more comparison between uniform sand and uniformly distributed one, this size range has been chosen to have the same d<sub>50</sub> with S-III equal to 2.6 mm.

### 4.2.1 Test procedures

The sieves used in this test were Sieve # 7 and 8, the particle size between 2.38 mm and 2.83 mm, with a total of about 40 kg sand. The slot sizes were 13, 15.6, 18.2, 20.8 and 23.4 mm and the height of sand were 260 and 390 mm. A total of six tests were carried out. The sample height for these experiments was limited to below 400 mm due to the limitation of sieved material in this uniform range (not more than 40 kg could be obtained for this range out of about 200 kg sand). Independence of flow rate from material height is proved in other experiments.

### 4.2.2 Test results

Table 4-2 shows the results of the six experimental results on U-II. These measured flow rate results are the average of flow rates shown in Appendix A graphs. Test #12 was repeated to

verify the repeatability of results. The effect of the sand height on the flow rate is not investigated for U-II.

Table 4-2 Test results for U-II samples

No	Sand Group	Size Range	Range Description	d50 (mm)	(D) Slot Opening (mm)	R=D/d50	Observed Arch Height (mm)	Sand Height (mm)	Stagnant Angle (°)	Measured Flow Rate (g/s)
8	U-II	2.38-2.83	uniform	2.6	13.03	5	21	390	39	160.75
9	U-II	2.38-2.83	uniform	2.6	15.6	6	30	260	36	234.53
10	U-II	2.38-2.83	uniform	2.6	18.2	7	30	390	37	318.62
11	U-II	2.38-2.83	uniform	2.6	20.8	8	35	260	36	412.57
12	U-II	2.38-2.83	uniform	2.6	23.4	9	55	390	35	511.21
13	U-II	2.38-2.83	uniform	2.6	23.4	9	40	260	35	522.4

### 4.3 S-I Fine Sand Ranged 0.5 mm to 2.38 mm

#### 4.3.1 Test procedures

Figure 4-1 shows the PSD of S-I with the sand size between 0.5 and 2.38 mm. About 75 kg of the sand was used in the apparatus with slot widths 4.2, 7, 8.4, 9.8, 11.2, 12.6 and 14 mm, and sand heights of about 350, 450, 700 and 750 mm. According to sand bulk density and apparatus volume, 75 kg of material is required to reach the maximum height.

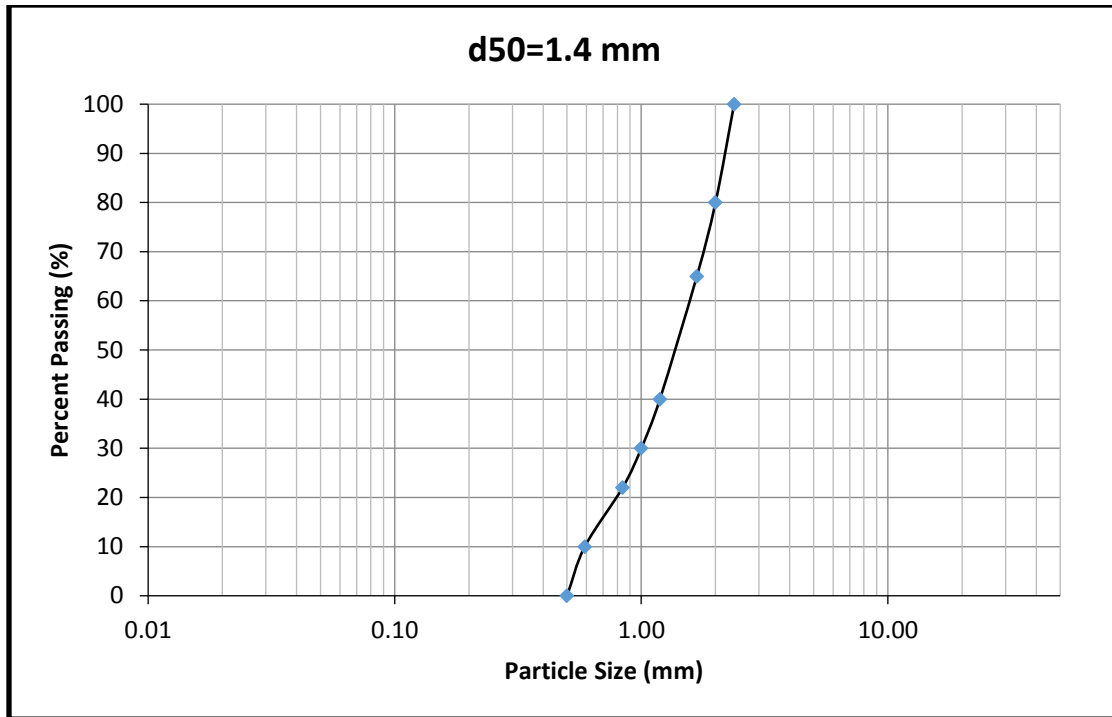


Figure 4-1 Particle size distribution of S-I sand group

### 4.3.2 Test results

Fourteen experiments were conducted on S-I with different slot widths. Some tests were repeated with varying heights of sand to examine the reproducibility of the test results. Table 4-3 shows the results for S-I samples. These measured flow rate results are the average of flow rates with very low standard deviations.

Table 4-3 Test results for S-I samples

No	Sand Group	Size Range	Range Description	d50 (mm)	(D) Slot Opening (mm)	R=D/d50	Observed Arch Height (mm)	Sand Height (mm)	Stagnant Angle (°)	Measured Flow Rate (g/s)
14	S-I	0.5-2.38	Fine	1.4	4.2	3	jammed	365	jammed	N/A
15	S-I	0.5-2.38	Fine	1.4	7	5	13	750	40	64.25
16	S-I	0.5-2.38	Fine	1.4	7	5	15	365	42	65.60

17	S-I	0.5-2.38	Fine	1.4	8.4	6	17	450	40	101.28
18	S-I	0.5-2.38	Fine	1.4	9.8	7	19	765	37	127.62
19	S-I	0.5-2.38	Fine	1.4	9.8	7	19	350	37	132.23
20	S-I	0.5-2.38	Fine	1.4	11.2	8	22	450	42	173.28
21	S-I	0.5-2.38	Fine	1.4	12.6	9	25	750	40	212.25
22	S-I	0.5-2.38	Fine	1.4	12.6	9	26	350	41	214.03
23	S-I	0.5-2.38	Fine	1.4	14	10	28	450	40	265.96
24	S-I	0.5-2.38	Fine	1.4	15.4	11	28	710	37	310.86
25	S-I	0.5-2.38	Fine	1.4	18.2	13	42	700	38	421.24
26	S-I	0.5-2.38	Fine	1.4	21	15	40	710	39	543.63
27	S-I	0.5-2.38	Fine	1.4	23.8	17	55	700	37	683.09

#### 4.4 S-II Coarse Sand Ranged 2.38 mm to 4.75 mm

##### 4.4.1 Test procedures

About 60 kg of sands per sample ranging in size between 2.38 and 4.75 mm were sieved for 10 tests. The slot widths for these tests are 18.2, 20, 21, 21.6, 23.4, 23.8 and 25.2 mm and sand heights were 300, 420 and 590 mm (30 kg, 42 kg and 60 kg of sand for each mentioned height respectively). Because of slot width limitations in the apparatus, it was not possible to conduct tests with wider slot sizes. The lower bound of the slot size was also selected at 18.2 mm to avoid material jamming.

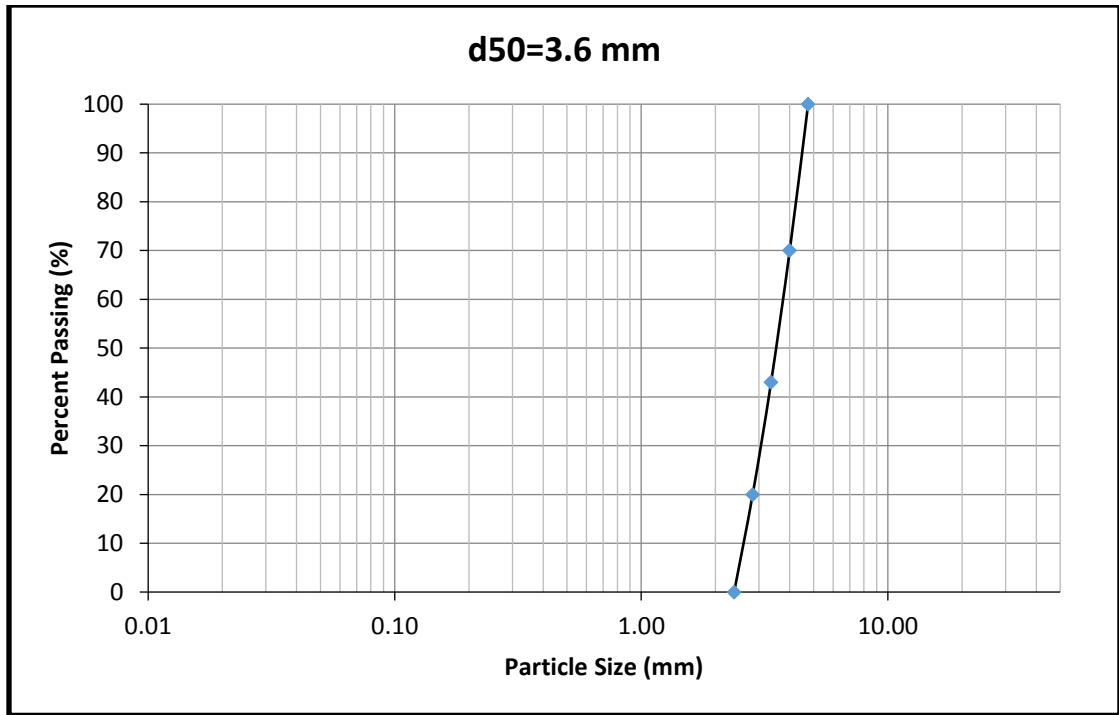


Figure 4-2 Particle size distribution of S-II samples

#### 4.4.2 Test results

Table 4-4 presents the results of 10 tests for S-II. These measured flow rate results are the average of flow rates with a maximum standard deviation of 3%.

Table 4-4 Test results for S-II samples

No	Sand Group	Size Range	Range Description	d50 (mm)	(D) Slot Opening (mm)	R=D/d50	Observed Arch Height (mm)	Sand Height (mm)	Stagnant Angle (°)	Measured Flow Rate (g/s)
28	S-II	2.38-4.75	Coarse	3.6	18.2	5.06	30	590	36	261.33
29	S-II	2.38-4.75	Coarse	3.6	18.2	5.06	29	300	36	269.43
30	S-II	2.38-4.75	Coarse	3.6	20	5.56	38	590	35	321.83
31	S-II	2.38-4.75	Coarse	3.6	20	5.56	30	590	41	325.00
32	S-II	2.38-4.75	Coarse	3.6	20	5.56	30	300	38	333.96

33	S-II	2.38-4.75	Coarse	3.6	21	5.8	30	590	36	360.07
34	S-II	2.38-4.75	Coarse	3.6	21.6	6	35	420	36	384.53
35	S-II	2.38-4.75	Coarse	3.6	23.4	6.5	39	590	36	448.71
36	S-II	2.38-4.75	Coarse	3.6	23.8	6.6	33	590	36	464.63
37	S-II	2.38-4.75	Coarse	3.6	25.2	7	45	590	37	519.11

## 4.5 S-III Size Range from 0.5 mm to 4.75 mm

### 4.5.1 Test procedures

This series of tests consisted of the wider PSD samples in S-III. The aim was to investigate the effect of coarse and fine material in the granular flow. In other words, if the effect of the finer side is dominant rather than the coarser side in a wider material range or vice versa. The S-III PSD was synthesized by mixing S-I and S-II in a specific proportion (Figure 5-3). Around 70 kg test materials per sample were prepared. The slot widths for these tests were 13, 14, 15.4, 16.9, 18.2, 20, 21, 21.6, 23.4, 23.8 and 25.2 mm. The heights were varied between 350 mm and 670 mm.

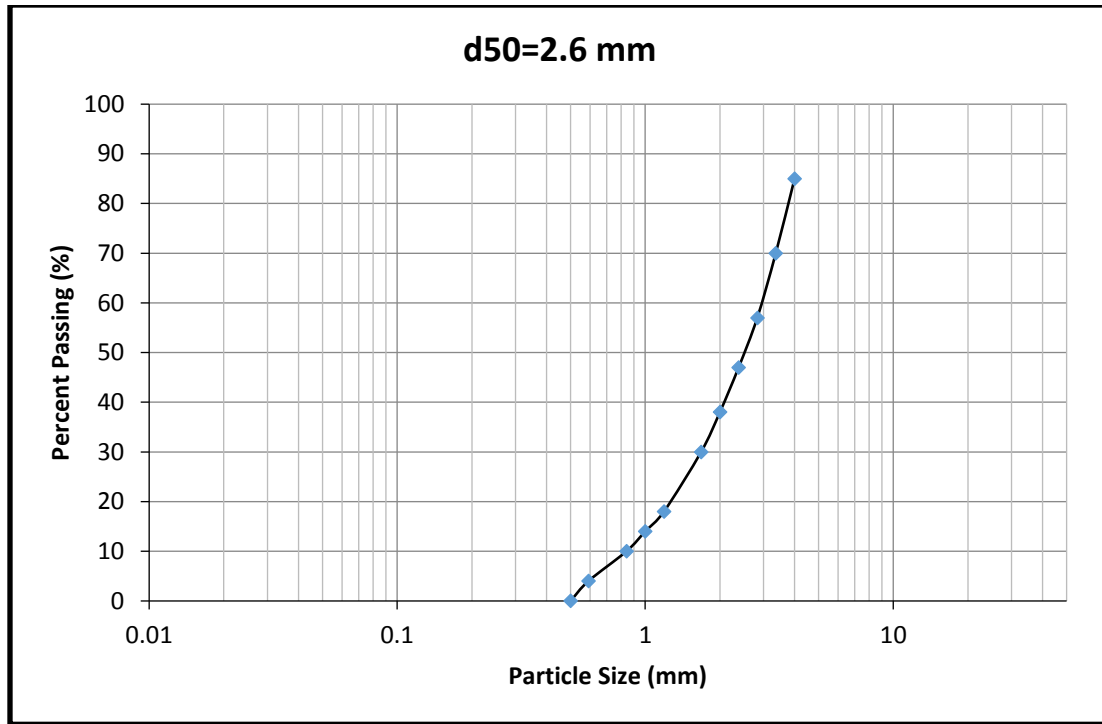


Figure 4-3 PSD of S-III samples

#### 4.5.2 Test results

The test matrix for S-III consisted of 15 experiments (Table 4-5). The measured flow rate results are the average of flow rates shown in Appendix A.

Table 4-5 Test results for S-III

No	Sand Group	Size Range	Range Description	d50 (mm)	(D) Slot Opening (mm)	R=D/d50	Observed Arch Height (mm)	Sand Height (mm)	Stagnant Angle (°)	Measured Flow Rate (g/s)
38	S-III	0.5-4.75	Full	2.6	13	5	jammed	510	jammed	N/A
39	S-III	0.5-4.75	Full	2.6	13	5	22	420	40	176.8
40	S-III	0.5-4.75	Full	2.6	14	5.4	16	510	37	208.98
41	S-III	0.5-4.75	Full	2.6	15.4	5.9	27	600	38	251.77

42	S-III	0.5-4.75	Full	2.6	15.4	5.9	28	350	40	263.77
43	S-III	0.5-4.75	Full	2.6	16.9	6.5	28	510	37	302.74
44	S-III	0.5-4.75	Full	2.6	18.2	7	31	510	36	350.85
45	S-III	0.5-4.75	Full	2.6	20	7.7	35	670	45	422.07
46	S-III	0.5-4.75	Full	2.6	20	7.7	32	350	40	429.4
47	S-III	0.5-4.75	Full	2.6	21	8.1	32	510	40	463.83
48	S-III	0.5-4.75	Full	2.6	21.6	8.3	37	510	37	480.06
49	S-III	0.5-4.75	Full	2.6	23.4	9	27	520	37	568.55
50	S-III	0.5-4.75	Full	2.6	23.8	9.2	38	640	41	591.53
51	S-III	0.5-4.75	Full	2.6	23.8	9.2	38	360	38	587.56
52	S-III	0.5-4.75	Full	2.6	25.2	9.7	30	560	35	658.32

## 4.6 Analysis and Discussion

Although the data logger recorded 10 mass measurements per second, the average discharge rates reported in tables and figures herein are based on 3-second measurements (average of 30 mass readings) to minimize noise in the data. The standard deviation of the flow rates based on the 3-second average is very low (see the figures on flow rate in Appendix A).

### 4.6.1 Effect of sand height

Some tests were carried out with different heights of sand to investigate the effect of sand height, hence, the effect of overburden stress on the granular flow rate. It is because the initial test results had shown that the overburden stress has little on the flow rate of granular material through an opening. Twelve pairs of tests (24 tests) were carried out with different sand groups. In each pair of tests, all other parameters (such as slot width, grain size distribution and degree of compaction) were kept constant, and only the sand height in the hopper was changed (decreased to almost half). As seen in Table 4-6, the difference in flow rate is about 2.5% with a maximum of

5% for a significant change in the height of sand. The results strongly suggest the existence of a free fall arch that provides a temporary impedance of flow after the free fall zone over the opening. The FFA theory explains why the overburden stress has little effect on granular flow rate.

Table 4-6 Comparison of results with different sand heights

No	Sand Group	Size Range	Range Description	d50 (mm)	(D) Slot Opening (mm)	R=D/d50	Observed Arch Height (mm)	Sand Height (mm)	Stagnant Angle (°)	Measured Flow Rate (g/s)	Deviation in Flow Rate (%)
2	U-I	1.19-1.68	uniform	1.4	4.8	3.4	9	570	40	26.88	1
3	U-I	1.19-1.68	uniform	1.4	4.8	3.4	9	310	41	27.20	
4	U-I	1.19-1.68	uniform	1.4	8	5.7	15	570	38	79.03	5
5	U-I	1.19-1.68	uniform	1.4	8	5.7	15	310	36	83.00	
6	U-I	1.19-1.68	uniform	1.4	11.2	8	20	570	37	159.17	2
7	U-I	1.19-1.68	uniform	1.4	11.2	8	27	310	33	161.94	
12	U-II	2.38-2.83	uniform	2.6	23.4	9	55	390	35	511.21	2
13	U-II	2.38-2.83	uniform	2.6	23.4	9	40	260	35	522.4	
15	S-I	0.5-2.38	Fine	1.4	7	5	13	750	40	64.25	2
16	S-I	0.5-2.38	Fine	1.4	7	5	15	365	42	65.60	
18	S-I	0.5-2.38	Fine	1.4	9.8	7	19	765	37	127.62	3
19	S-I	0.5-2.38	Fine	1.4	9.8	7	19	350	37	132.23	
21	S-I	0.5-2.38	Fine	1.4	12.6	9	25	750	40	212.25	1
22	S-I	0.5-2.38	Fine	1.4	12.6	9	26	350	41	214.03	
28	S-II	2.38-4.75	Coarse	3.6	18.2	5.06	30	590	36	261.33	3

29	S-II	2.38-4.75	Coarse	3.6	18.2	5.06	29	300	36	269.43	
31	S-II	2.38-4.75	Coarse	3.6	20	5.56	30	590	41	325.00	3
32	S-II	2.38-4.75	Coarse	3.6	20	5.56	30	300	38	333.96	
41	S-III	0.5-4.75	Full	2.6	15.4	5.9	27	600	38	251.77	5
42	S-III	0.5-4.75	Full	2.6	15.4	5.9	28	350	40	263.77	
45	S-III	0.5-4.75	Full	2.6	20	7.7	35	670	45	422.07	2
46	S-III	0.5-4.75	Full	2.6	20	7.7	32	350	40	429.4	
50	S-III	0.5-4.75	Full	2.6	23.8	9.2	38	640	41	591.53	1
51	S-III	0.5-4.75	Full	2.6	23.8	9.2	38	360	38	587.56	

This height independence is one of the crucial concepts which has been discussed over decades but not investigated widely for different particle size distributions. This is the fundamental difference between granular flow and fluid flow which depends on the fluid pressure or head. This concept which was introduced as Free Fall Arch (FFA) forms the basis of the hourglass design (Le Pennec et al., 1996). In all the tests, it is found that the granular flow rate is almost constant during the flow process except a few seconds at the beginning and the end of flow due to the absence of the FFA. Figures 4-4 to 4-8 show the granular flow rate in different experiments and different sand groups. Additional figures showing the discharge rate for different conditions are presented in Appendix A. As shown in these figures, although the discharge rate is constant regardless of material height in all cases, it shows more fluctuations of flow rates for tests with a wider range of sizes than uniform size particles. It might be because of particle segregation during the flow and size separation before reaching the orifice. This phenomenon needs to be investigated more deeply.

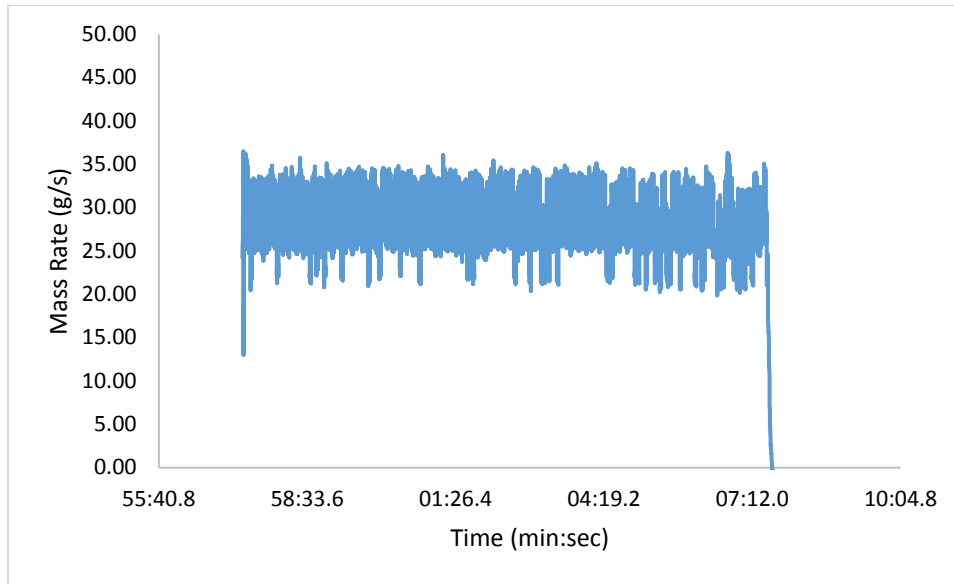


Figure 4-4: Granular flow rate vs. time for (U-I) sand group

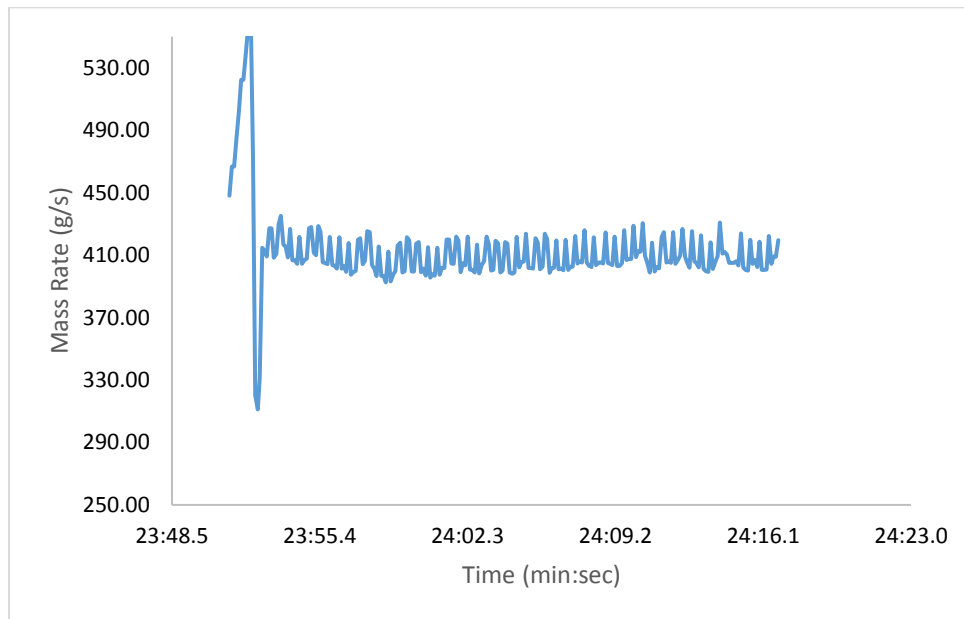


Figure 4-5 granular flow rate vs. time for (U-II) sand group

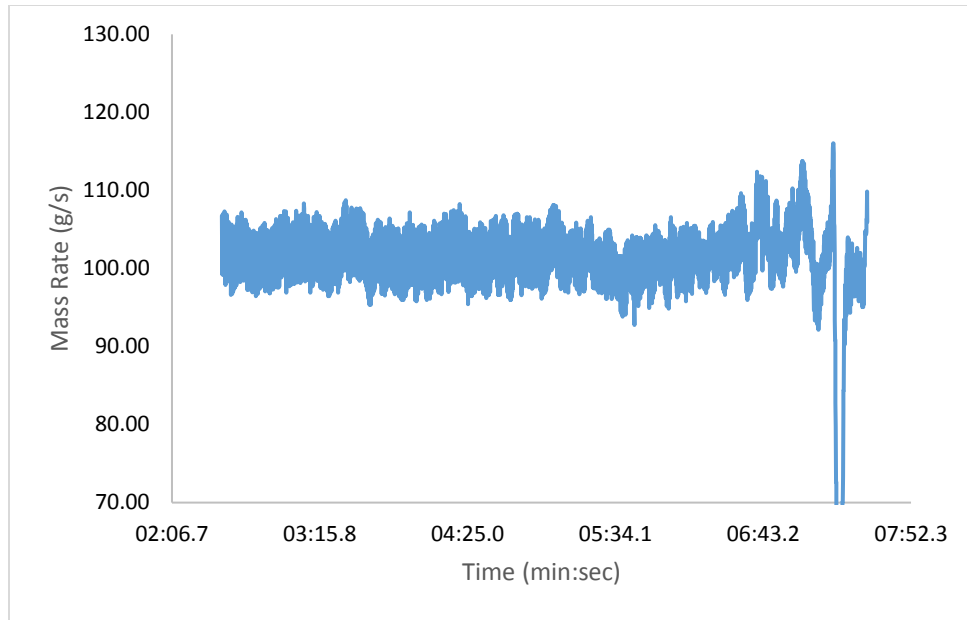


Figure 4-6 granular flow rate vs. time for (S-I) sand group

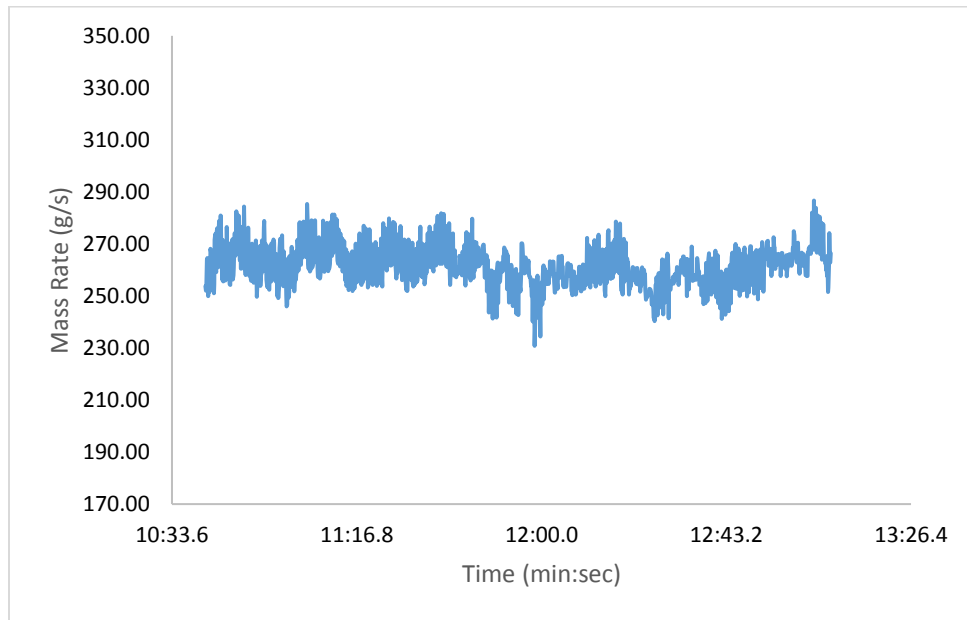


Figure 4-7 granular flow rate vs. time for (S-II) sand group

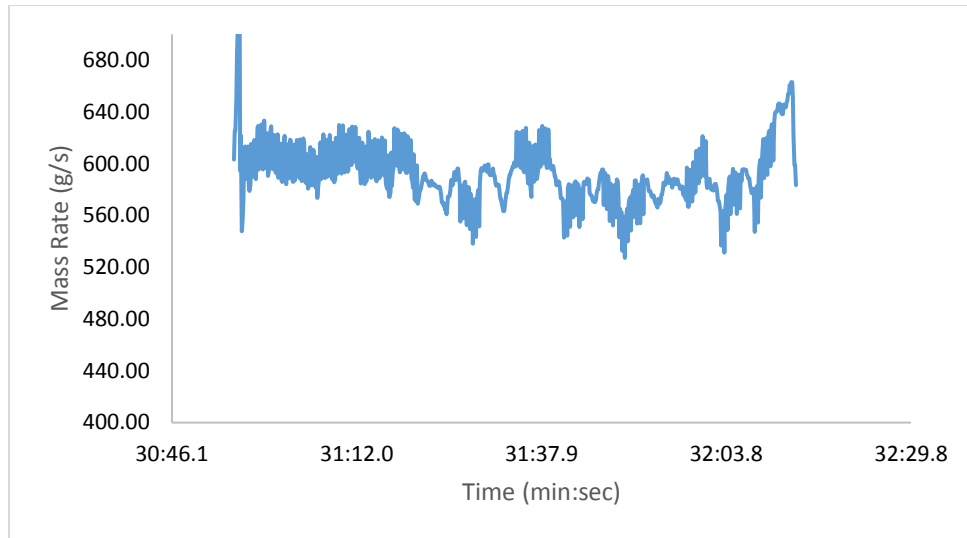


Figure 4-8 granular flow rate vs. time for (S-III) sand group

Besides, the cumulative discharged mass during the test has a linear trend confirming the independence of the granular mass flow rate from grains height over the slot (Figures 4-9 to 4-13). All other cumulative discharged mass graphs are presented in Appendix A.

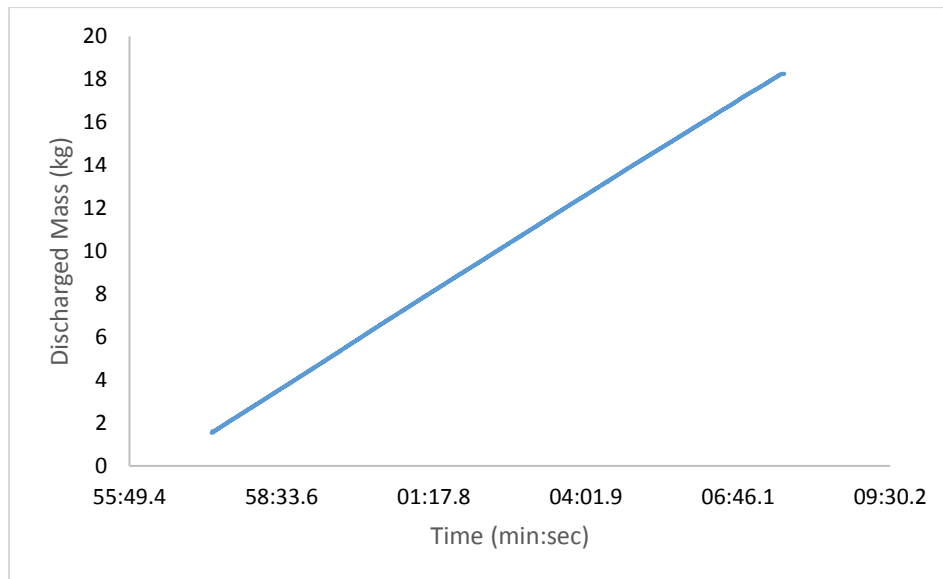


Figure 4-9 Cumulative discharged mass vs. time for (U-I) sand group

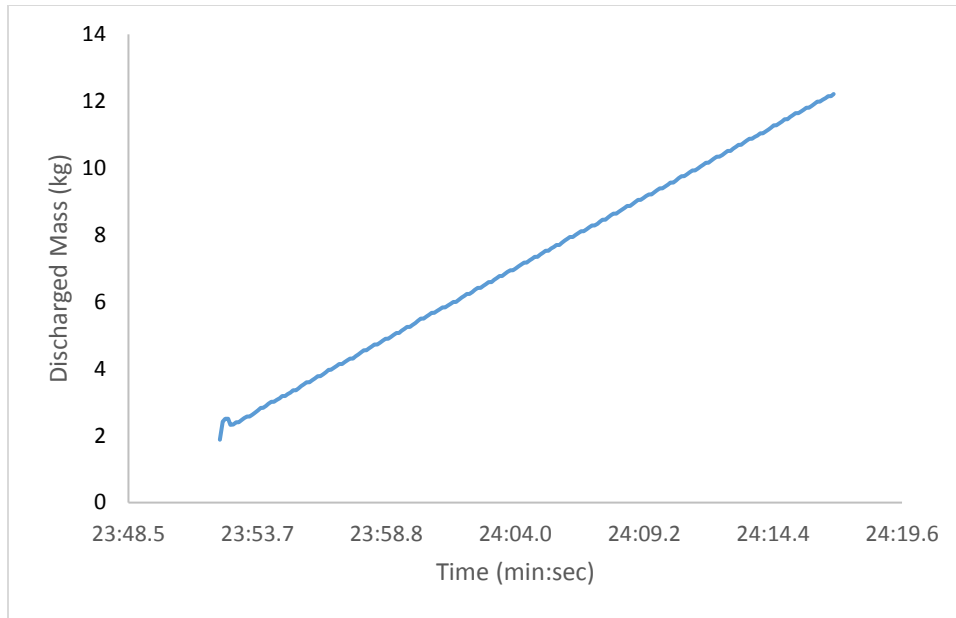


Figure 4-10 Cumulative discharged mass vs. time for (U-II) sand group

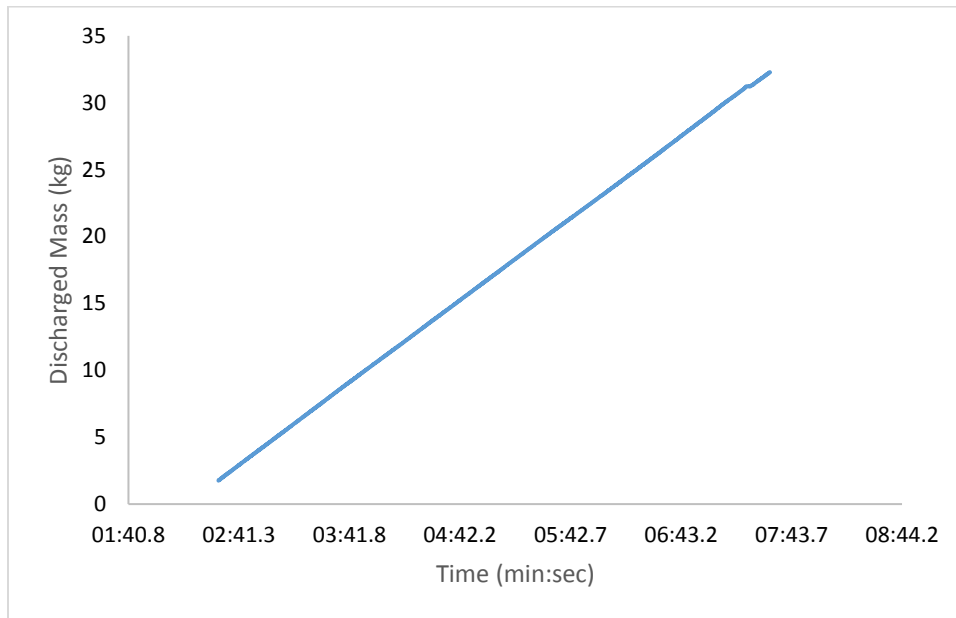


Figure 4-11 Cumulative discharged mass vs. time for (S-I) sand group

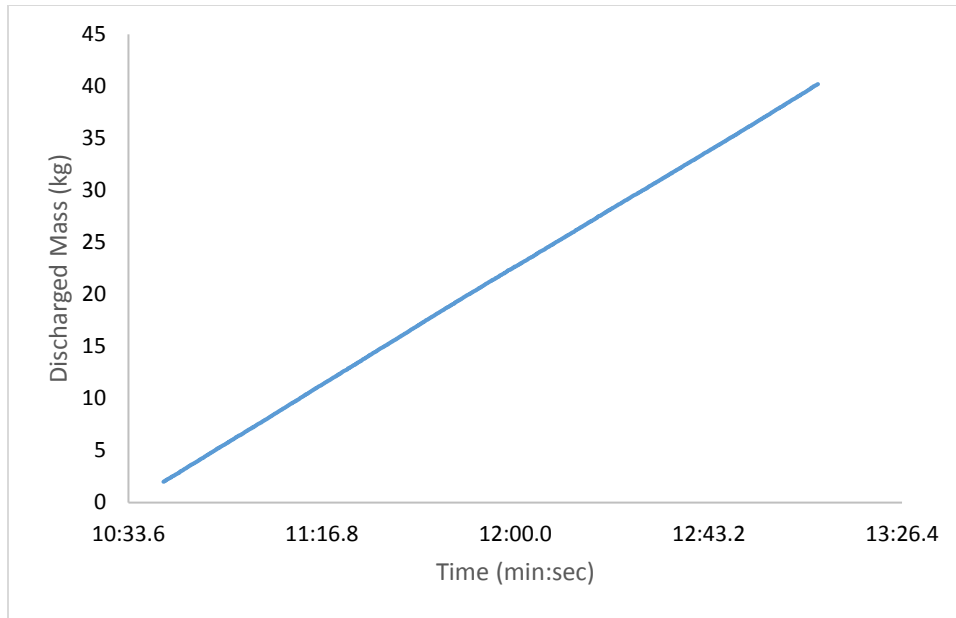


Figure 4-12 Cumulative discharged mass vs. time for (S-II) sand group

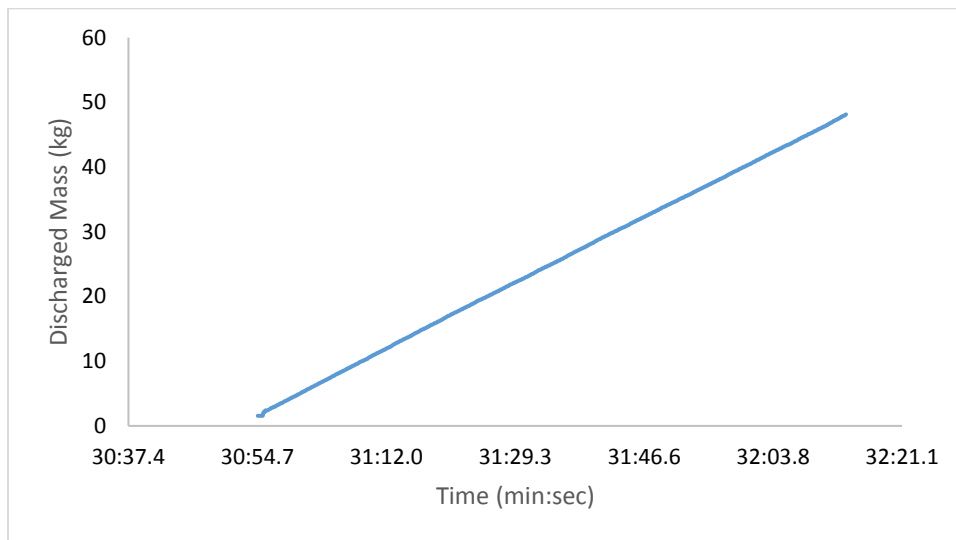


Figure 4-13 Cumulative discharged mass vs. time for (S-III) sand group

#### 4.6.2 Effect of grain size and PSD

Different PSD were used with the same slot size to study the effects of different particle size distributions (PSD). Table 4-7 shows the test parameters and results. It shows that the flow rate is inversely related to the characteristic particle size,  $d_{50}$ , i.e., with the increase in the particle

size, the discharge rate is decreased. Similar findings have been reported in the literature (Nedderman, 1992).

Table 4-7 Comparison of results with different particle size distributions

No	Sand Group	Size Range	Range Description	d50 (mm)	(D) Slot Opening (mm)	R=D/d50	Observed Arch Height (mm)	Sand Height (mm)	Stagnant Angle (°)	Measured Flow Rate (g/s)
7	U-I	1.19-1.68	uniform	1.4	11.2	8	27	310	33	161.94
20	S-I	0.5-2.38	Fine	1.4	11.2	8	22	450	42	173.28
8	U-II	2.38-2.83	Uniform	2.6	13	5	21	390	39	160.75
39	S-III	0.5-4.75	Full	2.6	13	5	22	420	40	176.8
23	S-I	0.5-2.38	Fine	1.4	14	10	28	450	40	265.96
40	S-III	0.5-4.75	Full	2.6	14	5.4	16	510	37	208.98
9	U-II	2.38-2.83	uniform	2.6	15.6	6	30	260	36	234.53
24	S-I	0.5-2.38	Fine	1.4	15.4	11	28	710	37	310.86
41	S-III	0.5-4.75	Full	2.6	15.4	5.9	27	600	38	251.77
10	U-II	2.38-2.83	uniform	2.6	18.2	7	30	390	37	318.62
25	S-I	0.5-2.38	Fine	1.4	18.2	13	42	700	38	421.24
28	S-II	2.38-4.75	Coarse	3.6	18.2	5.06	30	590	36	261.33
44	S-III	0.5-4.75	Full	2.6	18.2	7	31	510	36	350.85
31	S-II	2.38-4.75	Coarse	3.6	20	5.56	30	590	41	325.00
45	S-III	0.5-4.75	Full	2.6	20	7.7	35	670	45	422.07
11	U-II	2.38-2.83	uniform	2.6	20.8	8	35	260	36	412.57

26	S-I	0.5-2.38	Fine	1.4	21	15	40	710	39	543.63
33	S-II	2.38-4.75	Coarse	3.6	21	5.8	30	590	36	360.07
47	S-III	0.5-4.75	Full	2.6	21	8.1	32	510	40	463.83
34	S-II	2.38-4.75	Coarse	3.6	21.6	6	35	420	36	384.53
48	S-III	0.5-4.75	Full	2.6	21.6	8.3	37	510	37	480.06
12	U-II	2.38-2.83	uniform	2.6	23.4	9	55	390	35	511.21
35	S-II	2.38-4.75	Coarse	3.6	23.4	6.5	39	590	36	448.71
49	S-III	0.5-4.75	Full	2.6	23.4	9	27	520	37	568.55
27	S-I	0.5-2.38	Fine	1.4	23.8	17	55	700	37	683.09
36	S-II	2.38-4.75	Coarse	3.6	23.8	6.6	33	590	36	464.63
50	S-III	0.5-4.75	Full	2.6	23.8	9.2	38	640	41	591.53
37	S-II	2.38-4.75	Coarse	3.6	25.2	7	45	590	37	519.11
52	S-III	0.5-4.75	Full	2.6	25.2	9.7	30	560	35	658.32

To study the effect of particle size, according to the above table, 11 groups of experiments with 11 different slot opening size were considered. For investigating the effect of particle size, in group 3 with slot opening of 14 mm, test # 23 with  $d_{50} = 1.4$  mm has higher discharge rate than test # 40 with  $d_{50} = 2.6$  mm. In group 4 with slot opening of 15.4 mm, test # 24 with  $d_{50} = 1.4$  mm has higher discharge rate in compare with test # 9 and 41 with  $d_{50} = 2.6$  mm. In group 5 with slot opening of 18.2 mm, test # 25 with  $d_{50} = 1.4$  mm has higher discharge rate in comparison with test # 44 and 10 with  $d_{50} = 2.6$  mm and these two have higher rates than test # 28 with  $d_{50} = 3.6$  mm. As can be seen in other groups the same trend has been happened confirming that finer particles can pass through an orifice with higher rates than coarser particles.

To study the effect of particle size distribution (PSD) rather than particle size itself, it was decided to implement some tests at constant slot opening size with particles with the same  $d_{50}$  but different particle size distribution range. Table 4-8 shows these groups of tests more clearly.

Table 4-8 Comparison of results with different PSDs and the same  $d_{50}$  and the same opening size

No	Sand Group	Size Range	Range Description	$d_{50}$ (mm)	Slot Opening (mm)	$R=D/d_{50}$	Observed Arch Height (mm)	Sand Height (mm)	Stagnant Angle (°)	Measured Flow Rate (g/s)	Difference (%)
7	U-I	1.19-1.68	uniform	1.4	11.2	8	27	310	33	161.94	7
20	S-I	0.5-2.38	Fine	1.4	11.2	8	22	450	42	173.28	
8	U-II	2.38-2.83	Uniform	2.6	13	5	21	390	39	160.75	10
39	S-III	0.5-4.75	Full	2.6	13	5	22	420	40	176.8	
9	U-II	2.38-2.83	uniform	2.6	15.4	6	30	260	36	228.85	10
41	S-III	0.5-4.75	Full	2.6	15.4	5.9	27	600	38	251.77	
10	U-II	2.38-2.83	uniform	2.6	18.2	7	30	390	37	318.62	10
44	S-III	0.5-4.75	Full	2.6	18.2	7	31	510	36	350.85	
11	U-II	2.38-2.83	uniform	2.6	21	8	35	260	36	420.16	10
47	S-III	0.5-4.75	Full	2.6	21	8.1	32	510	40	463.83	
12	U-II	2.38-2.83	uniform	2.6	23.4	9	55	390	35	511.21	11
49	S-III	0.5-4.75	Full	2.6	23.4	9	27	520	37	568.55	

Uniformly distributed sand has been compared with uniform size sand in all groups with the same slot opening size and the same  $d_{50}$ . It has been observed that uniformly distributed sand which has wider particle size in both sides, finer and coarser, the discharge rate is higher than uniform size sand. This shows the finer particles are more contributing and are more dominant in

discharge rate rather than coarser components of the sand particles. Table 4.8 illustrates that this difference in discharge rates is about 10%. This finding helps to consider the finer portion of particle size in predicting the discharge rate rather than the average size of  $d_{50}$ . This phenomenon can be due to previous finding mentioned in Section (2.1.4) which states that finer particles fill the voids between coarser particles reducing porosity and increasing density and causing higher flow rates. For Test # 9 and Test # 11, the rates for the slot opening sizes of 15.4 mm and 21 mm have been interpolated from measurements data for slot opening sizes of 15.6 mm and 20.8 mm.

#### **4.6.3 Effect of slot size and slot size/particle size ratio**

It is evident that particle discharge rate through an orifice is directly proportionate to orifice size. Increase in orifice size causes an increase in discharge rate, and this is confirmed in all experiments.

As in each group of sands (U-I, U-II, S-I, S-II and S-III) the average particle size or  $d_{50}$  is constant, it is decided to investigate the correlation between the particle discharge rate and the  $(D/d_{50})$  ratio in each of 5 defined sand group, because two apparent contributing parameters in the granular flow rate are  $D$  and  $d_{50}$ .

Figures 4-14 and 4-15 show the correlation graph in the uniform sand (U-I) and fine sand (S-I) with  $d_{50} = 1.4$  mm. In these figures, curvature with the power of two fits perfectly to define the correlation.

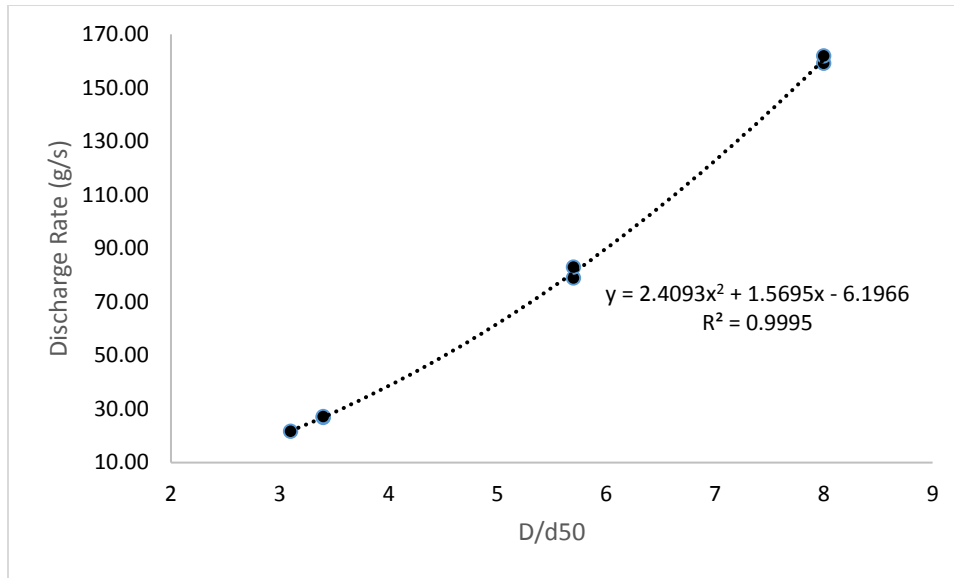


Figure 4-14 Granular flow vs. D/d50 for (U-I) sand group

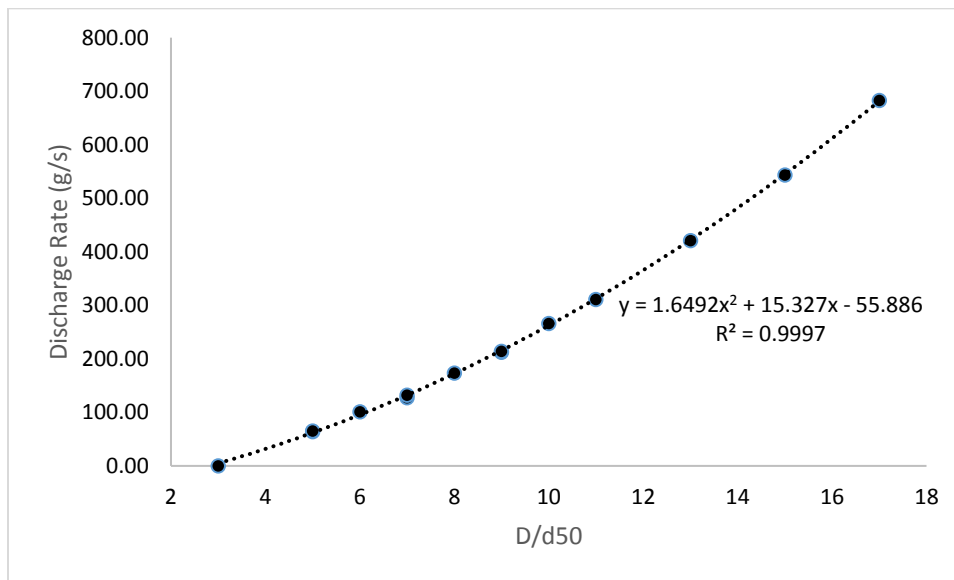


Figure 4-15 Granular flow vs. D/d50 for (S-I) sand group

As can be seen in Figures 4-16 and 4-17, for (U-II) and (S-III) in which  $d_{50} = 2.6$  mm, the curves tend to be more linear. It seems a more linear behavior should be expected for higher  $d_{50}$ , i.e., coarser materials.

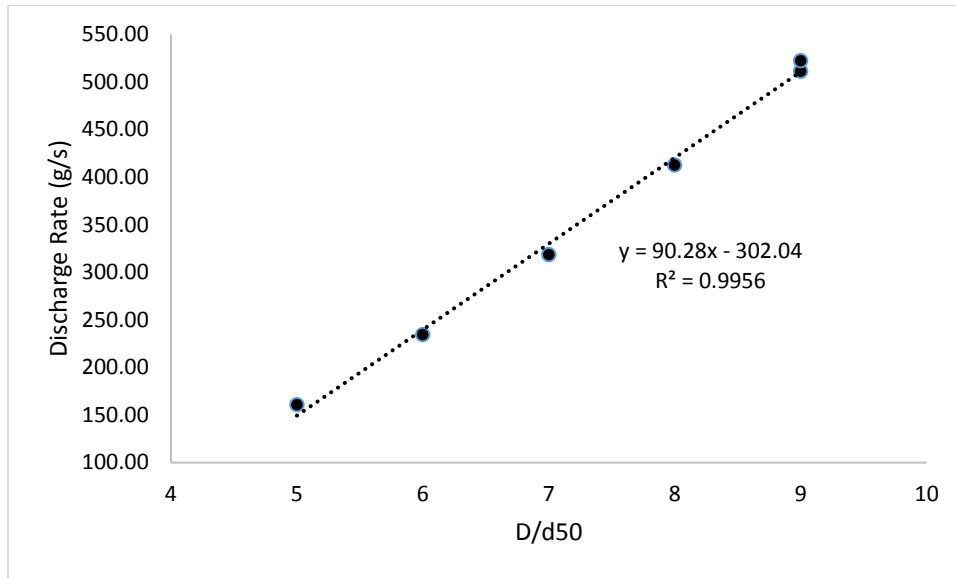


Figure 4-16 Granular flow vs. D/d50 for (U-II) sand group

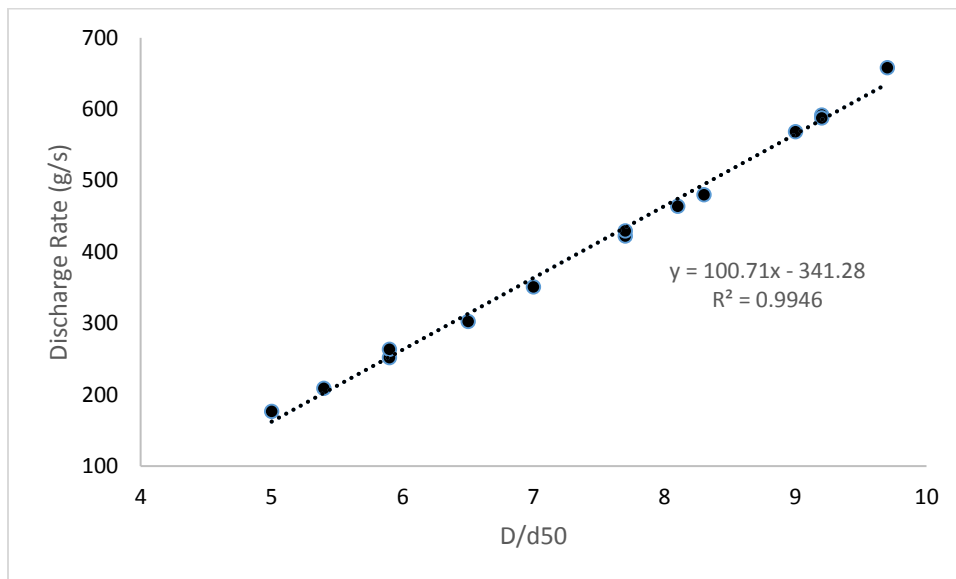


Figure 4-17 Granular flow vs. D/d50 for (S-III) sand group

The Figure 4-18 for coarse sand (S-II) confirms the idea mentioned before, i.e., coarser materials tend to behave more linearly as in this group, material with  $d_{50} = 3.6$  mm is more linear than (U-II) and (S-III) with  $d_{50} = 2.6$  mm.

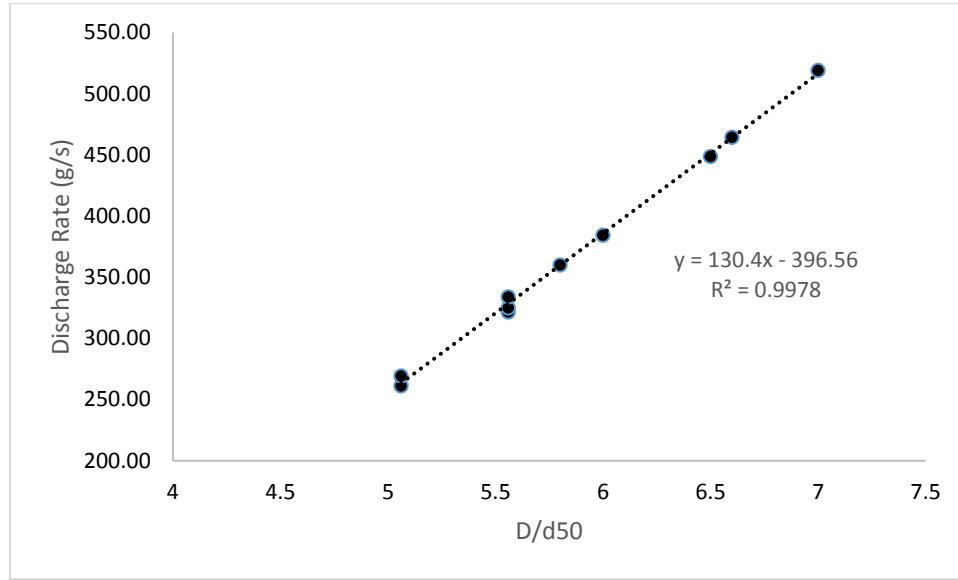


Figure 4-18 Granular flow vs. D/d50 for (S-II) sand group

#### 4.6.4 Comparison with Tang's (2017) analytical correlation

Tang (2017) proposed an equation to calculate the rate of flow of granular material through an opening. In Tang's equation, in addition to the slot size and particle size, porosity, stagnant zone angle and particles friction angle are needed to calculate the flow rate. As shown in Figure 4-19, the calculation requires the determination of the location and radius of the free fall arch. To calculate granular flow rates for the tests,  $d_{50}$  is used in Tang's equation as the characteristic particle size. According to Equation (4.1) and assuming uniform size particles, the angle between adjacent particles ( $\Delta\theta$  in Figure 4-19) is calculated. Table 4-9 shows the calculated results and the experimental measurements (based on the visual determination of the free fall radius and measured granular flow rate).

$$\frac{2(\cos \Delta\theta + \tan \varphi_p \sin \Delta\theta)}{m(M-2)(\sin \Delta\theta + \tan \varphi_p \cos \Delta\theta)} = \frac{(\cos \theta - \tan \varphi_p \sin \theta)}{(\sin \theta + \tan \varphi_p \cos \theta)} \quad (4.1)$$

where  $\Delta\theta$  is the angle between adjacent particles,  $\varphi_p$  is particles friction angle,  $\theta$  is half of the central angle of free fall arch which is equal to the complementary angle of the stagnant zone angle (figure below),  $M = \frac{\theta}{\sin(\Delta\theta/2)}$  and  $m = 2$  if  $M$  is an odd number otherwise  $m = 1$ .

After calculating  $\Delta\theta$ , the free fall arch radius  $R$  is obtained from Equation (4.2) and then based on Equation (4.2) free fall arch height  $s_0$  is calculated using Equation (4.3).

$$R = \frac{d_p}{2 \sin(\Delta\theta/2)} \quad (4.2)$$

$$s_0 = R - \frac{D_0}{2 \sin \theta} \quad (4.3)$$

where  $R$  is the FFA radius,  $d_p$  is the particle size which is assumed to be  $d_{50}$  here,  $s_0$  is the FFA height from the slot,  $D_0 = D - 1.5d_p$  and  $D$  is the slot width.

Finally, to calculate the flow rate, using Equation (4.4), the results are obtained for all the tests and compared with the actual experiments measurements (see Table 4-9).

$$Q = (1 - \varepsilon)D_0\sqrt{2gs_0} \quad (4.4)$$

where  $Q$  is the volumetric flow rate per unit length of sloe,  $\varepsilon$  is the porosity and  $g$  is gravitational acceleration.

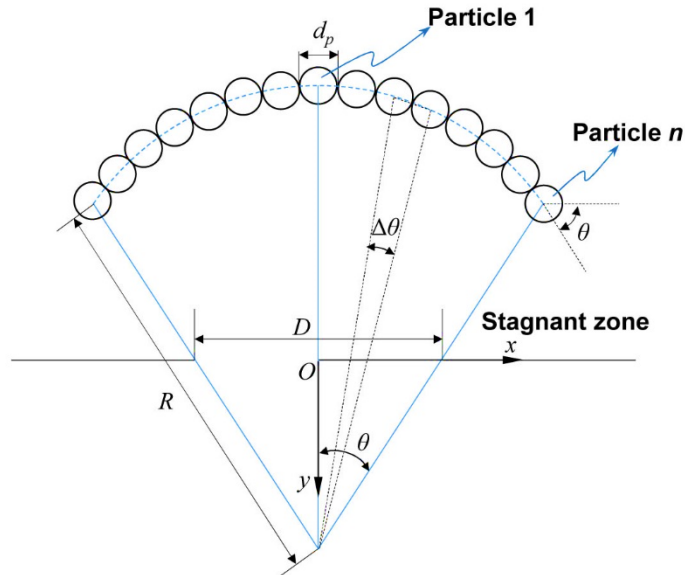


Figure 4-19 Schematic view of arch and calculation parameters (Tang, 2017)

Table 4-9 Comparison between experiments and Tang's presented correlation (2017)

No	Sand Group	Tang's Calculated FFA Radius (cm)	Visualized FFA Radius (cm)	Tang's Flow Rate Estimate (g/s)	Experiment's Flow Rate (g/s)	Difference (%)
1	U-I	0.87	1.09	61.19	21.74	181
2	U-I	1.16	1.1	81.13	26.88	202
3	U-I	0.93	1.11	70.44	27.20	159
4	U-I	1.46	1.81	147.80	79.03	87
5	U-I	1.78	1.79	168.55	83.00	103
6	U-I	1.67	2.42	215.72	159.17	36
7	U-I	6.68	3.06	486.16	161.94	200
8	U-II	2.1	2.63	285.35	160.75	78
9	U-II	3.31	0.87	452.23	234.53	93
10	U-II	2.71	3.69	452.37	318.62	42
11	U-II	3.31	4.26	581.53	412.57	41
12	U-II	4.26	4.72	757.96	511.21	48
13	U-II	4.26	4.82	757.96	522.4	45
14	S-I	1.02	N/A	66.67	N/A	N/A
15	S-I	1.01	1.59	102.52	64.25	60
16	S-I	0.87	1.82	90.57	65.60	38
17	S-I	1.02	2.05	118.24	101.28	17
18	S-I	1.49	2.27	176.1	127.62	38

19	S-I	1.49	2.27	176.1	132.23	33
20	S-I	0.87	2.7	117.61	173.28	-32
21	S-I	1.02	3.03	152.2	212.25	-28
22	S-I	0.93	3.15	135.22	214.03	-37
23	S-I	1.02	3.39	158.5	265.96	-40
24	S-I	1.49	3.38	253.46	310.86	-18
25	S-I	1.27	4.91	235.85	421.24	-44
26	S-I	1.13	4.85	191.82	543.63	-65
27	S-I	1.46	6.4	308.18	683.09	-55
28	S-II	4.58	3.66	621.95	261.33	138
29	S-II	4.58	3.56	621.95	269.43	131
30	S-II	5.89	6.6	786.59	321.83	144
31	S-II	2.4	3.87	428.05	325.00	32
32	S-II	3.28	3.78	545.73	333.96	63
33	S-II	4.58	3.76	707.32	360.07	96
34	S-II	4.58	4.28	725.61	384.53	89
35	S-II	4.58	4.75	780.49	448.71	74
36	S-II	4.58	4.16	792.68	464.63	71
37	S-II	3.75	5.45	731.71	519.11	41
38	S-III	N/A	N/A	N/A	N/A	N/A
39	S-III	1.89	2.75	270.59	176.8	53

40	S-III	2.7	2.13	371.76	208.98	78
41	S-III	2.37	3.3	367.65	251.77	46
42	S-III	1.89	3.45	308.24	263.77	17
43	S-III	2.76	3.44	442.94	302.74	46
44	S-III	3.31	3.76	532.94	350.85	52
45	S-III	1.38	4.5	221.76	422.07	-47
46	S-III	1.89	4.04	368.24	429.4	-14
47	S-III	1.89	4.08	378.82	463.83	-18
48	S-III	2.76	4.51	541.76	480.06	13
49	S-III	2.76	3.58	576.47	568.55	1
50	S-III	1.73	4.83	357.05	591.53	-40
51	S-III	2.37	4.73	512.94	587.56	-13
52	S-III	4.26	3.88	829.41	658.32	26

As can be seen from the Table 4-9, about 75% of tests have lower flow rates than calculated using Tang's equation. This has been illustrated in Figures 4-20 to 4-24 for different sand groups. There is no specific, meaningful trend or deviation between these two granular flow rates.

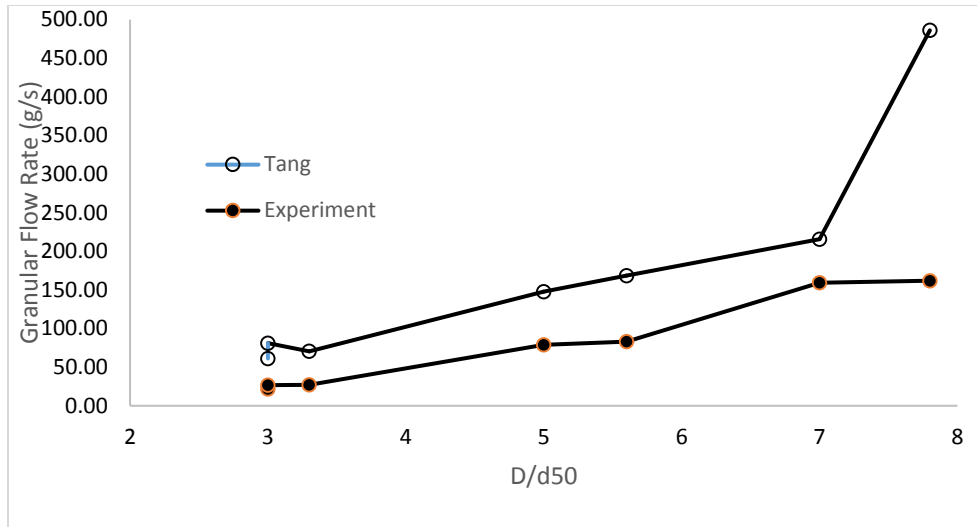


Figure 4-20 Comparison between experiment and Tang's correlation in (U-I)

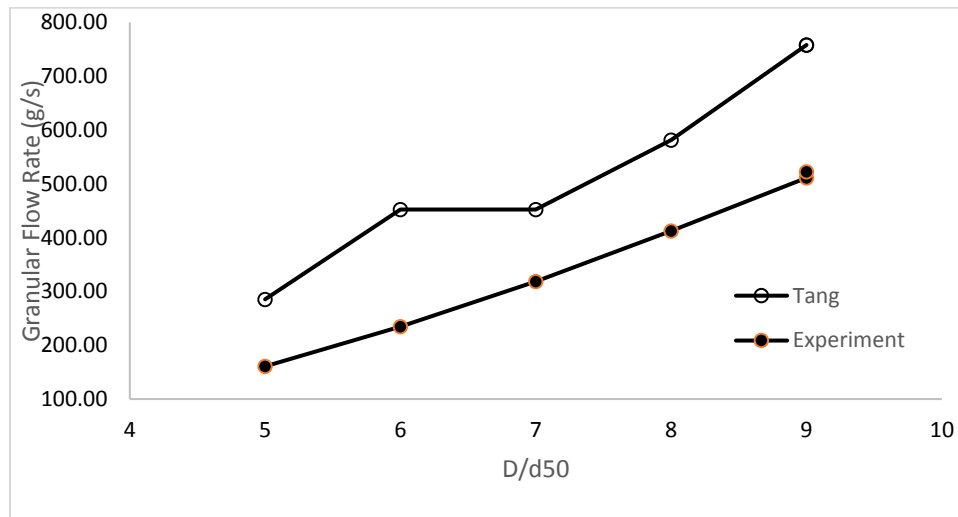


Figure 4-21 Comparison between experiment and Tang's correlation in (U-II)

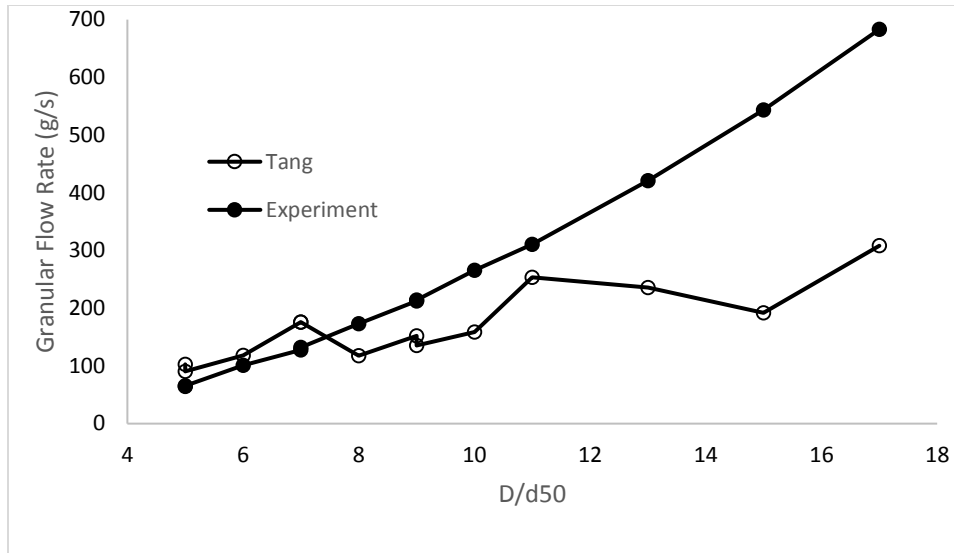


Figure 4-22 Comparison between experiment and Tang's correlation in (S-I)

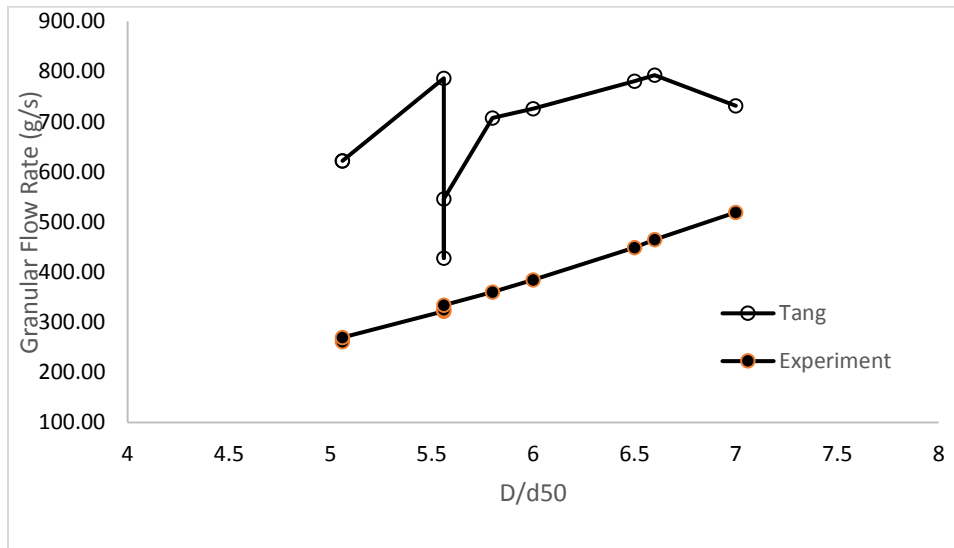


Figure 4-23 Comparison between experiment and Tang's correlation in (S-II)

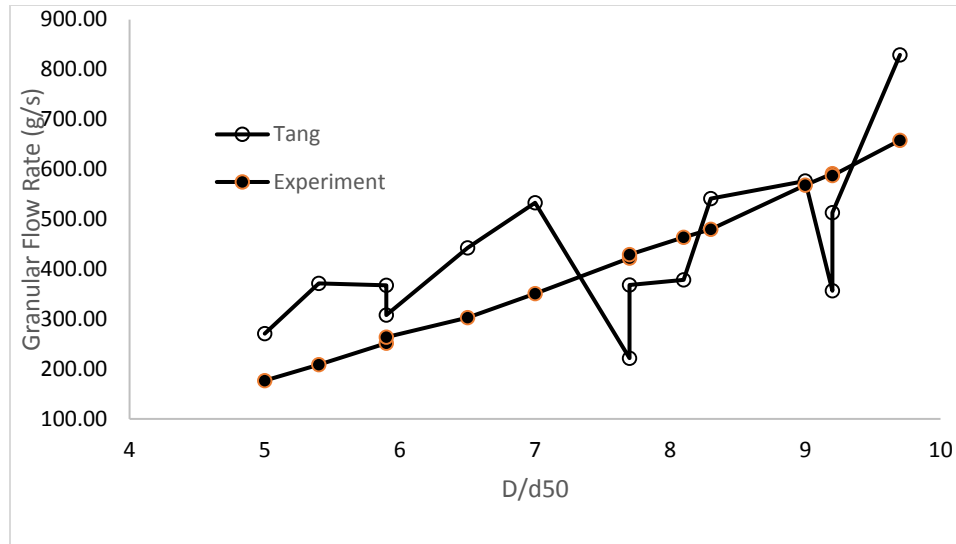


Figure 4-24 Comparison between experiment and Tang's correlation in (S-III)

#### 4.6.5 Comparison with modified Beverloo's law (Mayers and Sellers, 1978)

As discussed in chapter 2, Mayers and Sellers (1978) modified the Beverloo's equation for the slot in 1978. In Equation (4.5), except slot dimensions and particle size, parameters such as flowing density ( $\rho_f$ ) and Beverloo's shape coefficient ( $k$ ) should be entered. Table 4-10 provides a comparison between the calculated flow rate using the modified Beverloo's equation and experimental measurements. In this calculation, the density  $\rho_f$  of the material is assumed to be the minimum density, particle size  $d$  is assumed to be  $d_{50}$ , and  $k$  is assumed to be 1.4 (Beverloo et al. 1961).

$$W = 1.03 \rho_f \sqrt{g}(L - kd)(W_0 - kd)^{1.5} \quad (4.5)$$

where  $W$  is mass flow rate,  $\rho_f$  is flowing density,  $g$  is gravitational acceleration,  $L$  is slot length,  $k$  is Beverloo shape coefficient,  $d$  is grain diameter, and  $W_0$  is slot width.

Table 4-10 Comparison between experiments and modified Beverloo's equation (Mayers and Sellers, 1978)

No	Sand Group	Experiment (g/s)	Modified Beverloo (g/s)	Difference (%)
1	U-I	21.74	49.68	129
2	U-I	26.88	58.86	119
3	U-I	27.20	68.08	150
4	U-I	79.03	209.80	165
5	U-I	83.00	223.98	170
6	U-I	159.17	413.28	160
7	U-I	161.94	431.36	166
8	U-II	160.75	424.62	164
9	U-II	234.53	615.99	163
10	U-II	318.62	832.34	161
11	U-II	412.57	1069.36	159
12	U-II	511.21	1325.40	159
13	U-II	522.4	1325.40	154
14	S-I	N/A	48.33	N/A
15	S-I	64.25	172.24	168
16	S-I	65.60	172.24	163
17	S-I	101.28	251.11	148
18	S-I	127.62	339.30	166

19	S-I	132.23	339.30	157
20	S-I	173.28	435.93	152
21	S-I	212.25	540.30	155
22	S-I	214.03	540.30	152
23	S-I	265.96	651.89	145
24	S-I	310.86	770.25	148
25	S-I	421.24	1025.87	144
26	S-I	543.63	1304.80	140
27	S-I	683.09	1605.24	135
28	S-II	261.33	724.81	177
29	S-II	269.43	724.81	169
30	S-II	321.83	882.95	174
31	S-II	325.00	882.95	172
32	S-II	333.96	882.95	164
33	S-II	360.07	975.20	171
34	S-II	384.53	1032.00	168
35	S-II	448.71	1208.69	169
36	S-II	464.63	1249.20	169
37	S-II	519.11	1394.45	169
38	S-III	N/A	457.52	N/A
39	S-III	176.8	457.52	159

40	S-III	208.98	534.97	156
41	S-III	251.77	649.97	158
42	S-III	263.77	649.97	146
43	S-III	302.74	781.19	158
44	S-III	350.85	901.26	157
45	S-III	422.07	1076.67	155
46	S-III	429.4	1076.67	151
47	S-III	463.83	1178.52	154
48	S-III	480.06	1241.09	159
49	S-III	568.55	1435.15	152
50	S-III	591.53	1479.53	150
51	S-III	587.56	1479.53	152
52	S-III	658.32	1638.38	149

Table 4-10 shows that the Beverloo's equation overestimates the discharge rate with an average error of about 157%. Comparison between experiments and Beerloo's equation have been shown in Figures 4-25 to 4-29. The difference between the experimental results and the modified Beverloo's amounts can be attributed to the following reasons:

- 1- The shape factor or sphericity of the grains has not been considered in this equation.
- 2- The density of the material in Beverloo's equation has been substituted by minimum density which is believed to be higher than actual density of the material resulting in higher flow rates. There is no standard approach to determine the density of the material when it is flowing.
- 3- The modified Beverloo's equation is developed for uniformly size particles whereas in the experiments the particles vary within a narrow range for uniform PSD and  $d_{50}$  is

assumed to be the representative or characteristic particle size which may not be correct.

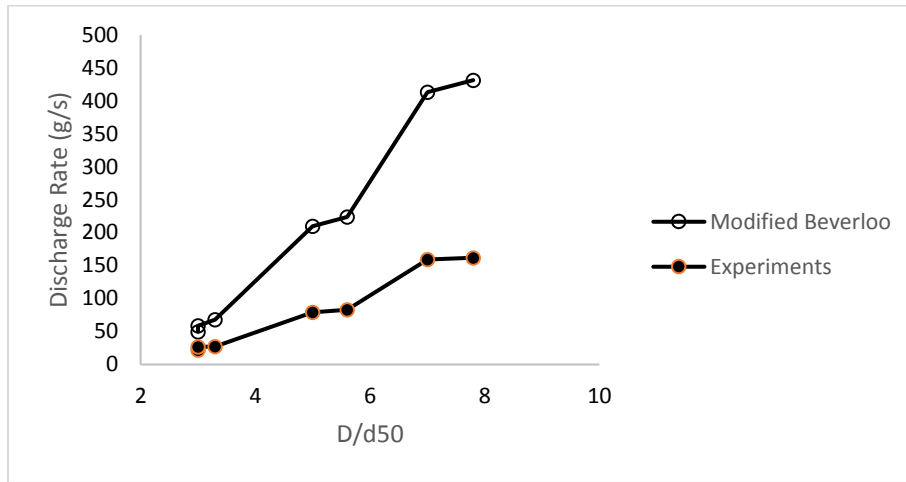


Figure 4-25 Comparison between experiments and modified Beverloo's correlation in

(U-I)

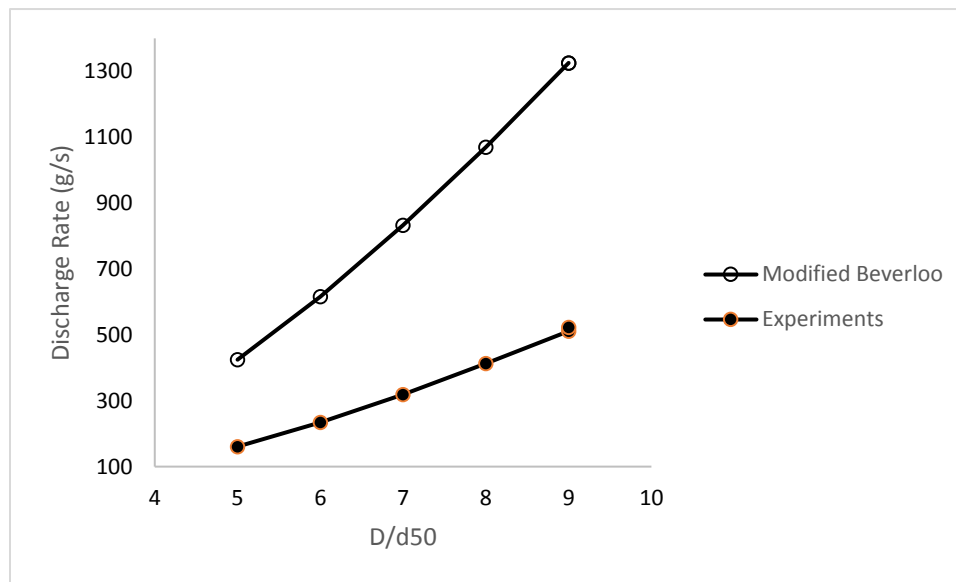


Figure 4-26 Comparison between experiments and modified Beverloo's correlation in (U-

II)

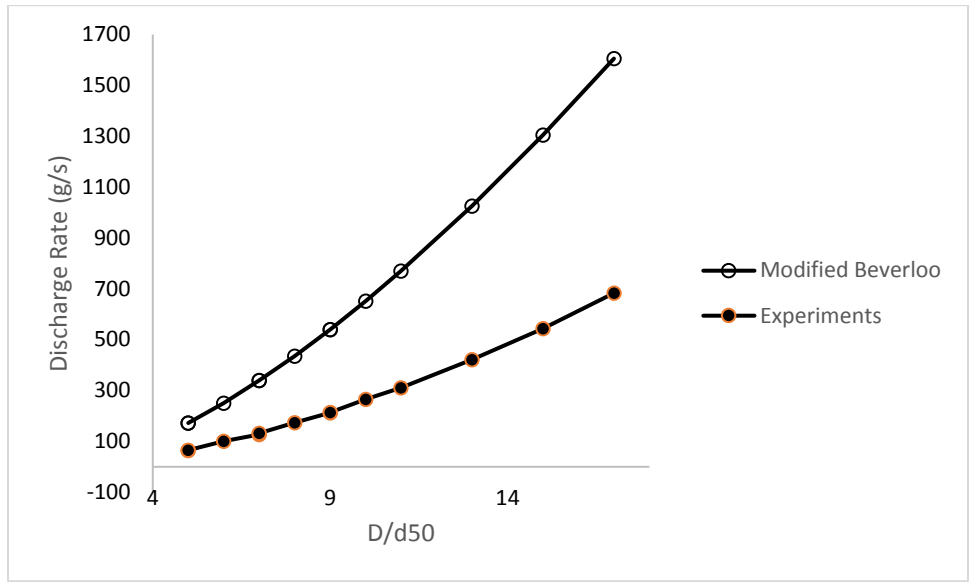


Figure 4-27 Comparison between experiments and modified Beverloo's correlation in (S-I)

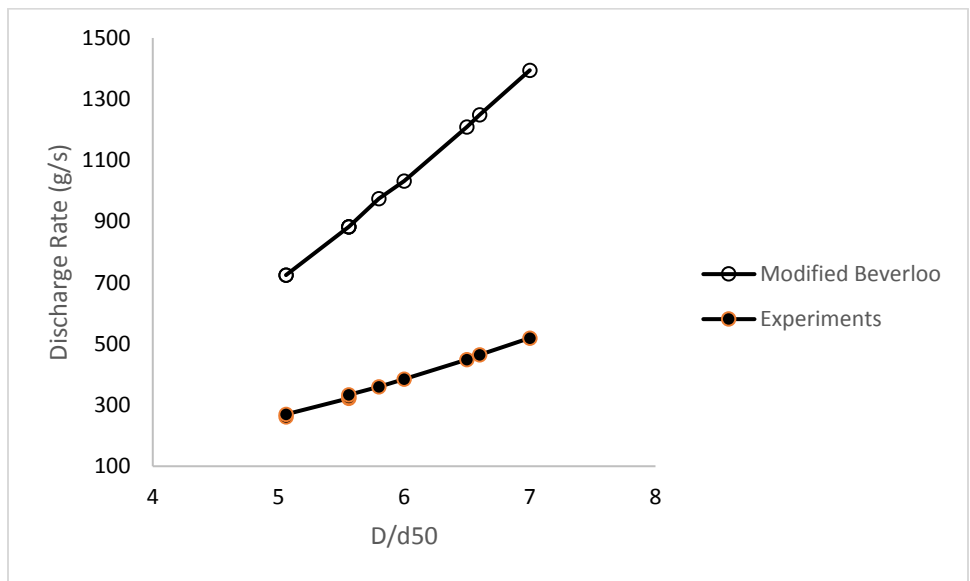


Figure 4-28 Comparison between experiments and modified Beverloo's correlation in (S-II)

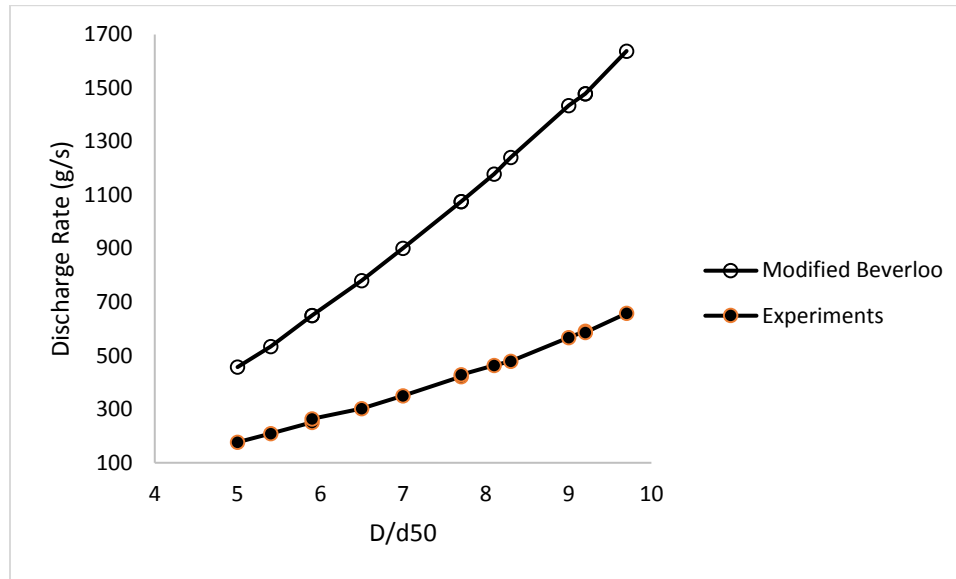


Figure 4-29 Comparison between experiments and modified Beverloo's correlation in (S-III)

#### 4.7 Determination of the Characteristic Particle Size

It is a hypothesis in this research that for non-uniform size material, the coarser particles dominate the formation of free fall arch which controls the discharge rate. Although  $d_{50}$  is commonly used as the characteristic size, it may not be correct.

As discussed in Section 4.6.2, it is seen that comparing the tests using uniform size (narrow range of particle size) and uniformly distributed size particles (wider range of particle size) with the same  $d_{50}$ , the uniformly distributed sand has a higher discharge rate than uniform sand. In these experiments and also in the literature, it has been shown that fine grain soil has a higher discharge rate than coarse grain soil. Contrary to the present hypothesis, it is seen that finer particles dominate the granular flow rate. The increase in discharge rate is about 10% in comparison with uniform-size sand. To investigate the effect of density,

Table 4-11 shows the increase of about 12% in (S-III) bulk density compared with the same for (U-II), although they have the same  $d_{50}=2.6$  mm. However, the bulk densities of (S-I) and (U-I) with the same  $d_{50}=1.4$  mm are almost equal. Additional experimental observations are necessary to investigate the density effect.

Table 4-11 Bulk density and porosity of all sand groups

Group	Size Range (mm)	Description	Bulk Density (g/cm <sup>3</sup> )	Porosity
U-I	1.19-1.68	Uniform	1.65	0.38
U-II	2.38-2.83	Uniform	1.64	0.38
S-I	0.5-2.38	Fine	1.64	0.38
S-II	2.38-4.75	Coarse	1.69	0.36
S-III	0.5-4.75	Full	1.84	0.31

As discussed in Section 4.6.5, the modified Beverloo's equation overestimates the discharge rate by about 150% on average, indicating the dominant particle size should be larger than  $d_{50}$ . To obtain lower rates, larger particle sizes should be used in the equation. Although this is in agreement with the present hypothesis, it does not agree with the experimental results. Also, by back calculating the characteristic particle size based on the modified Beverloo's equation, the size that gives the observed flow rate is larger than the maximum particle size in the distribution for all cases which is physically not acceptable. It is believed that other than particle size, the particle shape, and material density should be considered to give a more reasonable characteristic size. At this point, the results cannot be used to determine the characteristic particle size.

Table 4-12 Equivalent particle size based on modified Beverloo to provide the same results as experiments

No	Sand Group	Size Range	Range Description	$d_{50}$ (mm)	(D) Slot Opening (mm)	R=D/ $d_{50}$	Experiment (g/s)	Modified Beverloo based on $d_{50}$ (g/s)	Equivalent d (mm)	Equivalent d
1	U-I	1.19-1.68	uniform	1.4	4.3	3	21.74	49.68	2.0	1.41 $d_{50}$
2	U-I	1.19-1.68	uniform	1.4	4.8	3	26.88	70.45	2.2	1.40 $d_{50}$
3	U-I	1.19-1.68	uniform	1.4	4.8	3.3	27.20	68.08	2.2	1.55 $d_{50}$
4	U-I	1.19-1.68	uniform	1.4	8	5	79.03	227.58	3.4	2.09 $d_{50}$
5	U-I	1.19-1.68	uniform	1.4	8	5.6	83.00	223.98	3.3	2.28 $d_{50}$
6	U-I	1.19-1.68	uniform	1.4	11.2	7	159.17	435.93	4.3	2.67 $d_{50}$

7	U-I	1.19-1.68	uniform	1.4	11.2	7.8	161.94	431.36	4.2	2.94 d <sub>50</sub>
8	U-II	2.38-2.83	Uniform	2.6	13.03	5	160.75	424.62	5.4	2.08 d <sub>50</sub>
9	U-II	2.38-2.83	uniform	2.6	15.6	6	234.53	615.99	6.1	2.36 d <sub>50</sub>
10	U-II	2.38-2.83	uniform	2.6	18.2	7	318.62	832.34	6.9	2.64 d <sub>50</sub>
11	U-II	2.38-2.83	uniform	2.6	20.8	8	412.57	1069.36	7.6	2.91 d <sub>50</sub>
12	U-II	2.38-2.83	uniform	2.6	23.4	9	511.21	1325.40	8.3	3.18 d <sub>50</sub>
13	U-II	2.38-2.83	uniform	2.6	23.4	9	522.4	1325.40	8.2	3.14 d <sub>50</sub>
14	S-I	0.5-2.38	Fine	1.4	4.2	3	Jammed	48.33	N/A	N/A
15	S-I	0.5-2.38	Fine	1.4	7	5	64.25	172.24	2.9	2.10 d <sub>50</sub>
16	S-I	0.5-2.38	Fine	1.4	7	5	65.60	172.24	2.9	2.09 d <sub>50</sub>
17	S-I	0.5-2.38	Fine	1.4	8.4	6	101.28	251.11	3.3	2.33 d <sub>50</sub>
18	S-I	0.5-2.38	Fine	1.4	9.8	7	127.62	339.30	3.8	2.71 d <sub>50</sub>
19	S-I	0.5-2.38	Fine	1.4	9.8	7	132.23	339.30	3.7	2.66 d <sub>50</sub>
20	S-I	0.5-2.38	Fine	1.4	11.2	8	173.28	435.93	4.1	2.92 d <sub>50</sub>
21	S-I	0.5-2.38	Fine	1.4	12.6	9	212.25	540.30	4.5	3.23 d <sub>50</sub>
22	S-I	0.5-2.38	Fine	1.4	12.6	9	214.03	540.30	4.5	3.21 d <sub>50</sub>
23	S-I	0.5-2.38	Fine	1.4	14	10	265.96	651.89	4.8	3.44 d <sub>50</sub>
24	S-I	0.5-2.38	Fine	1.4	15.4	11	310.86	770.25	5.2	3.73 d <sub>50</sub>
25	S-I	0.5-2.38	Fine	1.4	18.2	13	421.24	1025.87	5.9	4.22 d <sub>50</sub>
26	S-I	0.5-2.38	Fine	1.4	21	15	543.63	1304.80	6.6	4.69 d <sub>50</sub>
27	S-I	0.5-2.38	Fine	1.4	23.8	17	683.09	1605.24	7.2	5.11 d <sub>50</sub>

28	S-II	2.38-4.75	Coarse	3.6	18.2	5.06	261.33	724.81	7.6	2.11 d <sub>50</sub>
29	S-II	2.38-4.75	Coarse	3.6	18.2	5.06	269.43	724.81	7.5	2.09 d <sub>50</sub>
30	S-II	2.38-4.75	Coarse	3.6	20	5.56	321.83	882.95	8.1	2.25 d <sub>50</sub>
31	S-II	2.38-4.75	Coarse	3.6	20	5.56	325.00	882.95	8.1	2.24 d <sub>50</sub>
32	S-II	2.38-4.75	Coarse	3.6	20	5.56	333.96	882.95	8.0	2.22 d <sub>50</sub>
33	S-II	2.38-4.75	Coarse	3.6	21	5.8	360.07	975.20	8.4	2.32 d <sub>50</sub>
34	S-II	2.38-4.75	Coarse	3.6	21.6	6	384.53	1032.00	8.5	2.36 d <sub>50</sub>
35	S-II	2.38-4.75	Coarse	3.6	23.4	6.5	448.71	1208.69	9.0	2.50 d <sub>50</sub>
36	S-II	2.38-4.75	Coarse	3.6	23.8	6.6	464.63	1249.20	9.1	2.53 d <sub>50</sub>
37	S-II	2.38-4.75	Coarse	3.6	25.2	7	519.11	1394.45	9.5	2.64 d <sub>50</sub>
38	S-III	0.5-4.75	Full	2.6	13	5	Jammed	457.52	N/A	N/A
39	S-III	0.5-4.75	Full	2.6	13	5	176.8	457.52	5.4	2.06 d <sub>50</sub>
40	S-III	0.5-4.75	Full	2.6	14	5.4	208.98	534.97	5.6	2.16 d <sub>50</sub>
41	S-III	0.5-4.75	Full	2.6	15.4	5.9	251.77	649.97	6.0	2.32 d <sub>50</sub>
42	S-III	0.5-4.75	Full	2.6	15.4	5.9	263.77	649.97	5.9	2.27 d <sub>50</sub>
43	S-III	0.5-4.75	Full	2.6	16.9	6.5	302.74	781.19	6.5	2.48 d <sub>50</sub>
44	S-III	0.5-4.75	Full	2.6	18.2	7	350.85	901.26	6.8	2.62 d <sub>50</sub>
45	S-III	0.5-4.75	Full	2.6	20	7.7	422.07	1076.67	7.3	2.80 d <sub>50</sub>
46	S-III	0.5-4.75	Full	2.6	20	7.7	429.4	1076.67	7.2	2.78 d <sub>50</sub>
47	S-III	0.5-4.75	Full	2.6	21	8.1	463.83	1178.52	7.5	2.90 d <sub>50</sub>
48	S-III	0.5-4.75	Full	2.6	21.6	8.3	480.06	1241.09	7.8	2.98 d <sub>50</sub>

49	S-III	0.5-4.75	Full	2.6	23.4	9	568.55	1435.15	8.2	3.13 d <sub>50</sub>
50	S-III	0.5-4.75	Full	2.6	23.8	9.2	591.53	1479.53	8.2	3.16 d <sub>50</sub>
51	S-III	0.5-4.75	Full	2.6	23.8	9.2	587.56	1479.53	8.2	3.17 d <sub>50</sub>
52	S-III	0.5-4.75	Full	2.6	25.2	9.7	658.32	1638.38	8.5	3.28 d <sub>50</sub>

As can be seen in Table 4-12, with an increase in the slot size, the equivalent particle size increases although all equivalent particle sizes are out of particle size distribution range.

## 5 Conclusion and Recommendations

### 5.1 Summary of findings

1. The experiments show that the granular discharge rate is independent of the height of the granular material, hence, the overburden stress. The flow rates are almost constant for different heights. This is an important characteristic of granular flow which is unique in comparison with fluid flow. This characteristic is found not only in uniformly sized particles but also for uniformly distributed size particles. It seems that although discharge rate is almost constant in all the experiments, more fluctuates is observed for tests with a wider range of particle size than uniform size particles. This may be due to the segregation of materials during the discharging process.
2. As expected, the granular flow rate increases in all cases with an increase in the ratio of  $D/d_{50}$ . The increase is more linear in coarser particles rather than finer particles for both uniform size and uniformly distributed size tests. Also, the discharge rate is inversely proportional to the particle size but directly proportional to the slot size.
3. To determine the dominant size that has more effects on granular flow rate, uniformly distributed size material was tested and compared with uniform size material with similar  $d_{50}$ . For similar slot size and similar  $d_{50}$ , the uniformly distributed material has higher flow rates suggesting that finer particles have more effect than coarser particles. The difference in flow rates in most cases is around 10%. It can be concluded that, consistent with the literature (Section 2.1.4), finer particles fill the voids between coarser particles causing a decrease in porosity, increase in density and eventually increase in flow rate. This can be verified with comparing two densities of (S-III) and (U-II) with  $d_{50}=2.6$  mm but with observing the same density for (S-I) and (U-I) with  $d_{50}=1.4$  mm, no evident conclusion can be reached, and more investigations seem to be necessary.
4. When using Tang's Equation (2.8) to calculate the flow rate, there is no obvious trend of results when comparing with the experiments. In developing the analytical solution to calculate granular flow rate, Tang assumes that the stagnant zone angle is equal to the angle of repose. The stagnant zone angle plays a vital role in the discharge rate. The stagnant zone angle was observed to be larger than the angle of repose in the

experiments as more particles move down the face of the stagnant zone in the final stage of flow. Tang's equation, unlike other equations and findings, shows that the flow rate is directly proportionate to the particle size. This is contrary to the conclusions of this experimental study and other correlations such as modified Beverloo (Mayers and Sellers, 1978).

5. The modified Beverloo's equation, using  $d_{50}$  as the characteristic particle size, overestimates the flow rates by about 150%. In this calculation, the minimum flow density is used, and the effect of the particle shape is ignored. Moreover, the flow rate decreases with increase in particle size. However, to match the observed flow rate, the back-calculated characteristic particle size is outside the physical range of particle sizes in the material which seems physically unacceptable.

## **5.2 Limitations**

The shape factor or particles' shape parameter has not been addressed in this study. Also, the particle velocity at the orifice and flowing density have not been measured due to limitations and available facilities in the lab.

## **5.3 Recommendations for future work**

The following are recommended for further research in this area:

1. Investigation of the effect of sphericity and particle shape: Tests should be conducted using spherical particles such as glass beads to eliminate or reduce particles angularity and friction.
2. Develop an analytical equation for 3D conditions, as a 3D model is more realistic for some cases.
3. Improve Beverloo's equation for a more accurate calculation of flow rate.
4. Perform test with different particle size distributions besides uniform size and uniform size distribution.
5. Investigate the effect of density on the granular flow by examining and comparing grains with different densities but other characteristics identical.
6. Develop a numerical model to provide a deeper understanding of the flow process.

## References

- Ahn, Hojin, Zafer Başaranoğlu, Mustafa Yılmaz, Abdulcelil Buğutekin, and M. Zafer Gül. 2008. "Experimental Investigation of Granular Flow through an Orifice." *Powder Technology* 186 (1): 65-71. doi://doi.org/10.1016/j.powtec.2007.11.001.  
<http://www.sciencedirect.com/science/article/pii/S0032591007005591>.
- Al-Din, N. and D. J. Gunn. 1984. "The Flow of Non-Cohesive Solids through Orifices." *Chemical Engineering Science* 39 (1): 121-127. doi://doi.org/10.1016/0009-2509(84)80137-2. <http://www.sciencedirect.com/science/article/pii/0009250984801372>.
- Anand, Anshu, Jennifer S. Curtis, Carl R. Wassgren, Bruno C. Hancock, and William R. Ketterhagen. 2008. "Predicting Discharge Dynamics from a Rectangular Hopper using the Discrete Element Method (DEM)." *Chemical Engineering Science* 63 (24): 5821-5830. doi://doi.org/10.1016/j.ces.2008.08.015.  
<http://www.sciencedirect.com/science/article/pii/S0009250908004429>.
- Barletta, Diego, Giorgio Donsì, Giovanna Ferrari, and Massimo Poletto. 2003. "On the Role and the Origin of the Gas Pressure Gradient in the Discharge of Fine Solids from Hoppers." *Chemical Engineering Science* 58 (23): 5269-5278.
- Beverloo, W. A., H. A. Leniger, and de Velde van. 1961. "The Flow of Granular Solids through Orifices." *Chemical Engineering Science* 15 (3): 260-269.
- BROWN, R. L. 1961. "Minimum Energy Theorem for Flow of Dry Granules through Apertures." *Nature* 191 (4787): 458-461.
- Brown, R. L. and J. C. Richards. 1965. "Kinematics of the Flow of Dry Powders and Bulk Solids." *Rheologica Acta* 4 (3): 153-165.
- Cleary, Paul W. and Mark L. Sawley. 2002. "DEM Modelling of Industrial Granular Flows: 3D Case Studies and the Effect of Particle Shape on Hopper Discharge." *Applied Mathematical Modelling* 26: 89-111. doi:10.1016/S0307-904X(01)00050-6.  
<http://login.ezproxy.library.ualberta.ca/login?url=http://search.ebscohost.com/login.ezproxy.library.ualberta.ca/login.aspx?direct=true&db=edselp&AN=S0307904X01000506&site=eds-live&scope=site>.
- Davidson, J. F., and Nedderman, R. M. 1973. "The hour-glass theory of hopper flow." *Trans. Inst. Chem. Eng*, 51, 29-35.
- Dias, Ricardo P., José A. Teixeira, Manuel G. Mota, and Alexander I. Yelshin. 2004. "Particulate Binary Mixtures: Dependence of Packing Porosity on Particle Size Ratio." *Industrial & Engineering Chemistry Research* 43 (24): 7912-7919. doi:10.1021/ie040048b.  
<https://doi.org/10.1021/ie040048b>.

- Donsì, G., G. Ferrari, and M. Poletto. 1997. "Distribution of Gas Pressure Inside a Hopper Discharging Fine Powders." *Chemical Engineering Science* 52 (23): 4291-4302.
- Drescher, A., A. J. Waters, and C. A. Rhoades. 1995a. "Arching in Hoppers: I. Arching Theories and Bulk Material Flow Properties." *Powder Technology* 84 (2): 165-176.
- Drescher, A., A. J. Waters, and C. A. Rhoades. 1995b. "Arching in Hoppers: II. Arching Theories and Critical Outlet Size." *Powder Technology* 84 (2): 177-183.
- Franklin, F. C. and L. N. Johanson. 1955. "Flow of Granular Material through a Circular Orifice." *Chemical Engineering Science* 4 (3): 119-129. doi://doi.org/10.1016/0009-2509(55)80003-6. <http://www.sciencedirect.com/science/article/pii/0009250955800036>.
- Guo, Shuai and David Z. Zhu. 2017. "Soil and Groundwater Erosion Rates into a Sewer Pipe Crack." *Journal of Hydraulic Engineering* 143 (7): 1-5. doi:10.1061/(ASCE)HY.1943-7900.0001306. <http://login.ezproxy.library.ualberta.ca/login?url=http://search.ebscohost.com/login.ezproxy.library.ualberta.ca/login.aspx?direct=true&db=a9h&AN=122650936&site=ehost-live&scope=site>.
- Hermosilla, Rodolfo. 2012. "The Guatemala City Sinkhole Collapses." *Carbonates & Evaporites* 27 (2): 103-107. doi:10.1007/s13146-011-0074-1. <http://login.ezproxy.library.ualberta.ca/login?url=http://search.ebscohost.com/login.ezproxy.library.ualberta.ca/login.aspx?direct=true&db=a9h&AN=77873183&site=ehost-live&scope=site>.
- Hilton, J. E. and P. W. Cleary. 2011. "Granular Flow during Hopper Discharge." *Physical Review E* 84 (1): 011307.
- Janda, Alvaro, Iker Zuriguel, and Diego Maza. 2012. "Flow Rate of Particles through Apertures obtained from Self-Similar Density and Velocity Profiles." *Physical Review Letters* 108 (24): 248001.
- Khanam, Jasmina and Arunabha Nanda. 2005. "Flow of Granules through Cylindrical Hopper." *Powder Technology* 150 (1): 30-35. doi://doi.org/10.1016/j.powtec.2004.11.016. <http://www.sciencedirect.com/science/article/pii/S0032591004004826>.
- Lafond, Patrick G. 2014. "Particle Jamming during the Discharge of Fluid-Driven Granular Flow." 3617418, ProQuest Dissertations Publishing. <http://search.proquest.com/docview/1527095130>.
- Le Pennec, Thierry, Knut Jørgen Måløy, Alex Hansen, Madani Ammi, Daniel Bideau, and Xiaolun Wu. 1996. "Ticking Hour Glasses: Experimental Analysis of Intermittent Flow." *Physical Review E* 53 (3): 2257-2264.

- Li, Jintang, Paul A. Langston, Colin Webb, and Tom Dyakowski. 2004. "Flow of Sphero-Disc Particles in Rectangular Hoppers—a DEM and Experimental Comparison in 3D." *Chemical Engineering Science* 59 (24): 5917-5929. doi://doi.org/10.1016/j.ces.2004.07.022. <http://www.sciencedirect.com/login.ezproxy.library.ualberta.ca/science/article/pii/S0009250904004580>.
- Lin, P., S. Zhang, J. Qi, Y. M. Xing, and L. Yang. 2015. "Numerical Study of Free-Fall Arches in Hopper Flows." *Physica A: Statistical Mechanics and its Applications* 417: 29-40.
- Liu, Yu. 2014. "The Theoretical Calculation of the Flow Rate of Granular Matter from an Inclined Orifice." *Granular Matter* 16 (1): 133-139. doi:10.1007/s10035-013-0473-1. <https://doi-org.login.ezproxy.library.ualberta.ca/10.1007/s10035-013-0473-1>.
- Mamtani, K. 2011. "Effect of Particle Shape on Hopper Discharge Rate." MSc, University of Florida.
- Mankoc, C., A. Janda, R. Arévalo, J. M. Pastor, I. Zuriguel, A. Garcimartín, and D. Maza. 2007. "The Flow Rate of Granular Materials through an Orifice." *Granular Matter* 9 (6): 407-414.
- Mankoc, Cristian, Angel Garcimartín, Iker Zuriguel, Diego Maza, and Luis A. Pugnaloni. 2009. "Role of Vibrations in the Jamming and Unjamming of Grains Discharging from a Silo." *Physical Review E* 80 (1): 011309. doi:10.1103/PhysRevE.80.011309. <https://link-aps-org.login.ezproxy.library.ualberta.ca/doi/10.1103/PhysRevE.80.011309>.
- Meza-Diaz, B., B. Tremblay, and Q. Doan. 2003. "Mechanisms of Sand Production through Horizontal Well Slots in Primary Production." .
- Myers, M.E., Sellers, M., 1978. Rate of discharge from wedge-shaped hoppers. Project Report, Department of Chemical Engineering, University of Cambridge.
- Nedderman, R. M. 1992. *Statics and Kinematics of Granular Materials*. Cambridge, England: Cambridge University Press.
- Nedderman, R. M. and C. Laohakul. 1980. "The Thickness of the Shear Zone of Flowing Granular Materials." *Powder Technology* 25 (1): 91-100. doi://doi.org/10.1016/0032-5910(80)87014-8. <http://www.sciencedirect.com/science/article/pii/0032591080870148>.
- Rao, K. Kesava and Prabhu R. Nott. 2008. *An Introduction to Granular Flow*. Cambridge Series in Chemical Engineering. Cambridge ;New York: Cambridge University Press.
- Rubio-Largo, S., A. Janda, D. Maza, I. Zuriguel, and R. C Hidalgo. 2015. "Disentangling the Free-Fall Arch Paradox in Silo Discharge." *Physical Review Letters* 114 (23): 238002.
- Sheldon, Hannah G. and Douglas J. Durian. 2010. "Granular Discharge and Clogging for Tilted Hoppers." *Granular Matter* 12 (6): 579-585. doi:10.1007/s10035-010-0198-3. <http://login.ezproxy.library.ualberta.ca/login?url=http://search.ebscohost.com/login.ezproxy>.

[library.ualberta.ca/login.aspx?direct=true&db=a9h&AN=54633046&site=eds-live&scope=site](http://library.ualberta.ca/login.aspx?direct=true&db=a9h&AN=54633046&site=eds-live&scope=site).

- Sukumaran, B ( 1 ) and Ashmawy, A K ( 2 ). 2003. "Influence of Inherent Particle Characteristics on Hopper Flow Rate." *Powder Technology* 138 (1): 46-50.  
doi:10.1016/j.powtec.2003.08.039.  
<http://login.ezproxy.library.ualberta.ca/login?url=http://search.ebscohost.com/login.ezproxy.library.ualberta.ca/login.aspx?direct=true&db=edselc&AN=edselc.2-52.0-0344862100&site=eds-live&scope=site>.
- Tang, Y. 2017. "Mechanisms of Soil Erosion due to Defective Sewer Pipes." PhD Dissertation, University of Alberta.
- Tao, He, Baosheng Jin, Wenqi Zhong, Xiaofang Wang, Bing Ren, Yong Zhang, and Rui Xiao. 2010. "Discrete Element Method Modeling of Non-Spherical Granular Flow in Rectangular Hopper." *Chemical Engineering and Processing: Process Intensification* 49 (2): 151-158.  
doi://doi.org/10.1016/j.cep.2010.01.006.  
<http://www.sciencedirect.com/login.ezproxy.library.ualberta.ca/science/article/pii/S0255270110000073>.
- Terzaghi, K. 1943. "Theoretical Soil Mechanics." Chapman and Hall.
- Tian, Y., P. Lin, S. Zhang, C. L. Wang, J. F. Wan, and L. Yang. 2015. "Study on Free Fall Surfaces in Three-Dimensional Hopper Flows." *Advanced Powder Technology* 26 (4): 1191-1199.
- To, Kiwing, Pik-Yin Lai, and H. K. Pak. 2001. "Jamming of Granular Flow in a Two-Dimensional Hopper." *Physical Review Letters* 86 (1): 71-74.  
doi:10.1103/PhysRevLett.86.71. <https://link.aps.org/doi/10.1103/PhysRevLett.86.71>.
- Vivanco, Francisco, Sergio Rica, and Francisco Melo. 2012. "Dynamical Arching in a Two Dimensional Granular Flow." *Granular Matter* 14 (5): 563-576.
- Wu, Jintao, Jizhong Chen, and Yongrong Yang. 2008. "A Modified Kinematic Model for Particle Flow in Moving Beds." *Powder Technology* 181 (1): 74-82.  
doi://doi.org/10.1016/j.powtec.2007.06.014.  
<http://www.sciencedirect.com/login.ezproxy.library.ualberta.ca/science/article/pii/S0032591007002999>.
- Zuriguel, Iker, Angel Garcimartín, Diego Maza, Luis A. Pugnaloni, and J. M. Pastor. 2005a. "Jamming during the Discharge of Granular Matter from a Silo." *Physical Review E* 71 (5): 051303.
- Zuriguel, Iker, Angel Garcimartín, Diego Maza, Luis A. Pugnaloni, and J. M. Pastor. 2005b. "Jamming during the Discharge of Granular Matter from a Silo." *Physical Review E* 71 (5):

051303. doi:10.1103/PhysRevE.71.051303. <https://link-aps-org.login.ezproxy.library.ualberta.ca/doi/10.1103/PhysRevE.71.051303>.

Zuriguel, Iker, Luis A. Pugnaloni, Angel Garcimartín, and Diego Maza. 2003. "Jamming during the Discharge of Grains from a Silo Described as a Percolating Transition." *Physical Review E* 68 (3): 030301. doi:10.1103/PhysRevE.68.030301. <https://link.aps.org/doi/10.1103/PhysRevE.68.030301>.

## **Appendix A All Experimental Results in Graphs**

This appendix presents the granular flow rate and cumulative discharged mass versus time for all the experiments.

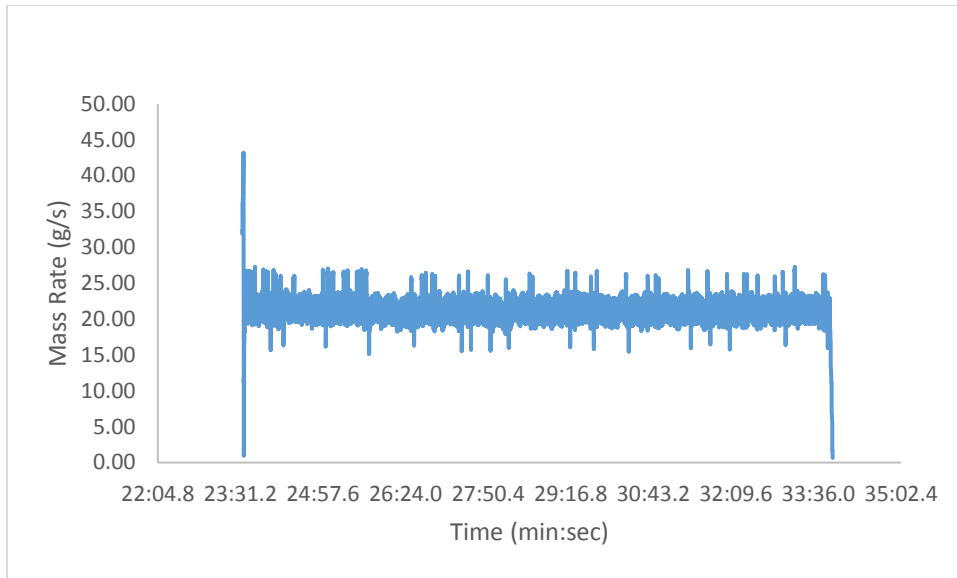


Figure A-1 a Experiment # 1 Granular flow rate vs. time

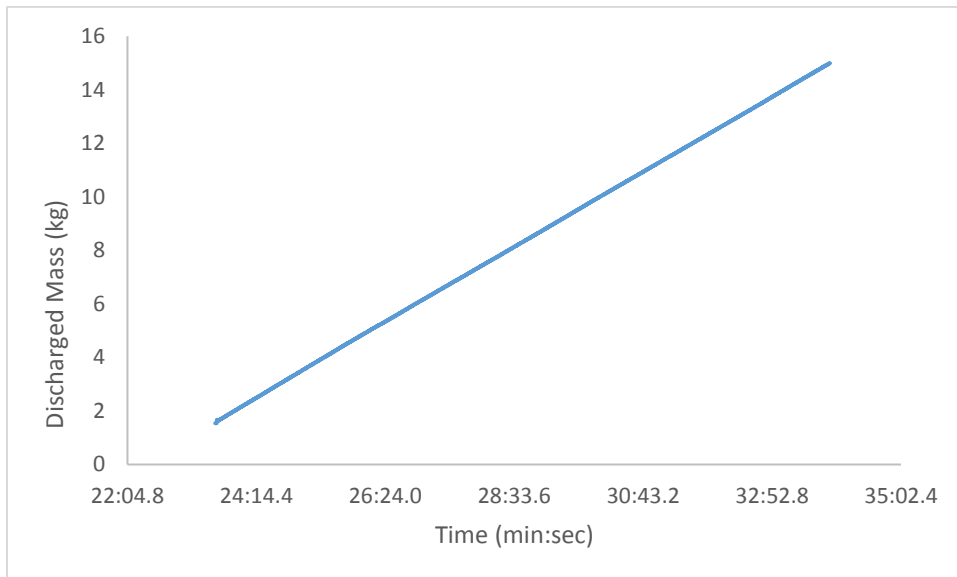


Figure A-2 b Experiment # 1 Cumulative discharge mass vs. time

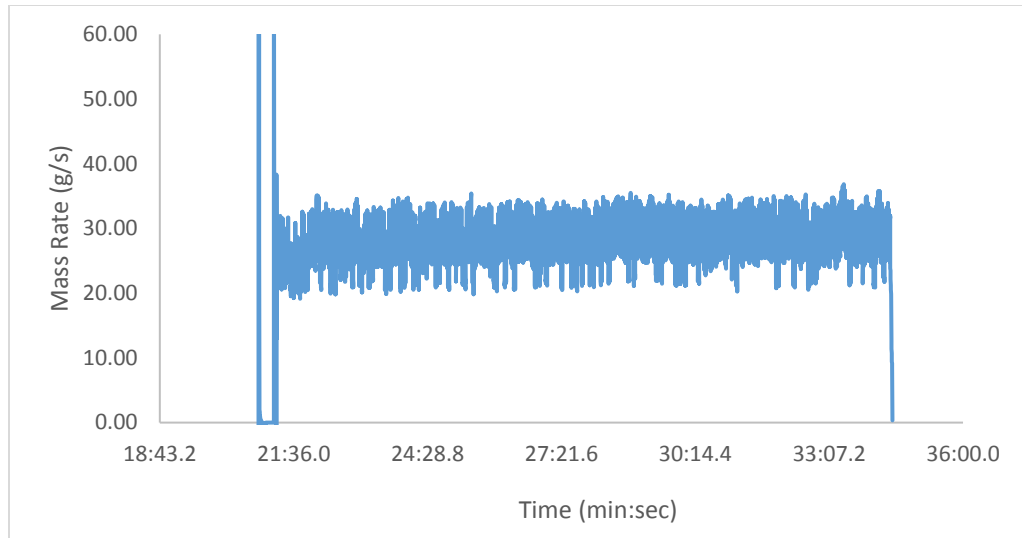


Figure A-2 a Experiment # 2 Granular flow rate vs. time

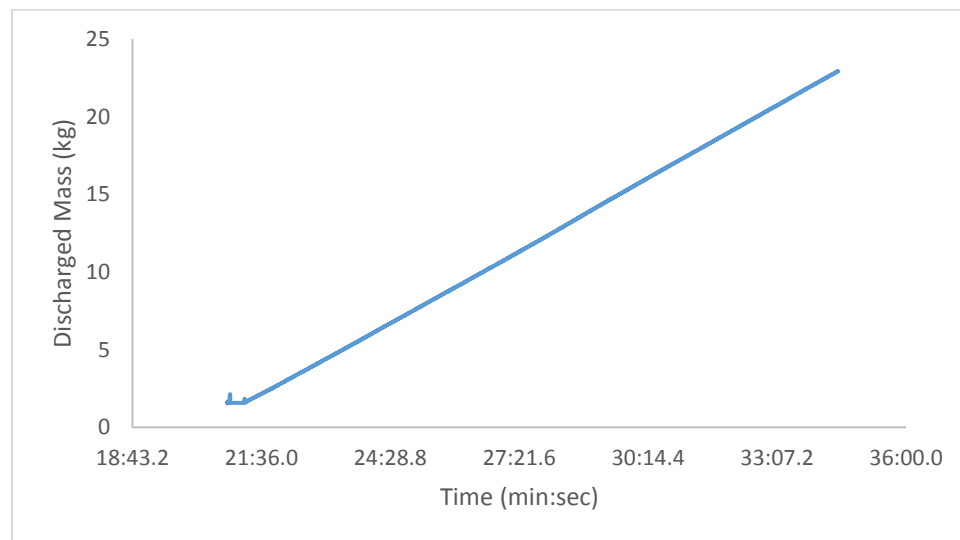


Figure A-2 b Experiment # 2 Cumulative discharge mass vs. time

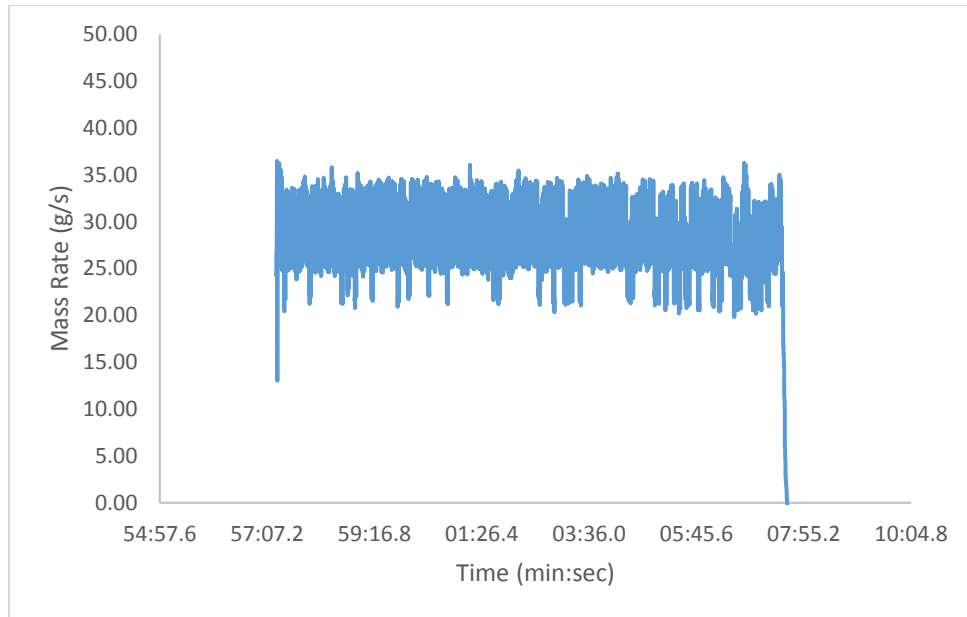


Figure A-3 a Experiment # 3 Granular flow rate vs. time

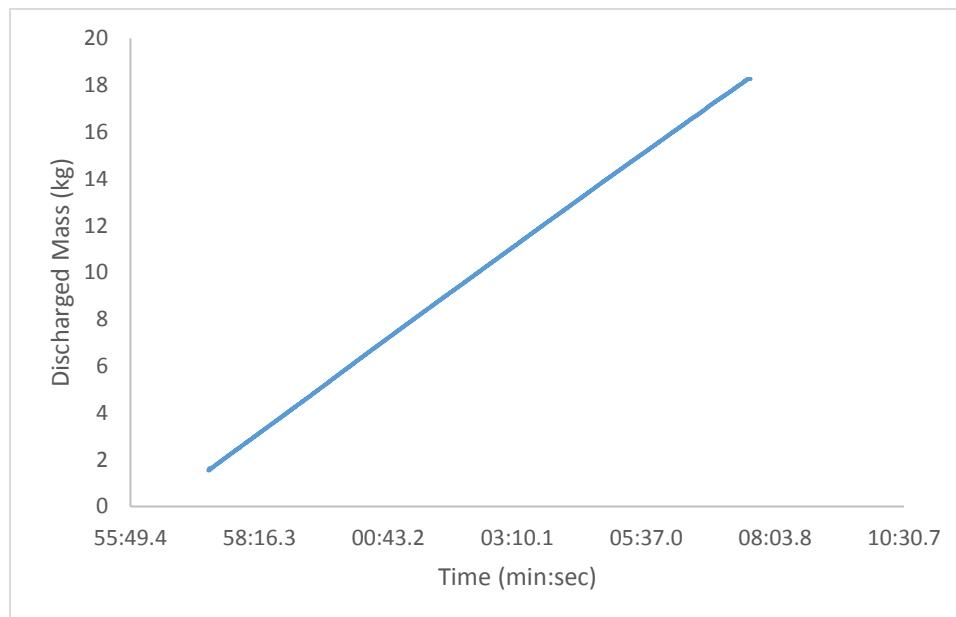


Figure A-3 b Experiment # 3 Cumulative discharge mass vs. time

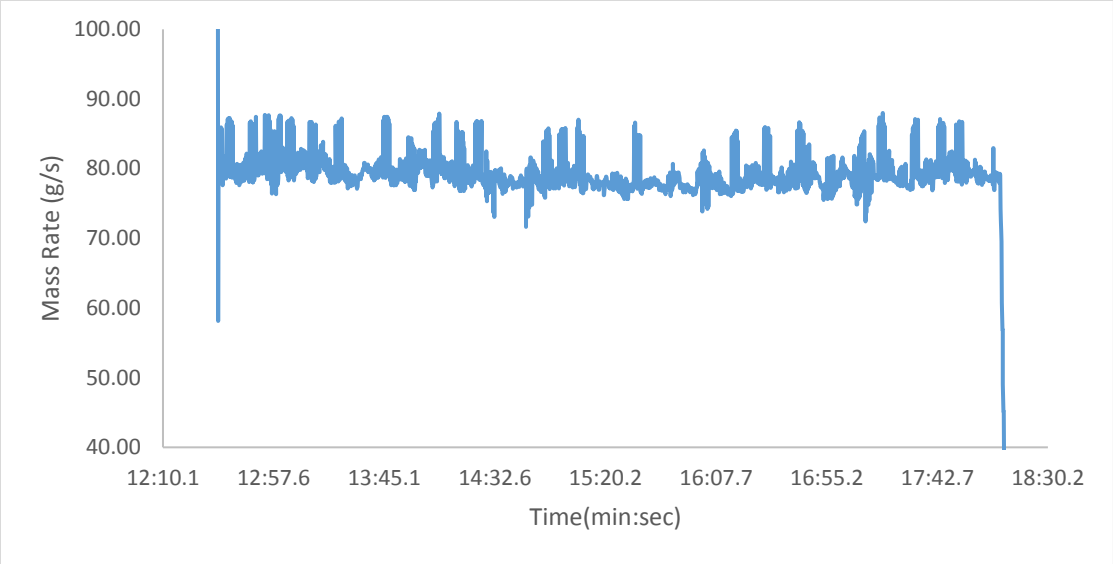


Figure A-4 a Experiment # 4 Granular flow rate vs. time

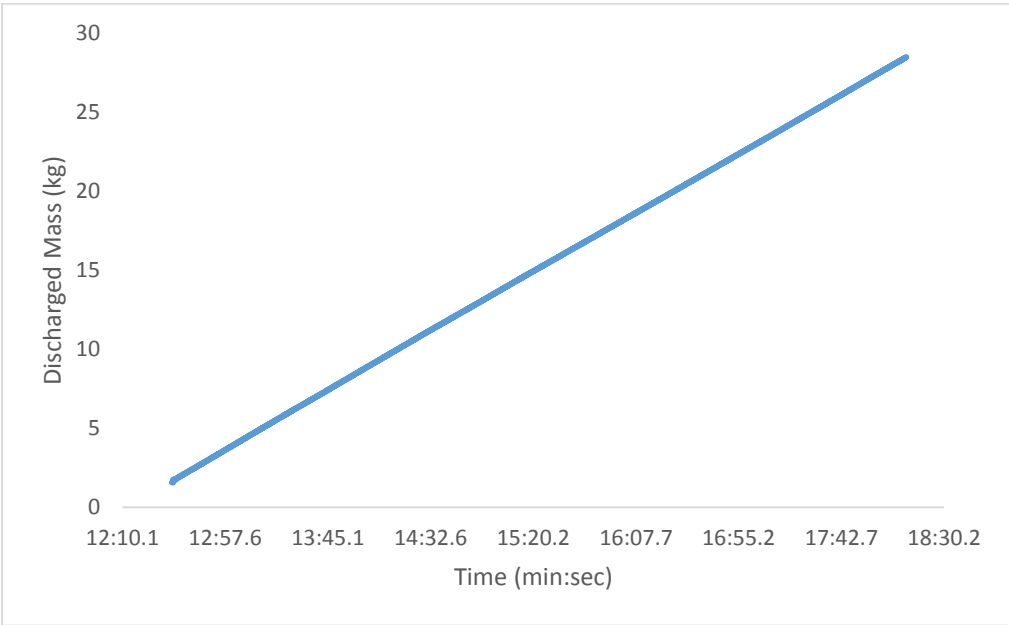


Figure A-4 b Experiment # 4 Cumulative discharge mass vs. time

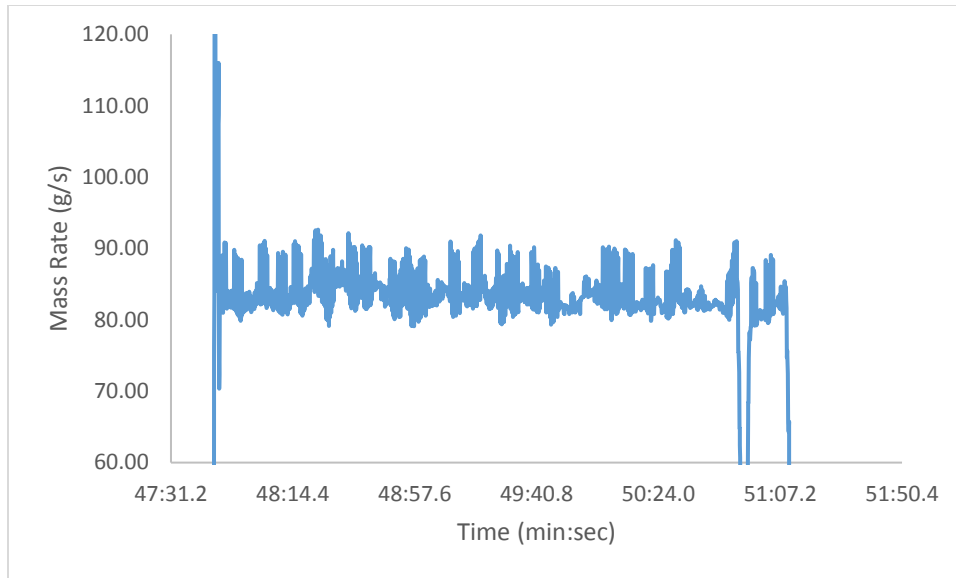


Figure A-5 a Experiment # 5 Granular flow rate vs. time

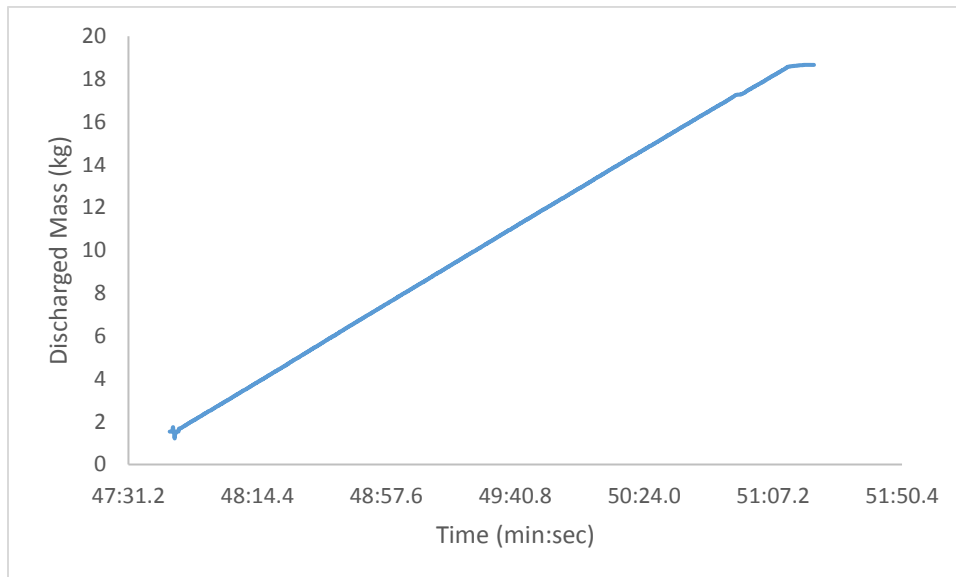


Figure A-5 b Experiment # 5 Cumulative discharge mass vs. time

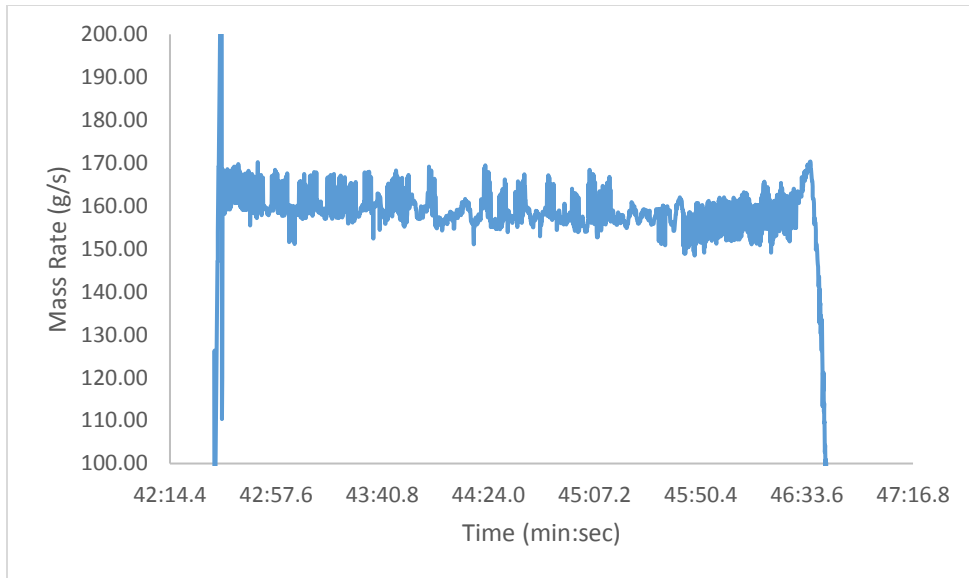


Figure A-6 a Experiment # 6 Granular flow rate vs. time

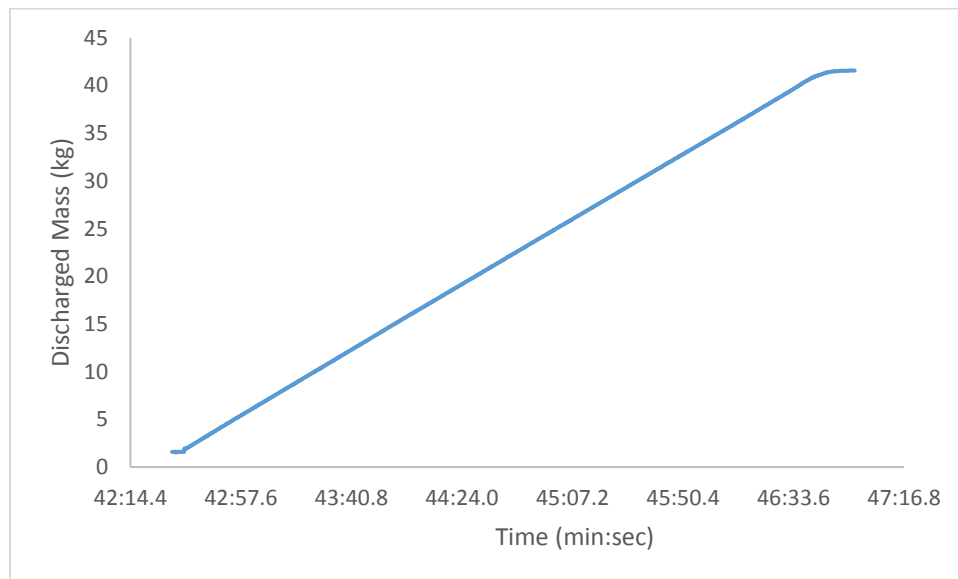


Figure A-6 b Experiment # 6 Cumulative discharge mass vs. time

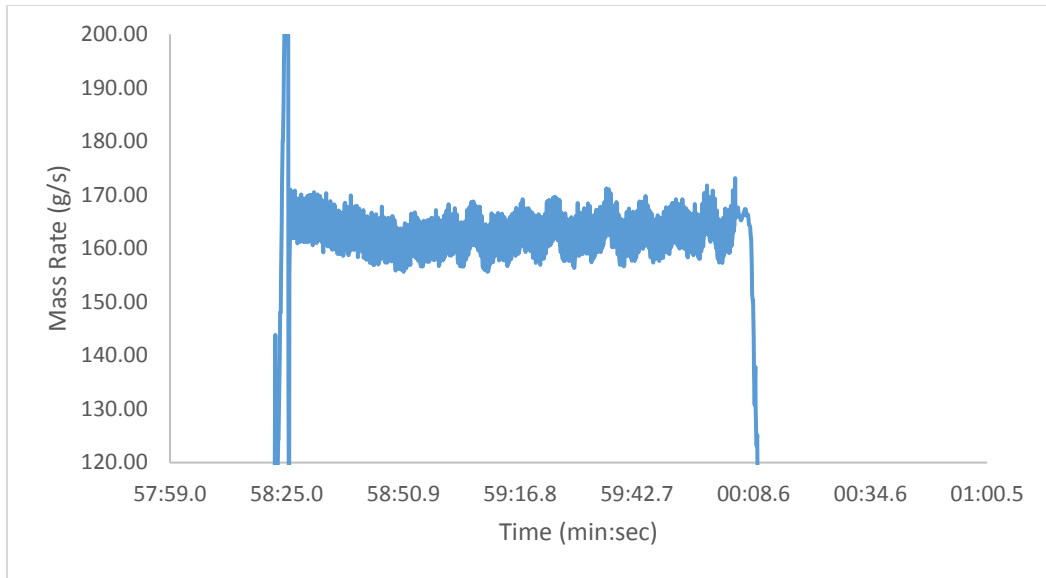


Figure A-7 a Experiment # 7 Granular flow rate vs. time

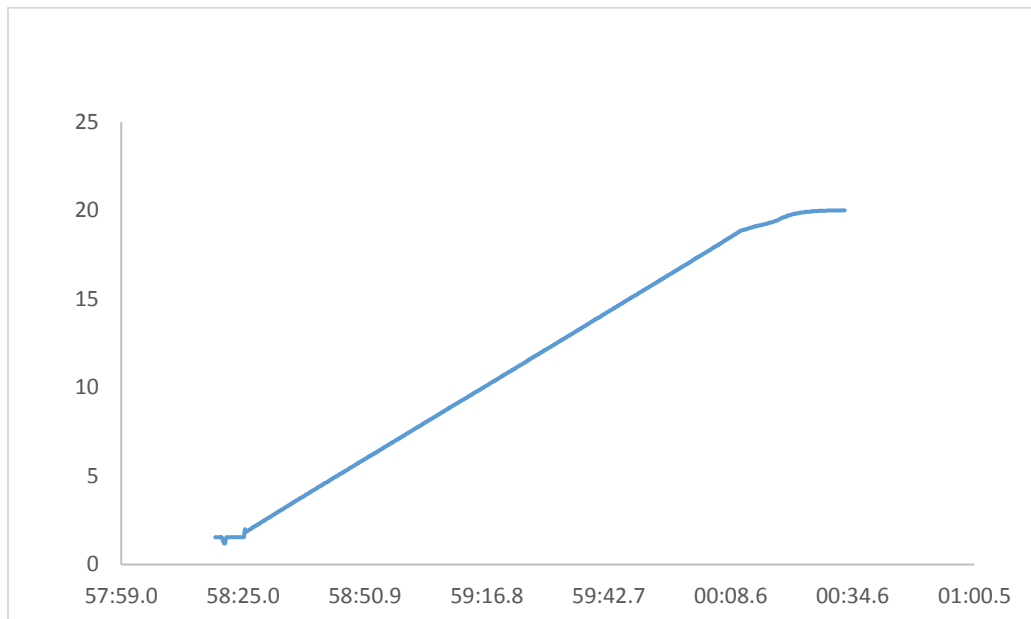


Figure A-7 b Experiment # 7 Cumulative discharge mass vs. time

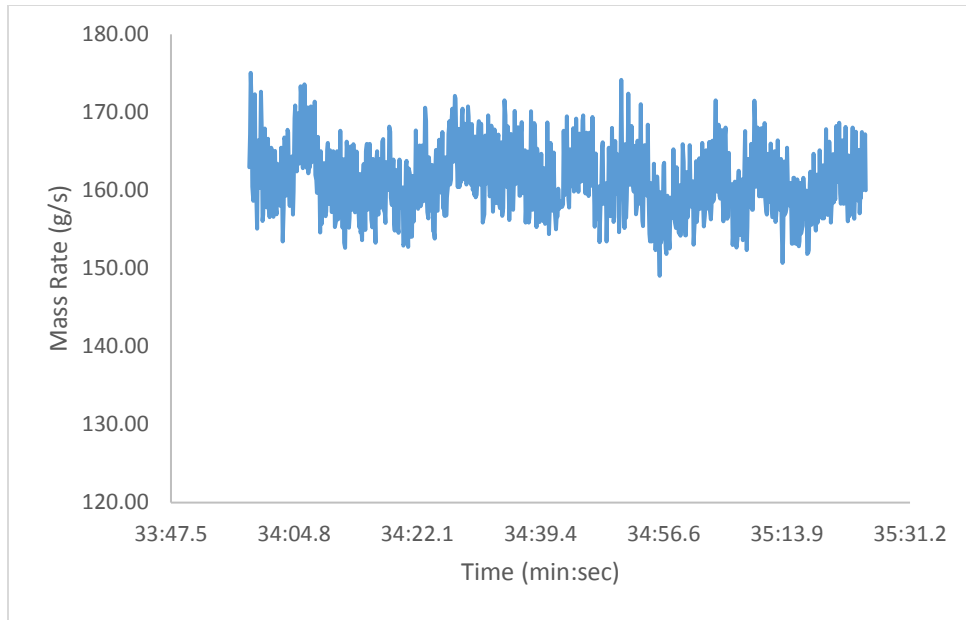


Figure A-8 a Experiment # 8 Granular flow rate vs. time

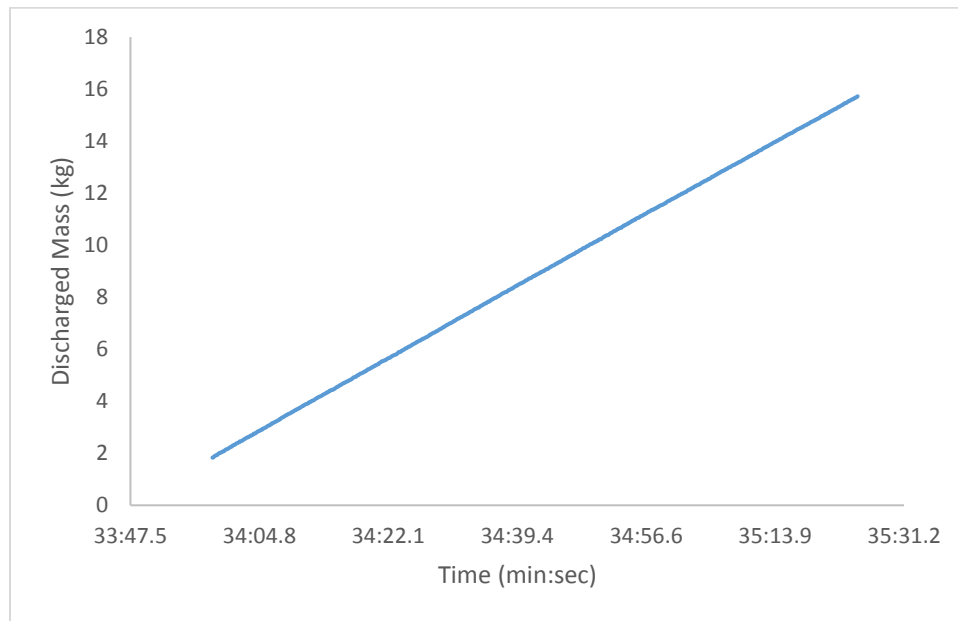


Figure A-8 b Experiment # 8 Cumulative discharge mass vs. time

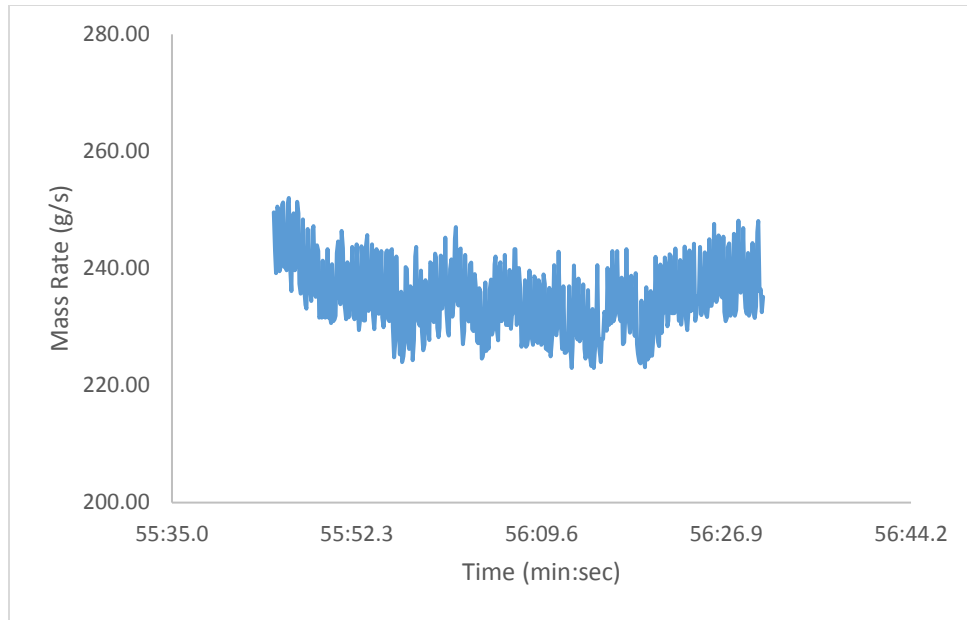


Figure A-9 a Experiment # 9 Granular flow rate vs. time

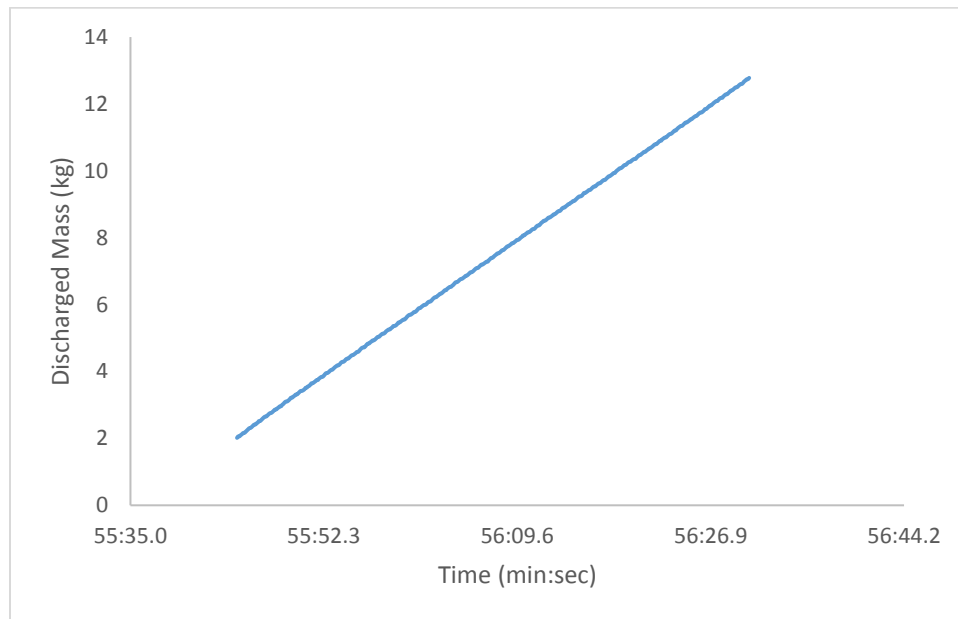


Figure A-9 b Experiment # 9 Cumulative discharge mass vs. time

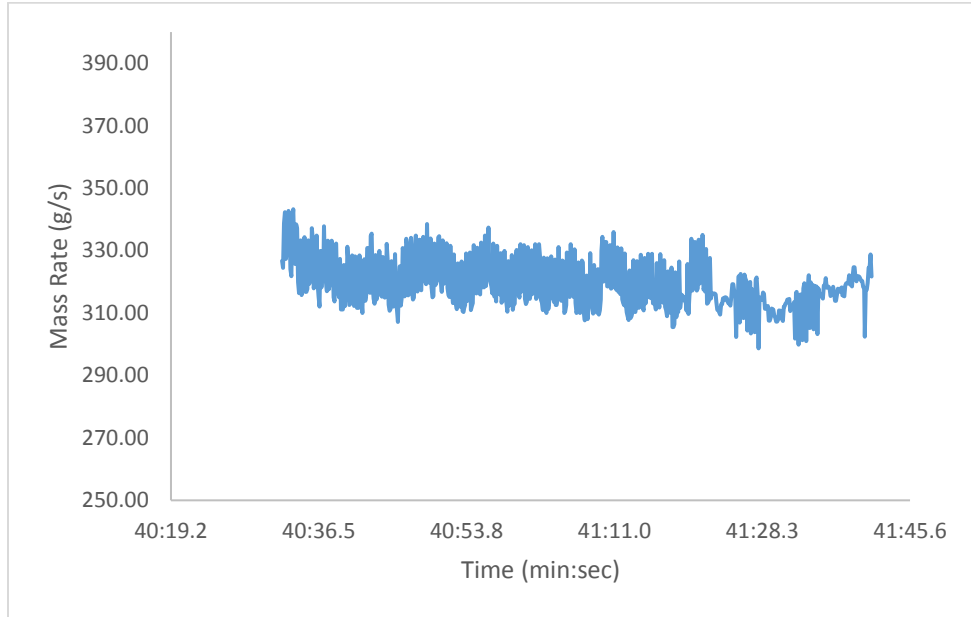


Figure A-10 a Experiment # 10 Granular flow rate vs. time

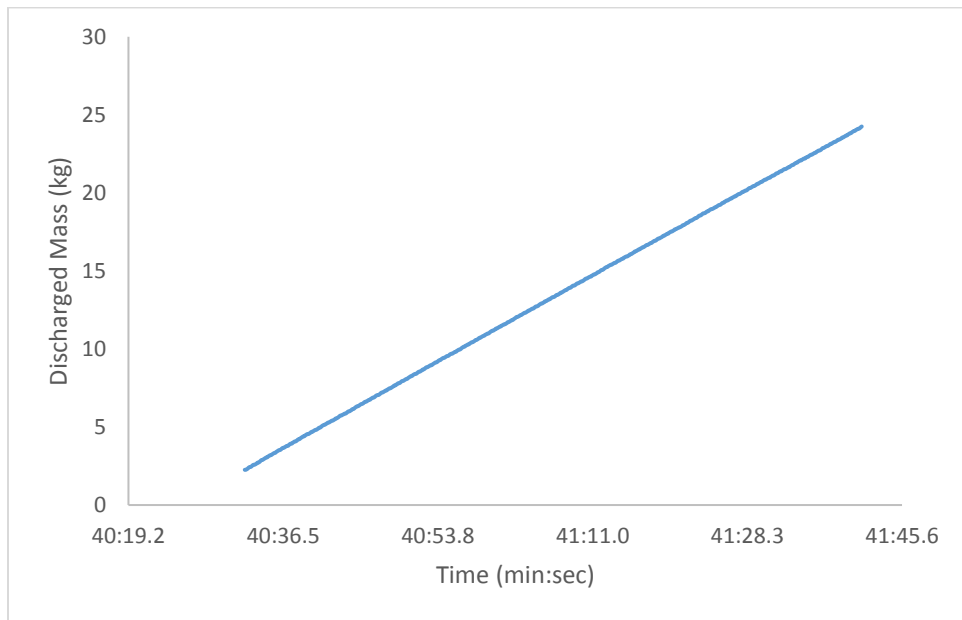


Figure A-10 b Experiment # 10 Cumulative discharge mass vs. time

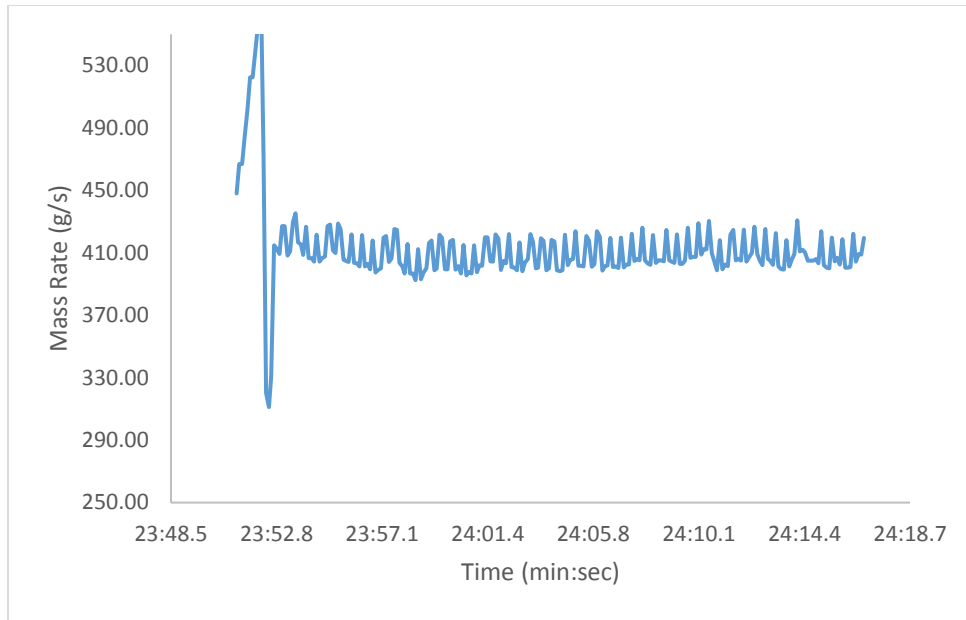


Figure A-11 a Experiment # 11 Granular flow rate vs. time

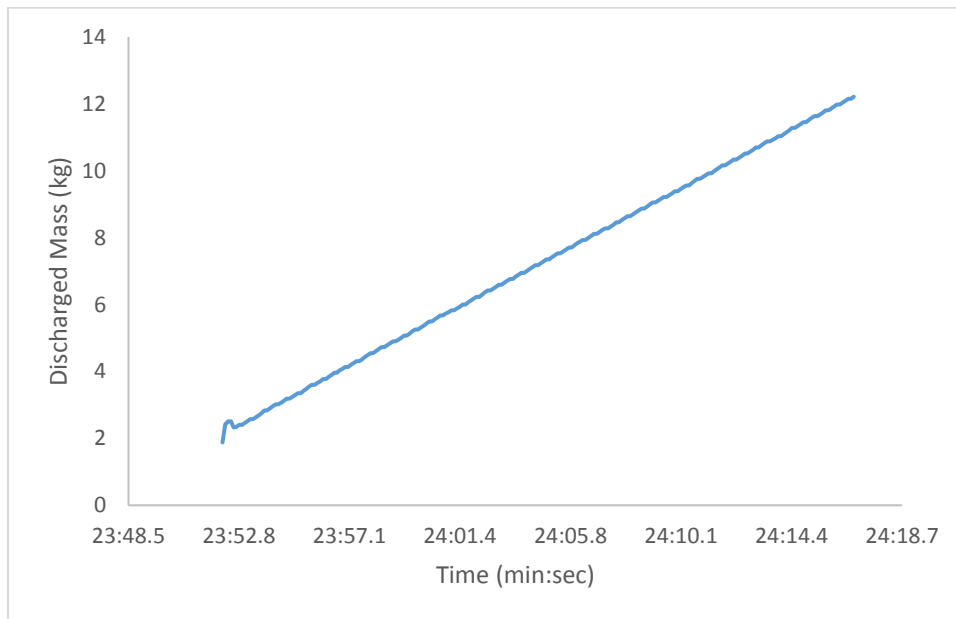


Figure A-11 b Experiment # 11 Cumulative discharge mass vs. time

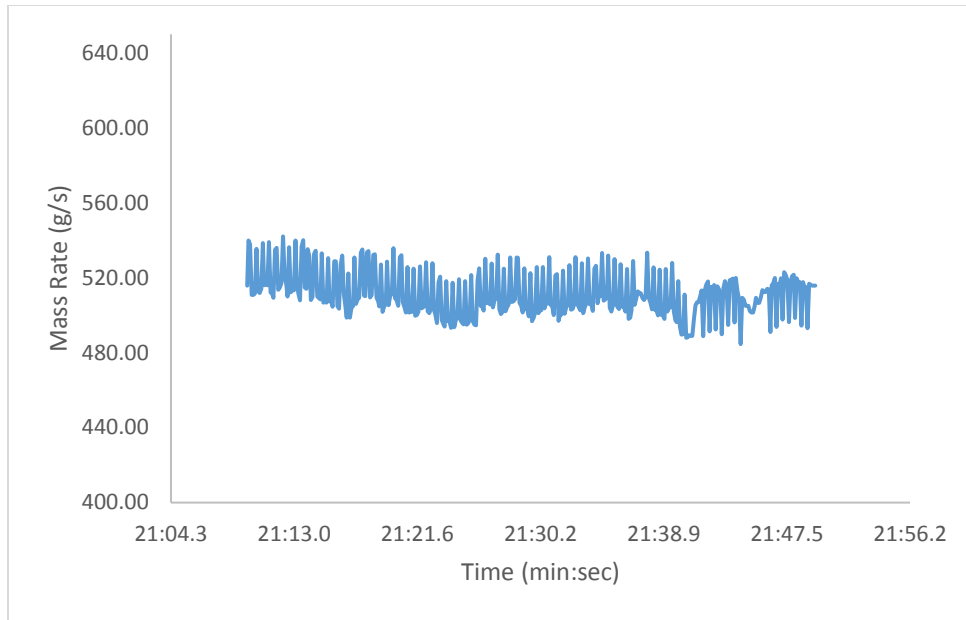


Figure A-12 a Experiment # 12 Granular flow rate vs. time

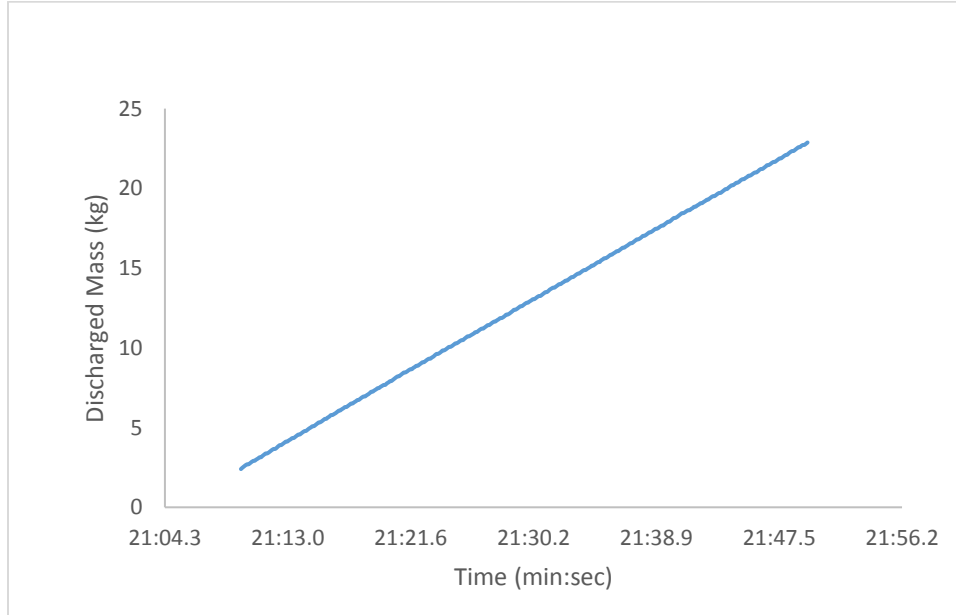


Figure A-12 b Experiment # 12 Cumulative discharge mass vs. time

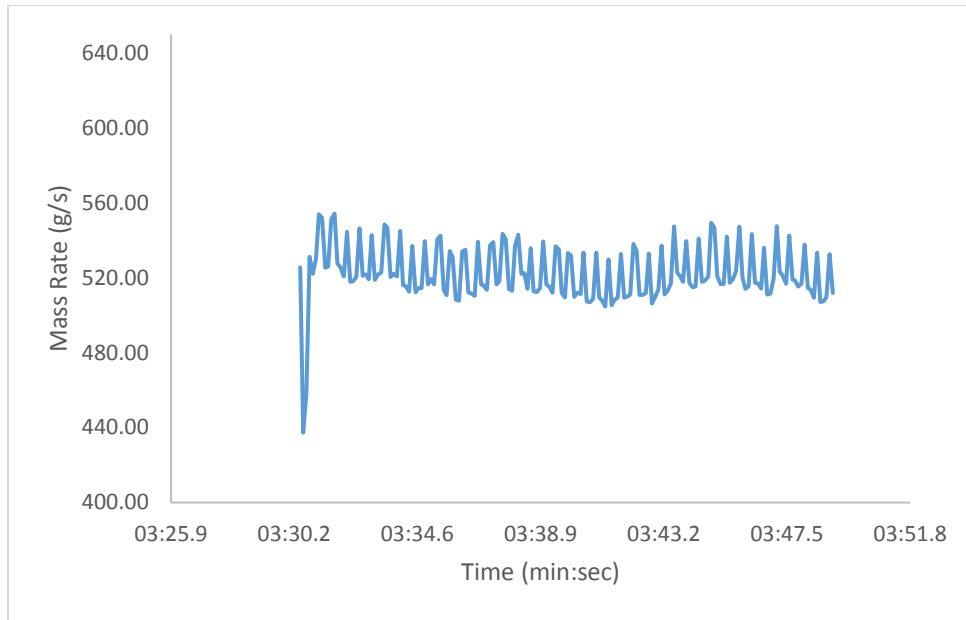


Figure A-13 a Experiment # 13 Granular flow rate vs. time

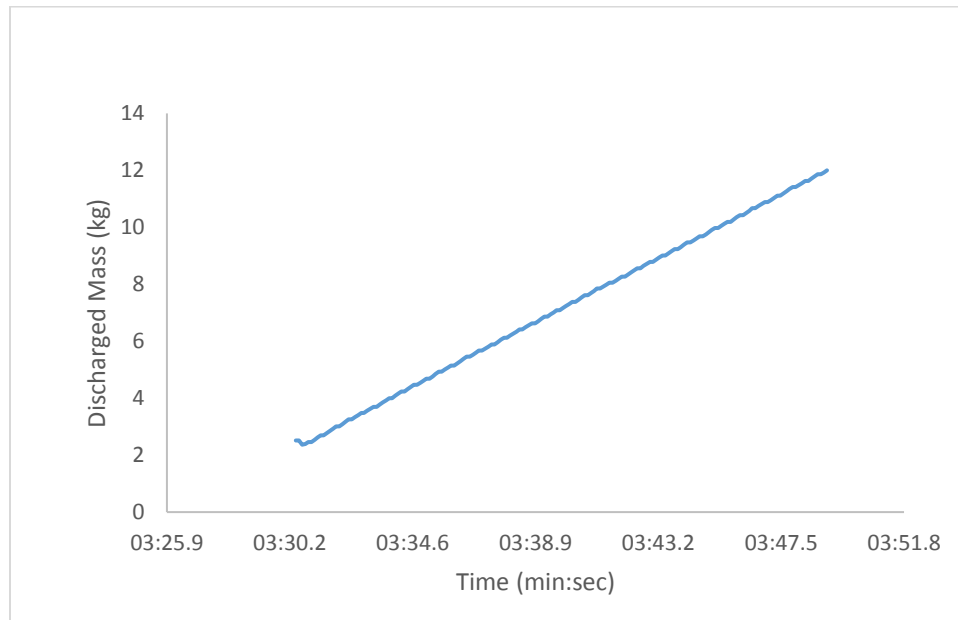


Figure A-13 b Experiment # 13 Cumulative discharge mass vs. time

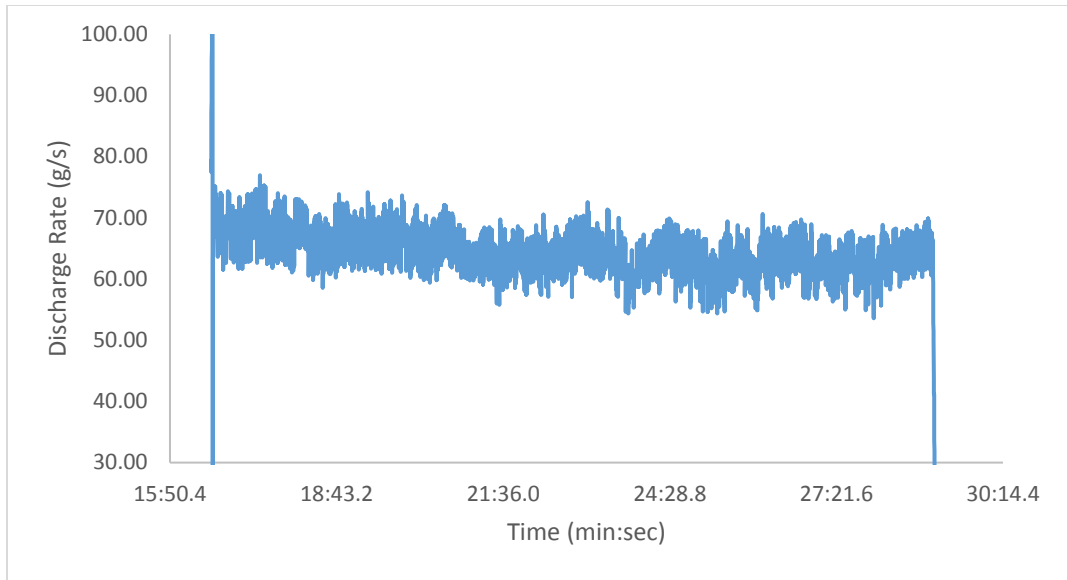


Figure A-14 a Experiment # 15 Granular flow rate vs. time

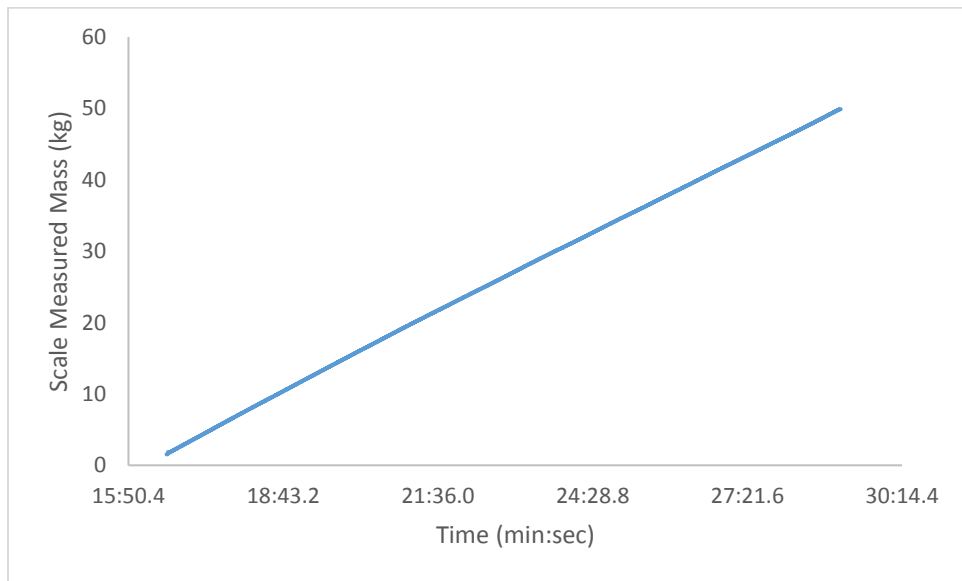


Figure A-14 b Experiment # 15 Cumulative discharge mass vs. time

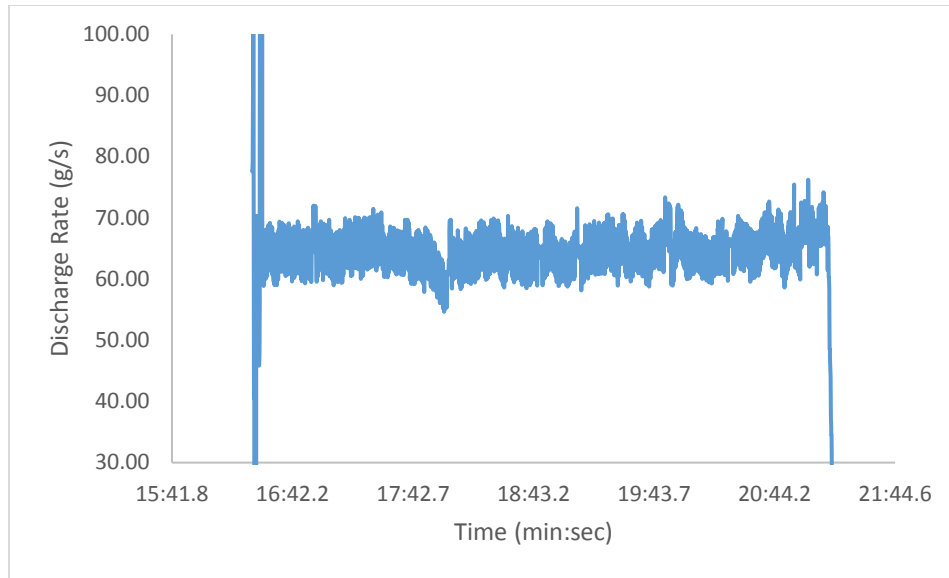


Figure A-15 a Experiment # 16 Granular flow rate vs. time

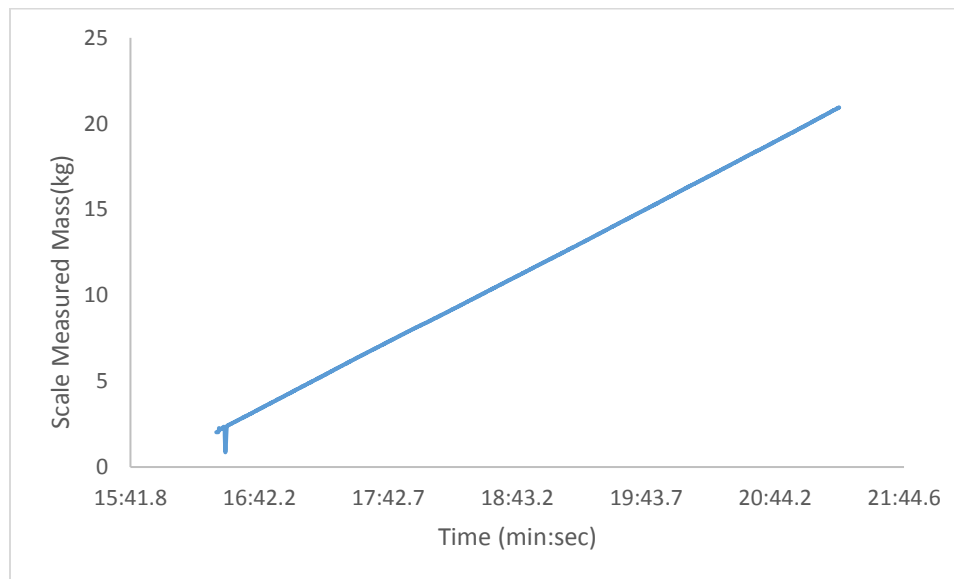


Figure A-15 b Experiment # 16 Cumulative discharge mass vs. time

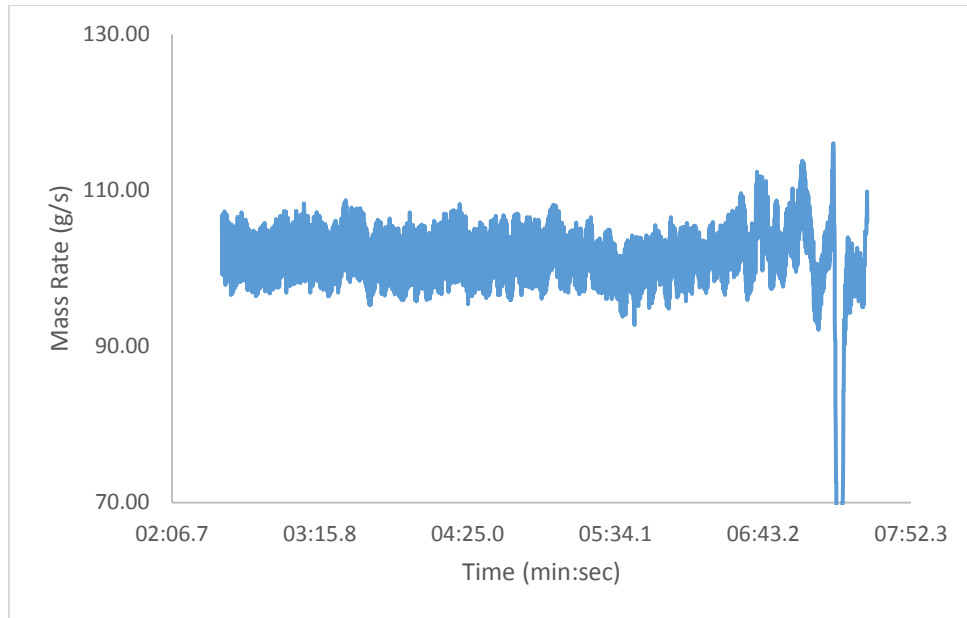


Figure A-16 a Experiment # 17 Granular flow rate vs. time

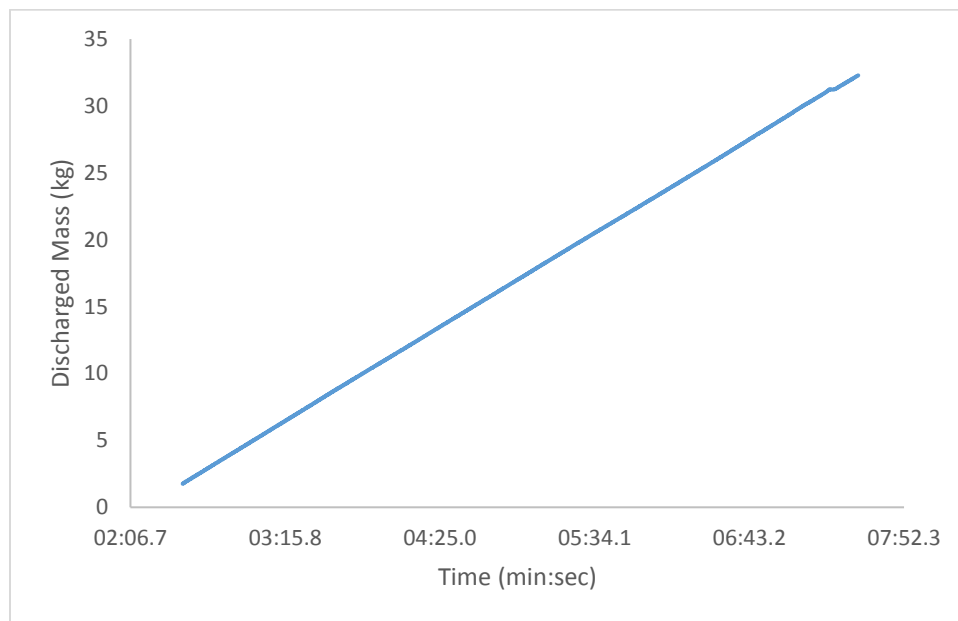


Figure A-16 b Experiment # 17 Cumulative discharge mass vs. time

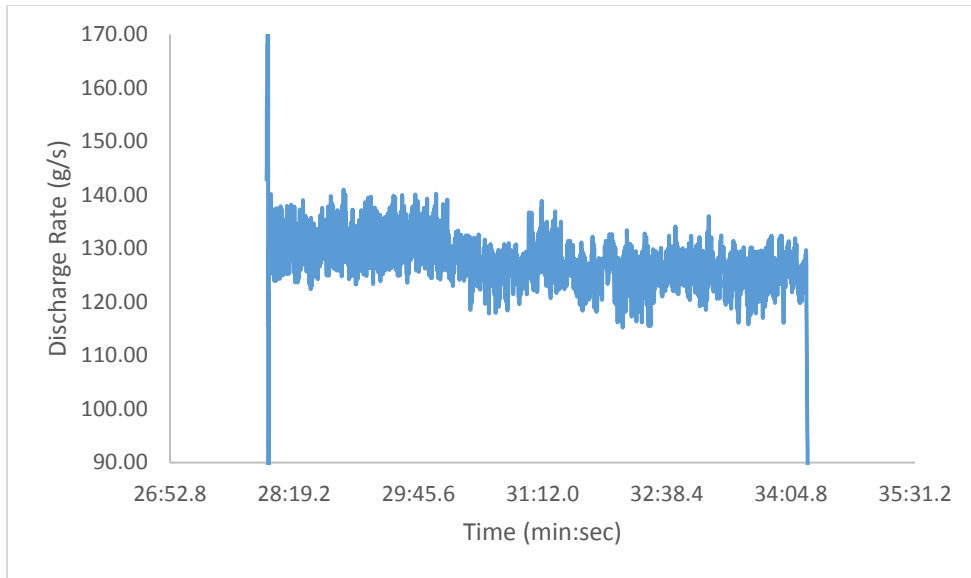


Figure A-17 a Experiment # 18 Granular flow rate vs. time

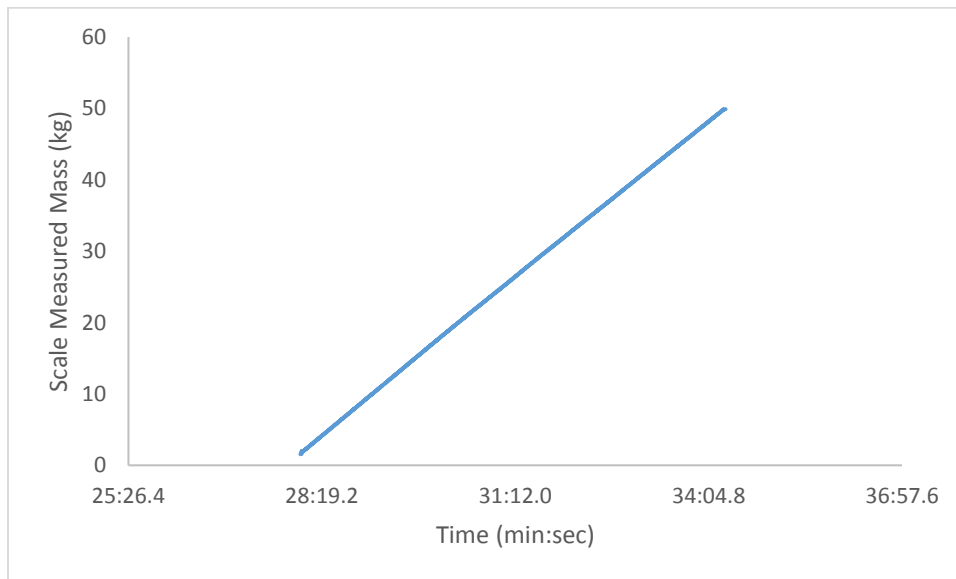


Figure A-17 b Experiment # 18 Cumulative discharge mass vs. time

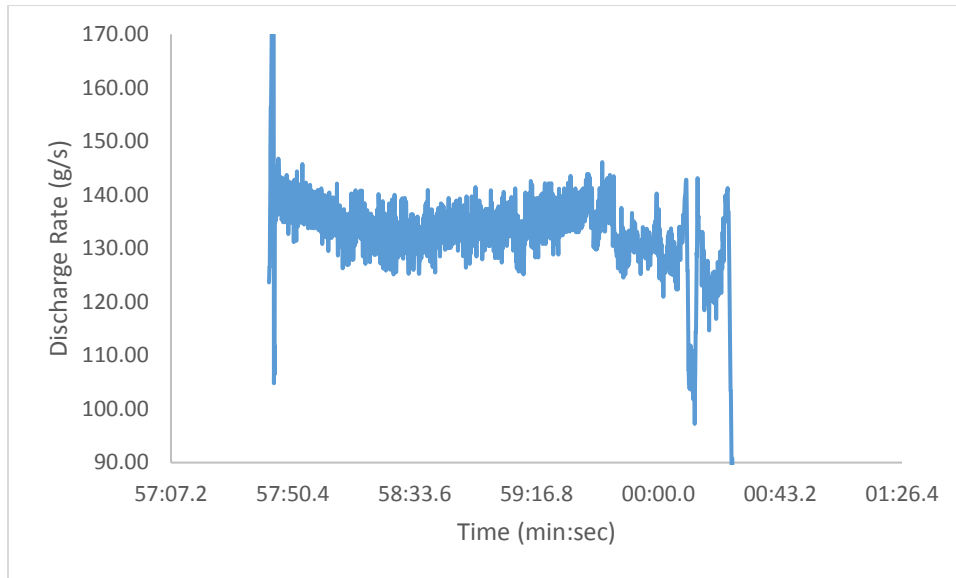


Figure A-18 a Experiment # 19 Granular flow rate vs. time

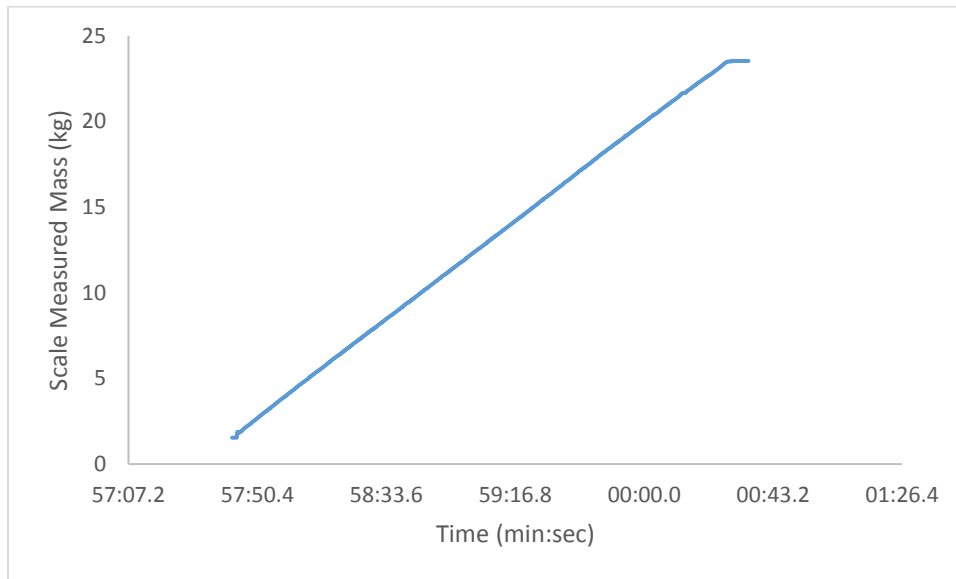


Figure A-18 b Experiment # 19 Cumulative discharge mass vs. time

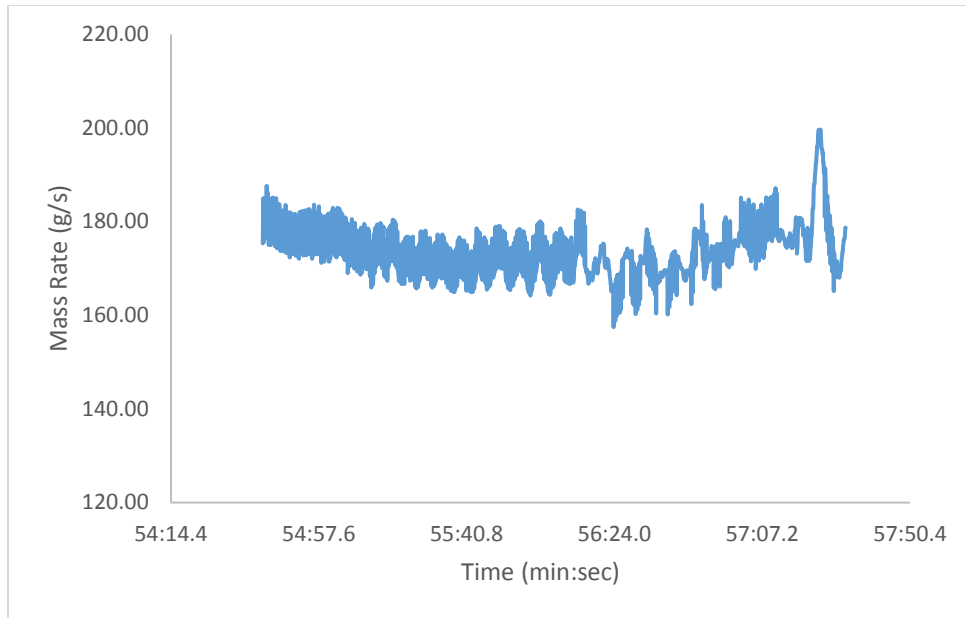


Figure A-19 a Experiment # 20 Granular flow rate vs. time

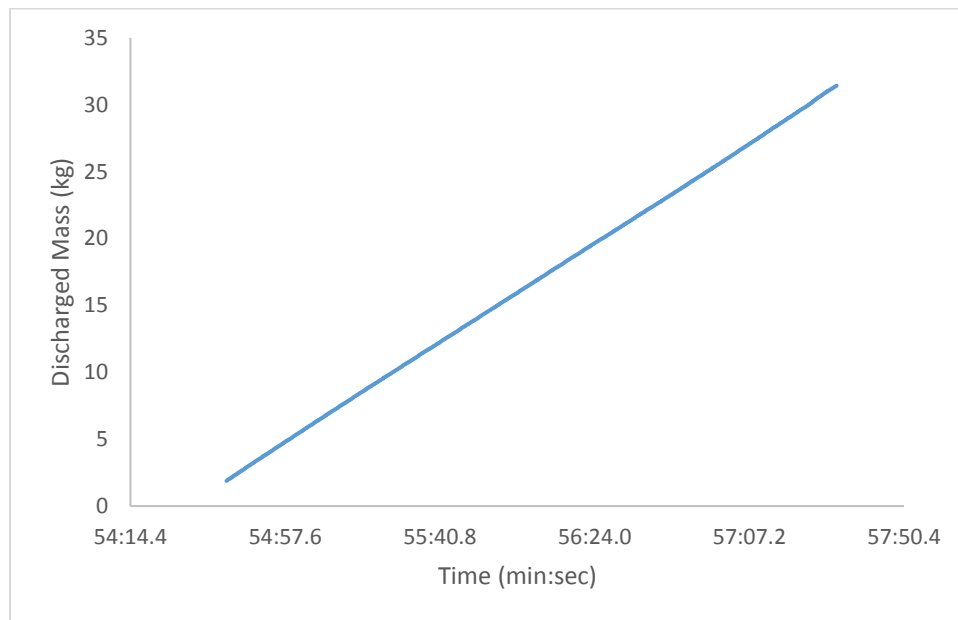


Figure A-19 b Experiment # 20 Cumulative discharge mass vs. time

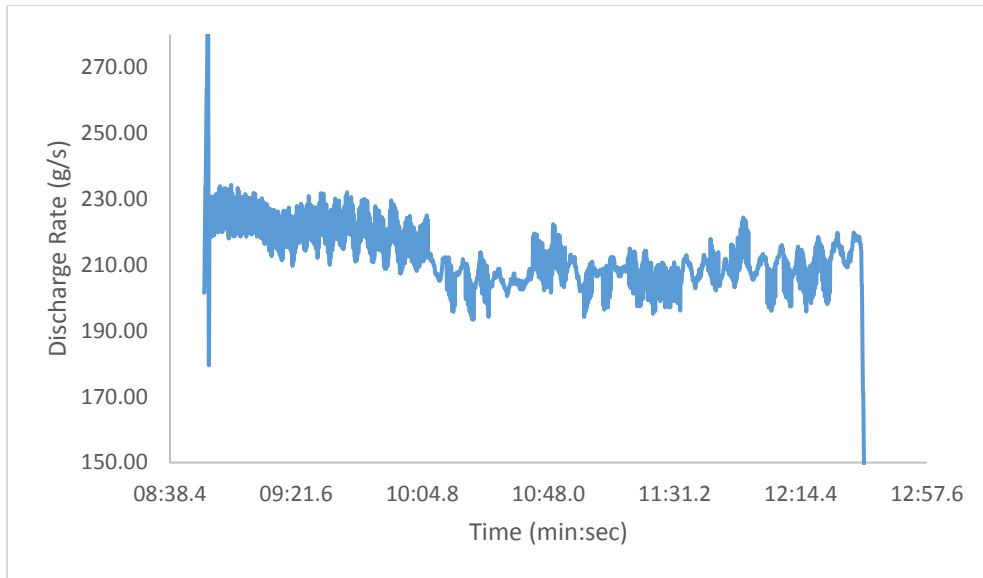


Figure A-20 a Experiment # 21 Granular flow rate vs. time

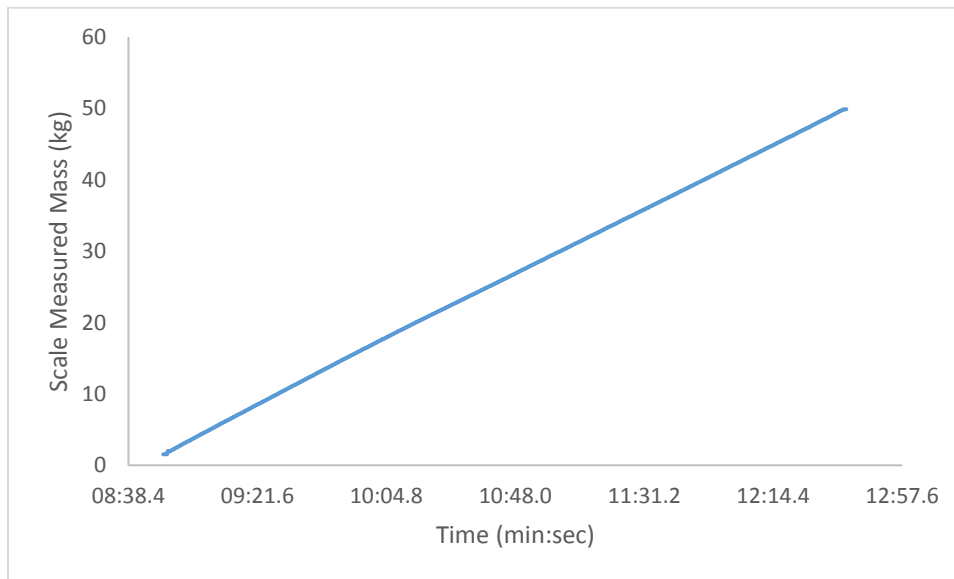


Figure A-20 b Experiment # 21 Cumulative discharge mass vs. time

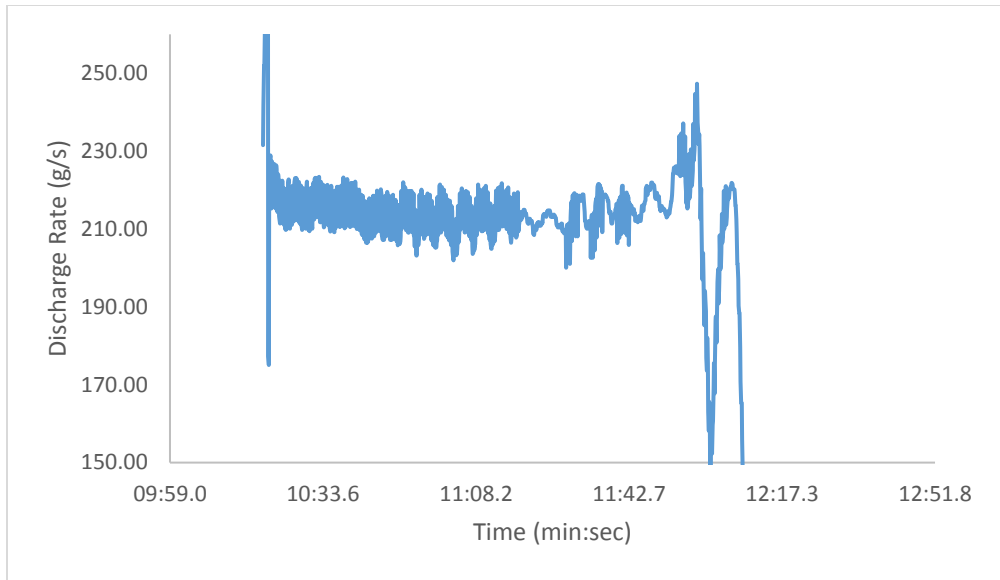


Figure A-21 a Experiment # 22 Granular flow rate vs. time

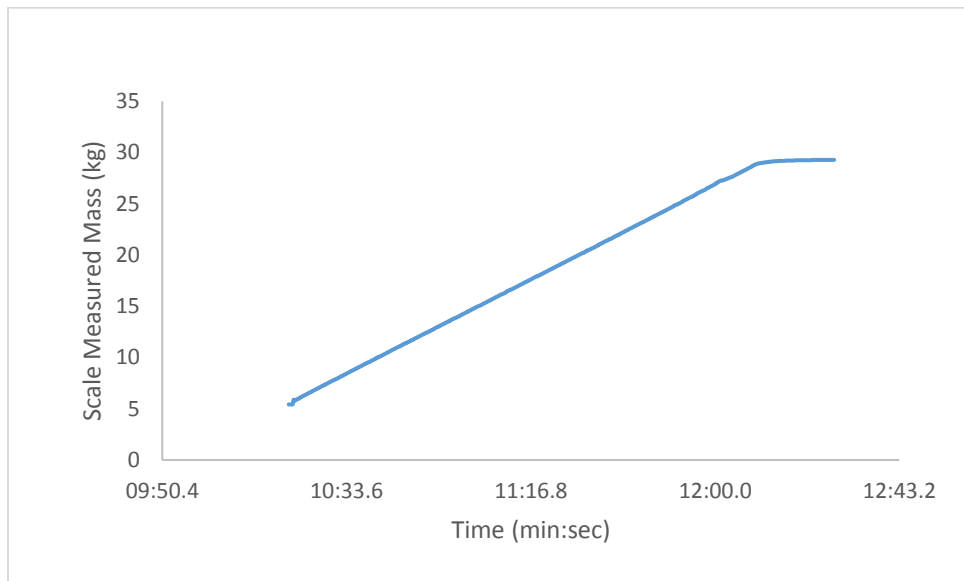


Figure A-21 b Experiment # 22 Cumulative discharge mass vs. time

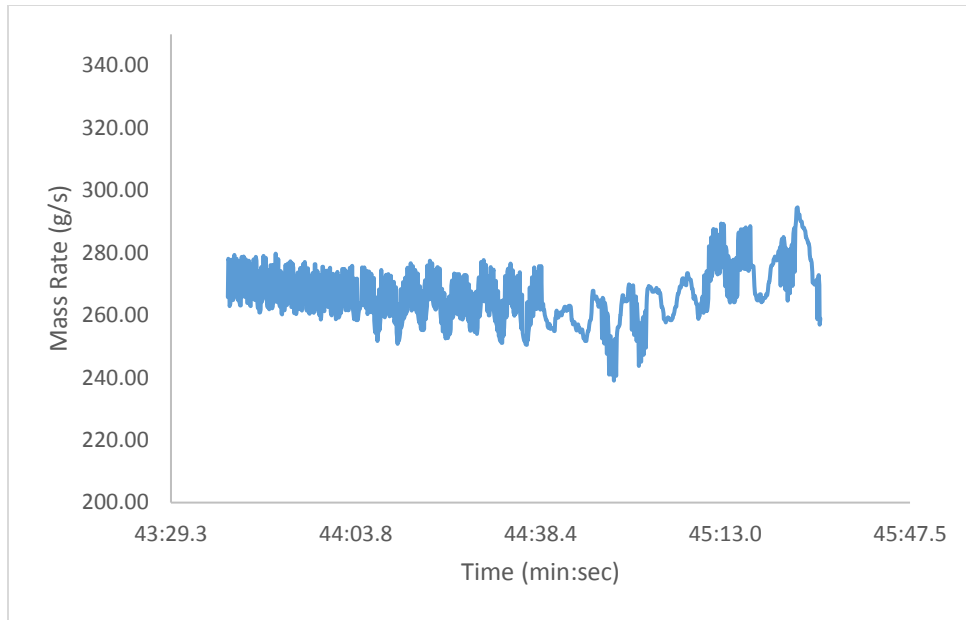


Figure A-22 a Experiment # 23 Granular flow rate vs. time

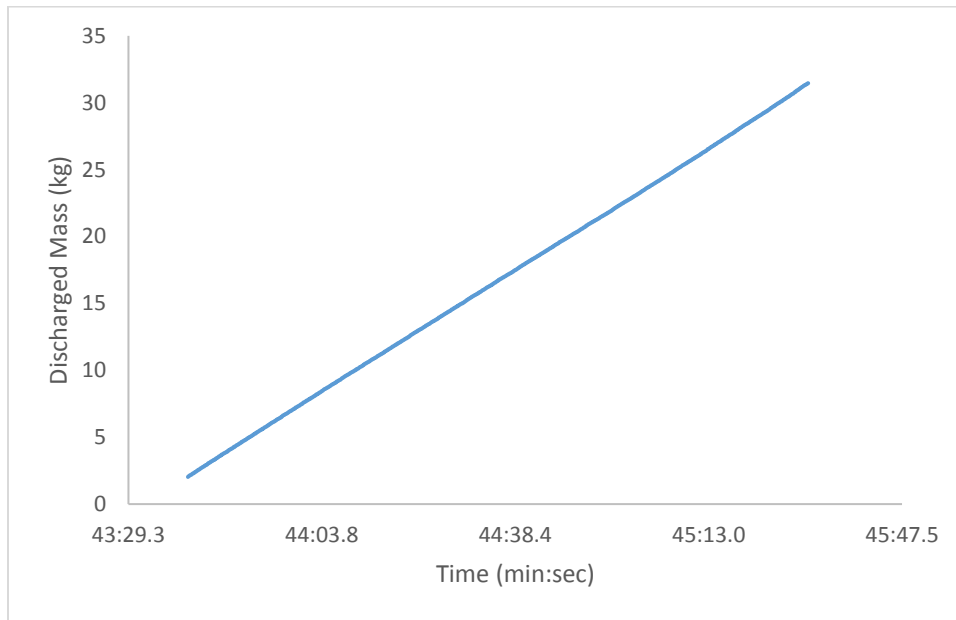


Figure A-22 b Experiment # 23 Cumulative discharge mass vs. time

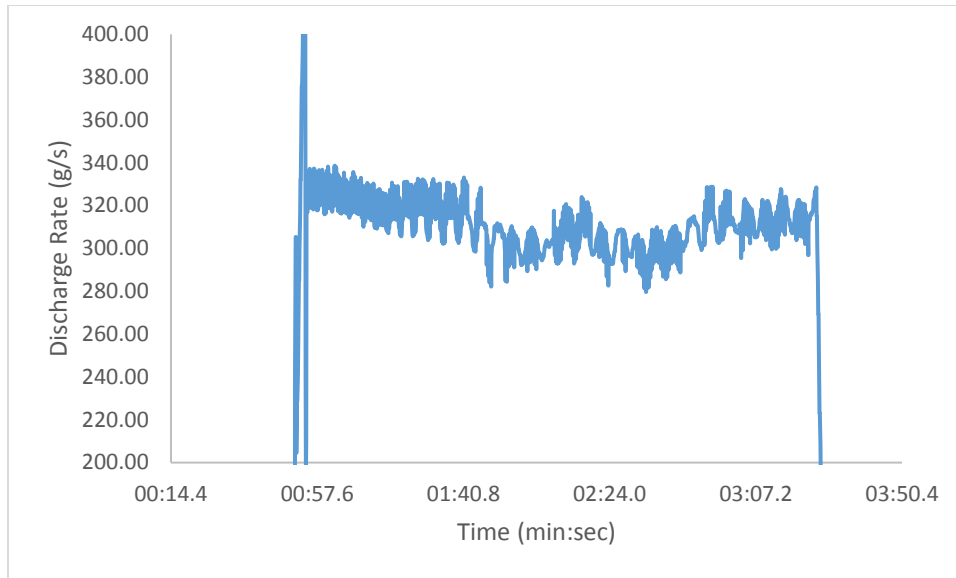


Figure A-23 a Experiment # 24 Granular flow rate vs. time

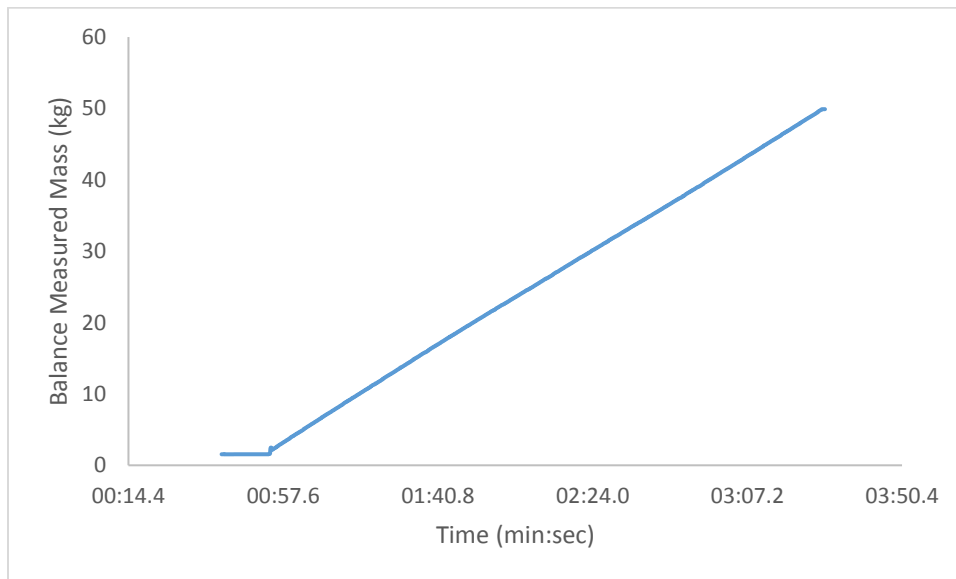


Figure A-23 b Experiment # 24 Cumulative discharge mass vs. time

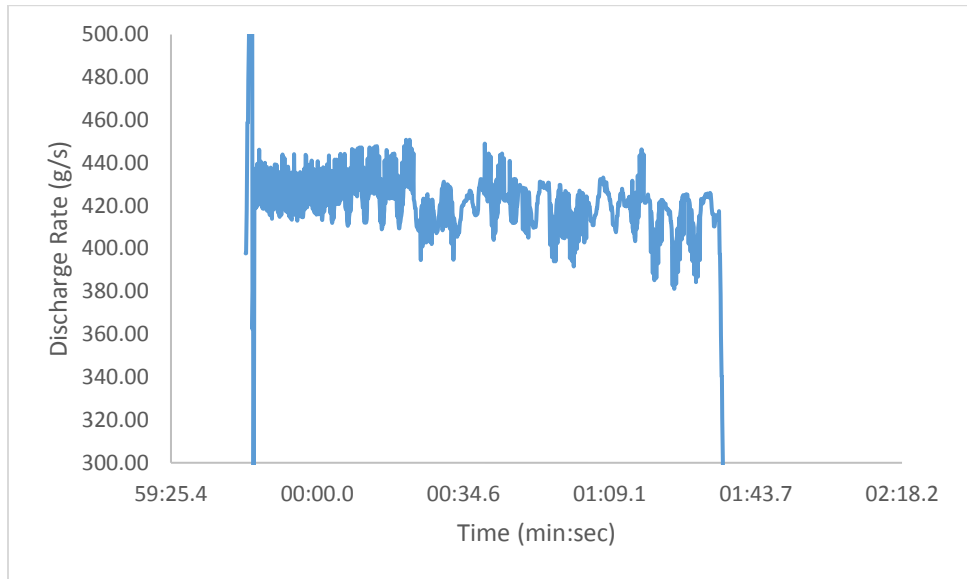


Figure A-24 a Experiment # 25 Granular flow rate vs. time

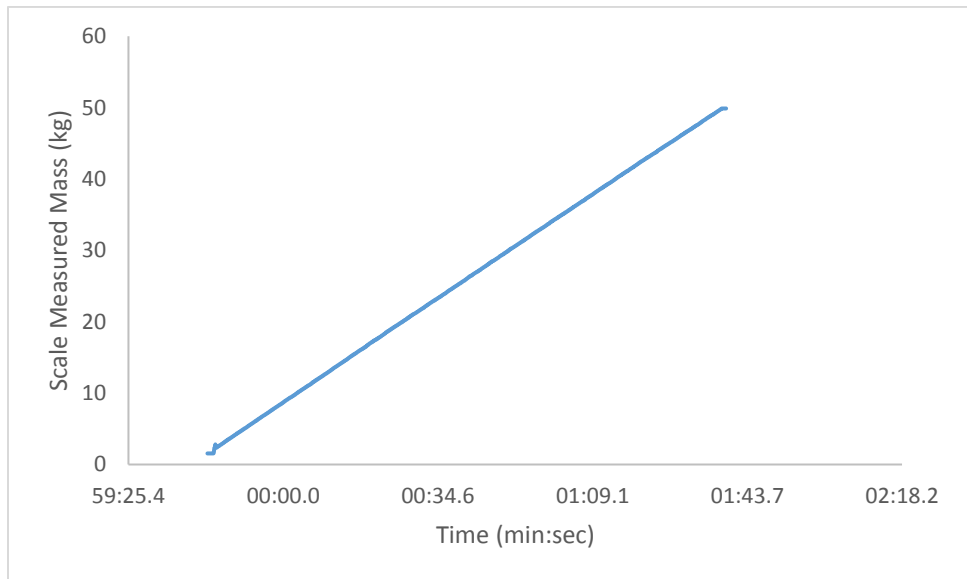


Figure A-24 b Experiment # 25 Cumulative discharge mass vs. time

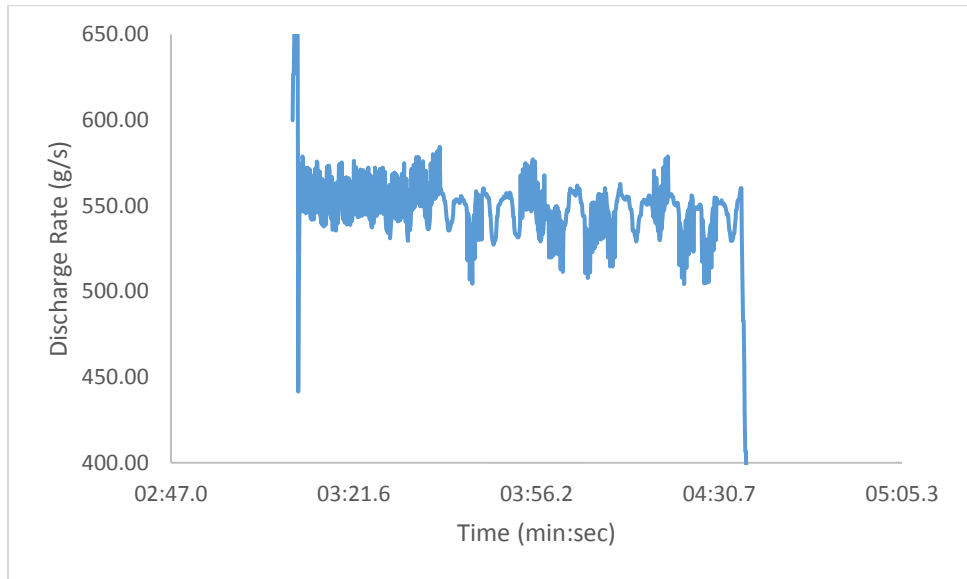


Figure A-25 a Experiment # 26 Granular flow rate vs. time

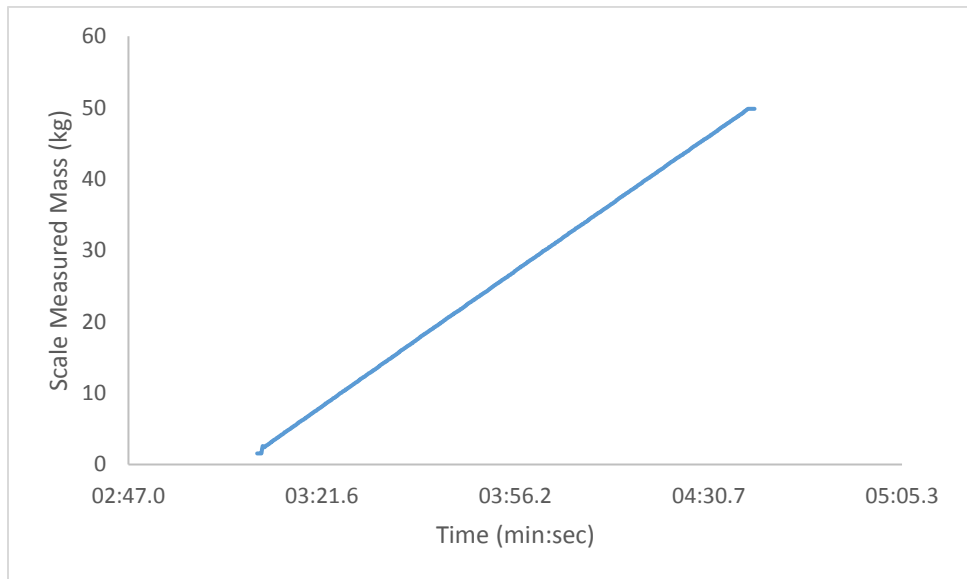


Figure A-25 b Experiment # 26 Cumulative discharge mass vs. time

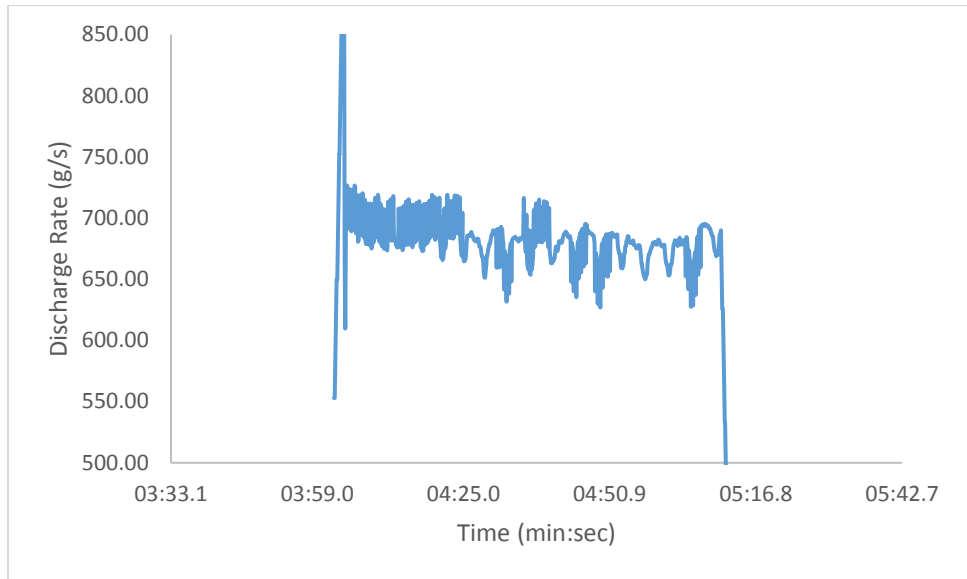


Figure A-26 a Experiment # 27 Granular flow rate vs. time

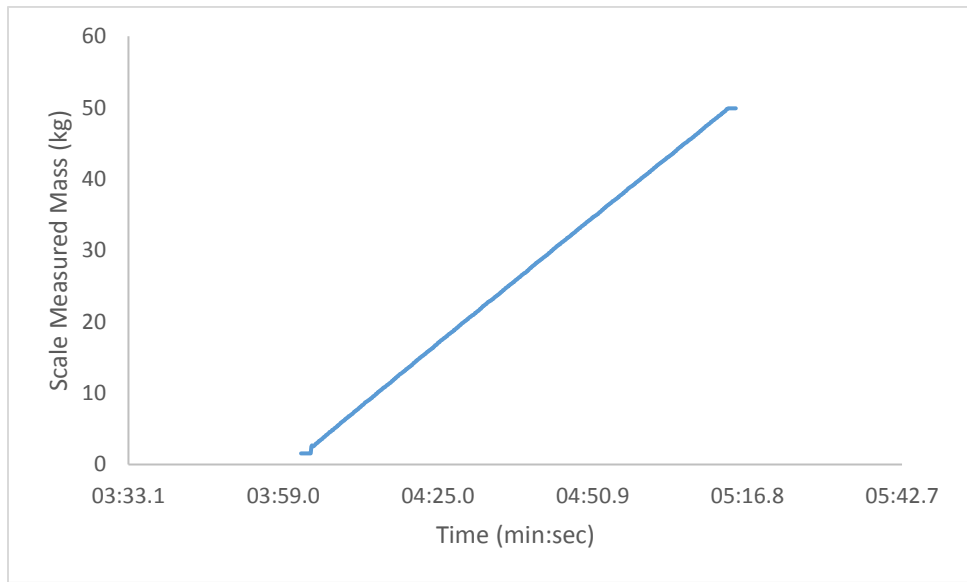


Figure A-26 b Experiment # 27 Cumulative discharge mass vs. time

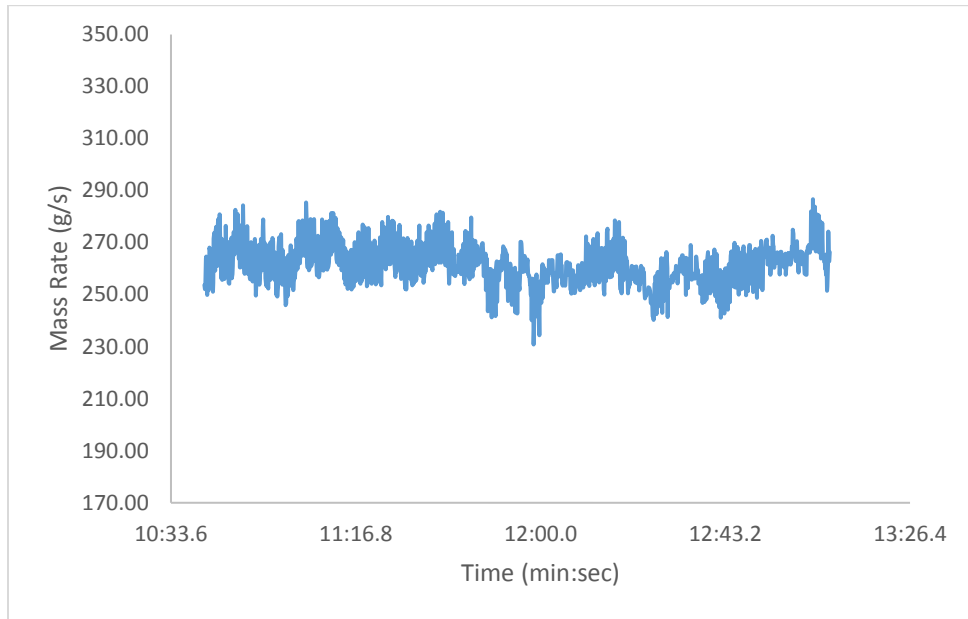


Figure A-27 a Experiment # 28 Granular flow rate vs. time

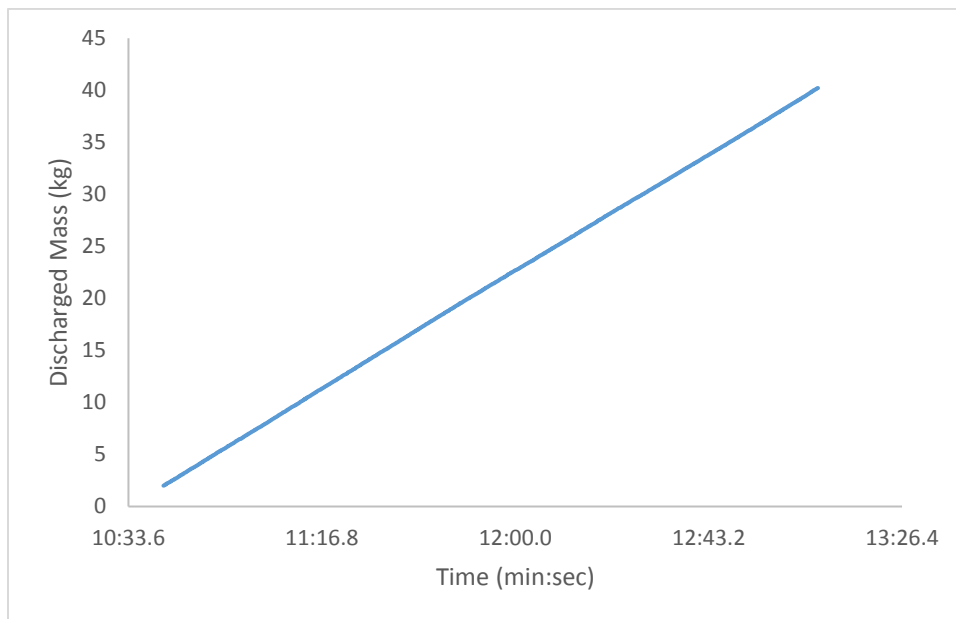


Figure A-27 b Experiment # 28 Cumulative discharge mass vs. time

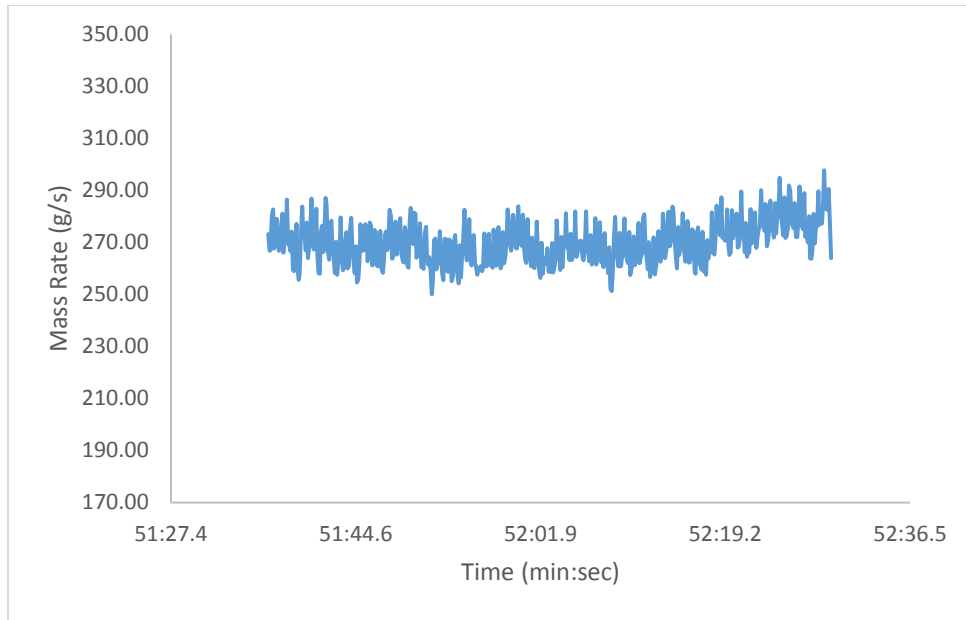


Figure A-28 a Experiment # 29 Granular flow rate vs. time

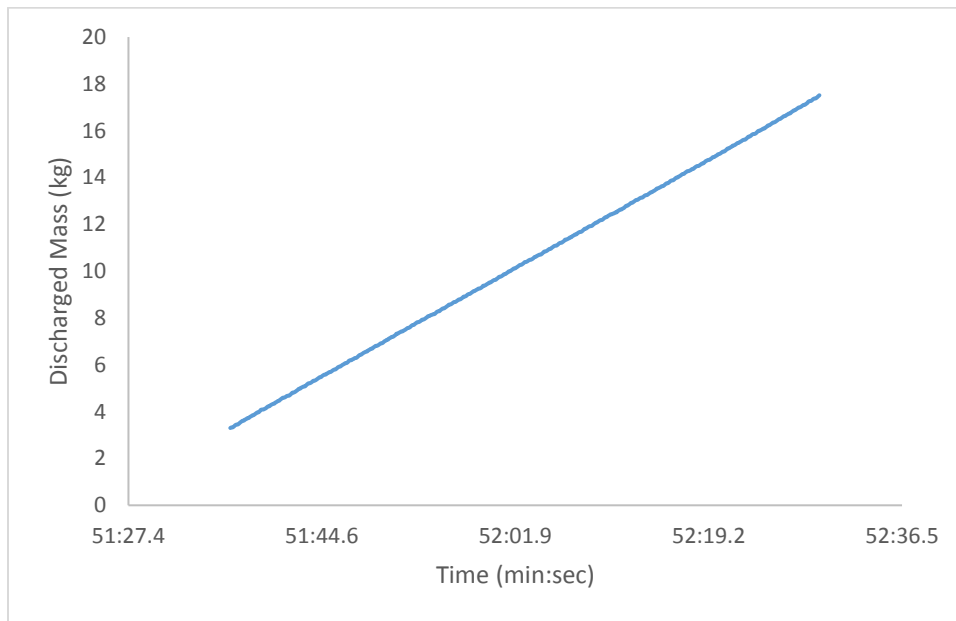


Figure A-28 b Experiment # 29 Cumulative discharge mass vs. time

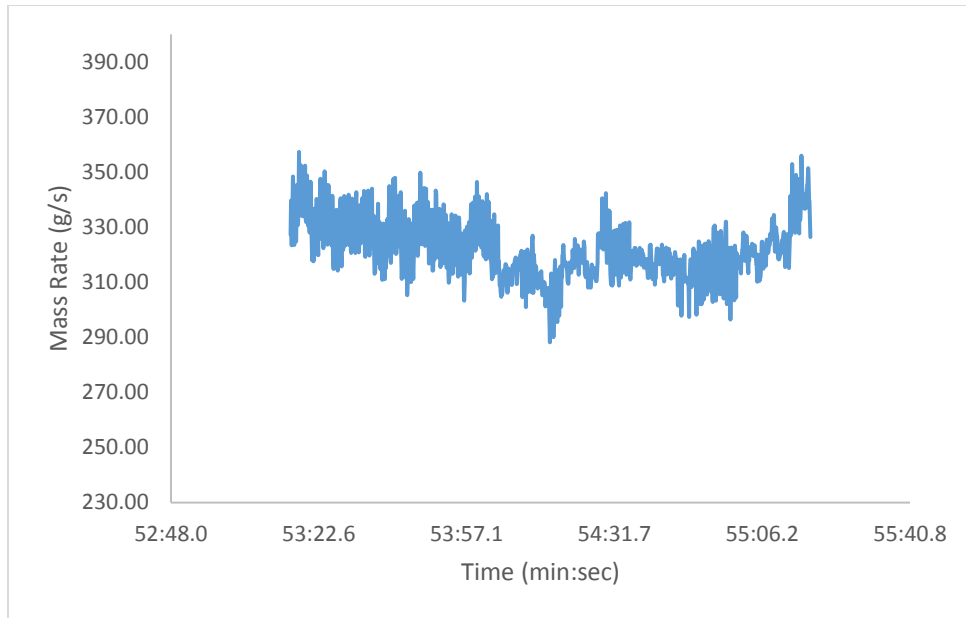


Figure A-29 a Experiment # 30 Granular flow rate vs. time

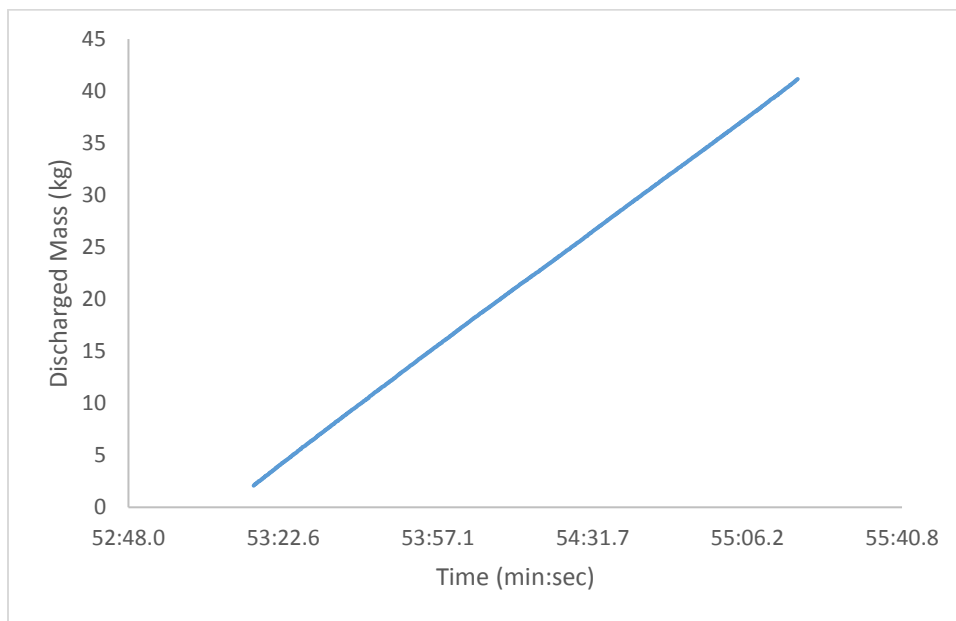


Figure A-29 b Experiment # 30 Cumulative discharge mass vs. time

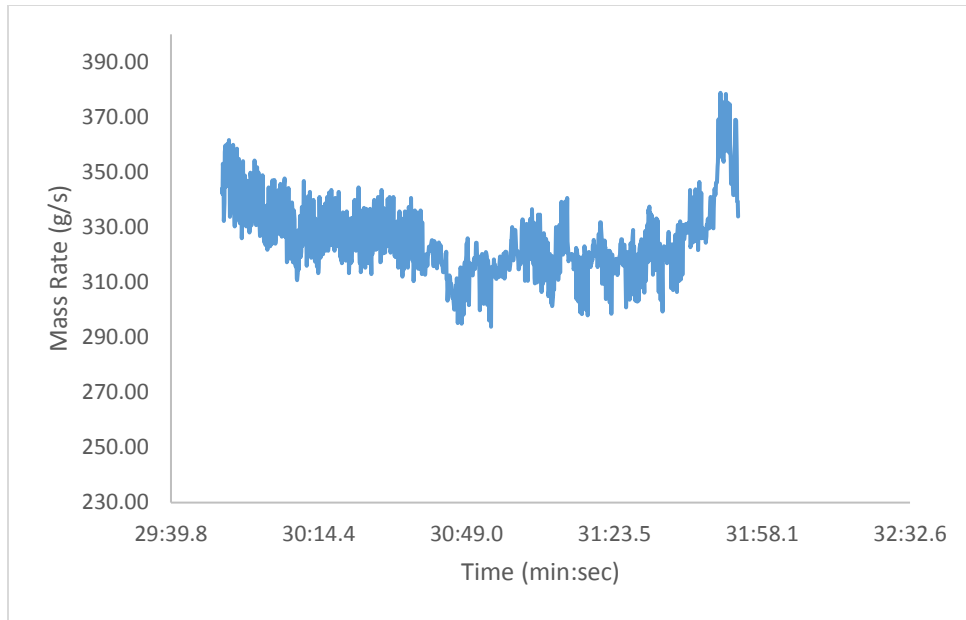


Figure A-30 a Experiment # 31 Granular flow rate vs. time

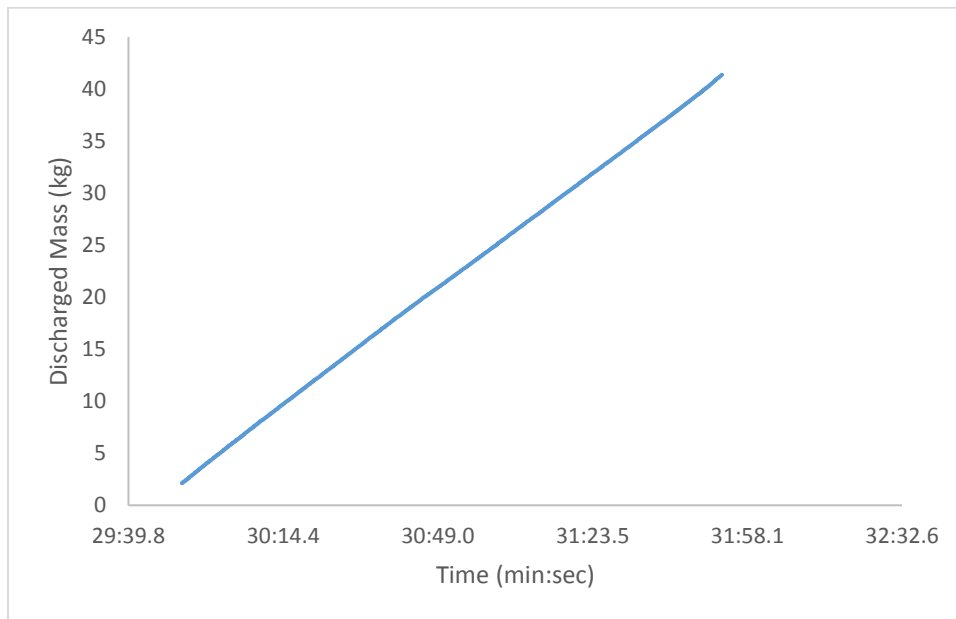


Figure A-30 b Experiment # 31 Cumulative discharge mass vs. time

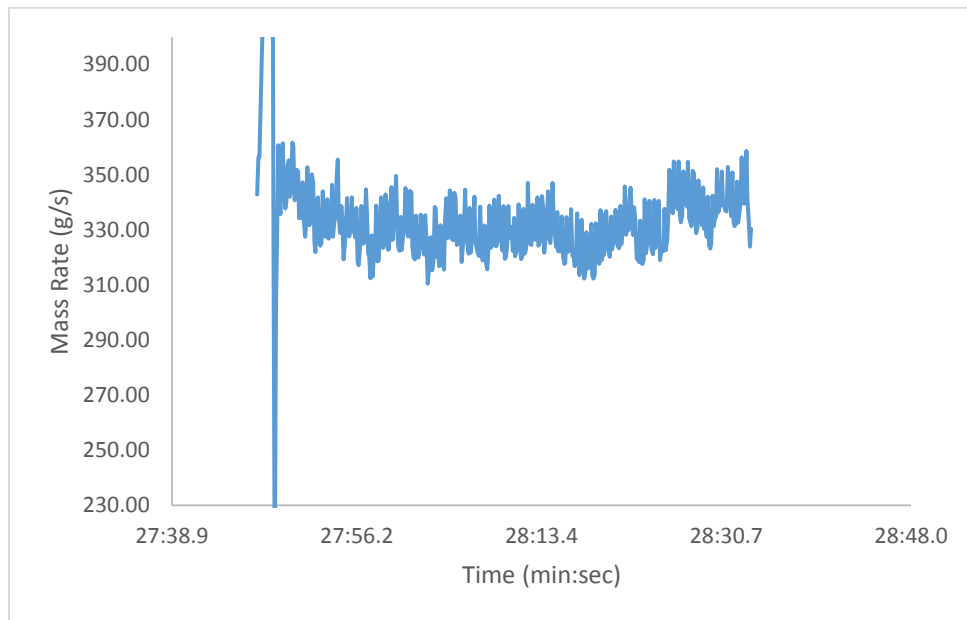


Figure A-31 a Experiment # 32 Granular flow rate vs. time

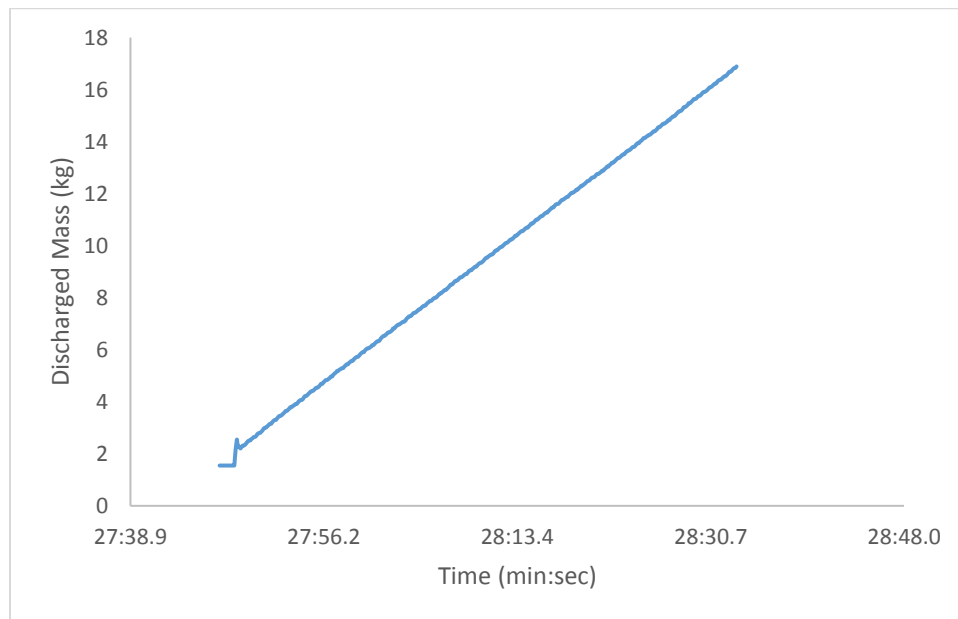


Figure A-31 b Experiment # 32 Cumulative discharge mass vs. time

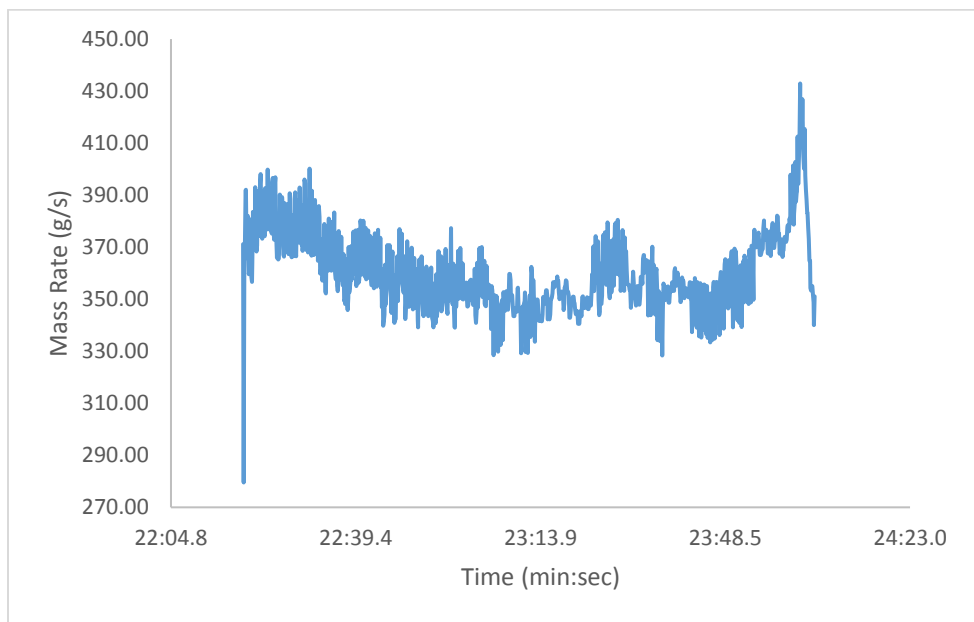


Figure A-32 a Experiment # 33 Granular flow rate vs. time

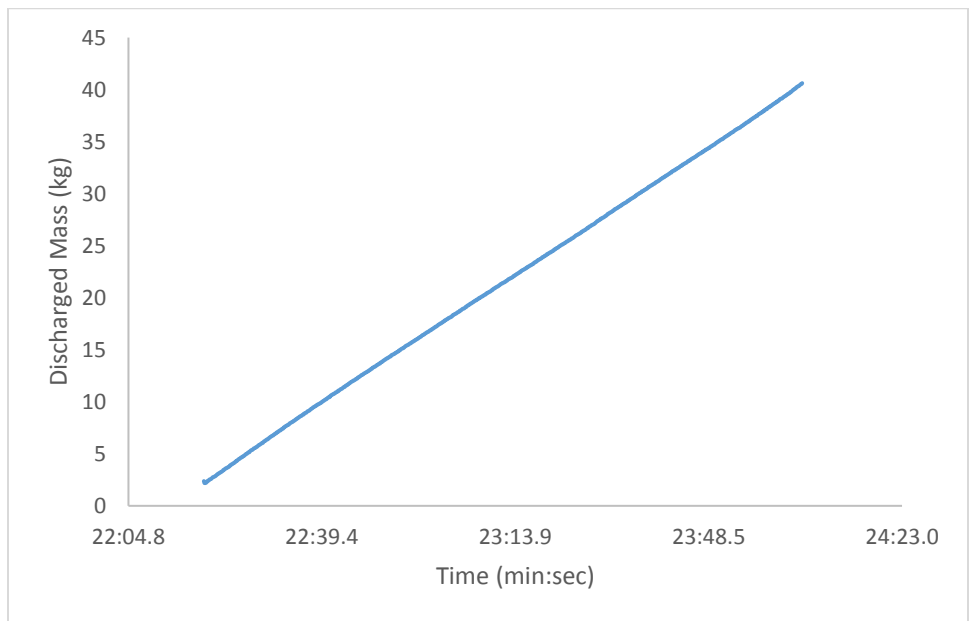


Figure A-32 b Experiment # 33 Cumulative discharge mass vs. time

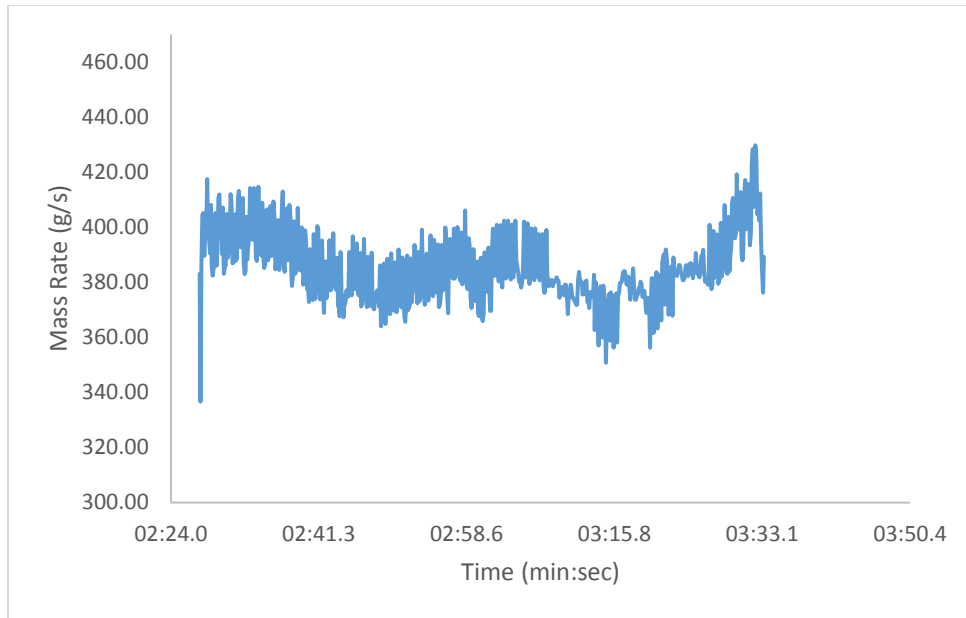


Figure A-33 a Experiment # 34 Granular flow rate vs. time

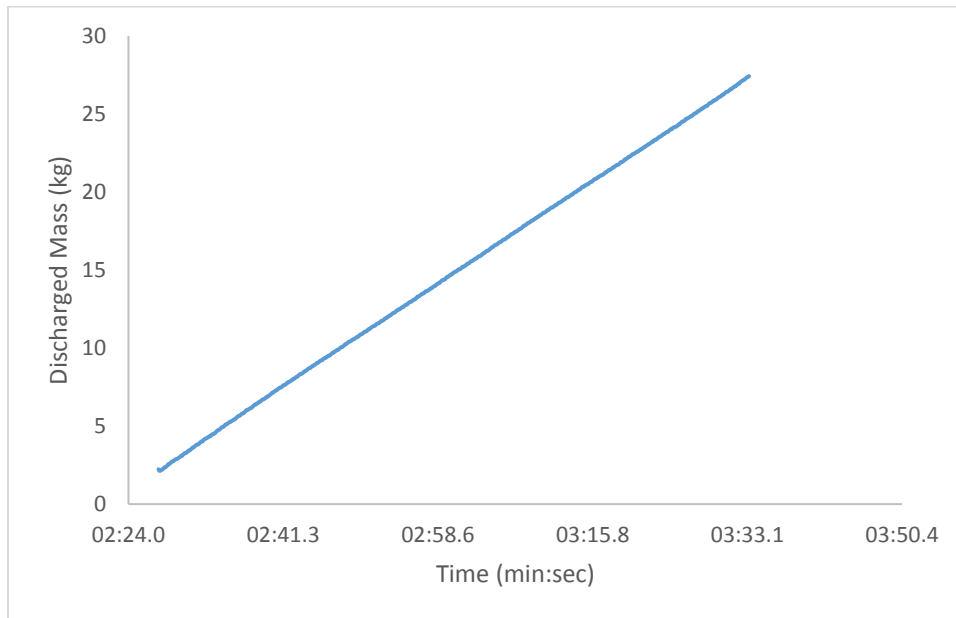


Figure A-33 b Experiment # 34 Cumulative discharge mass vs. time

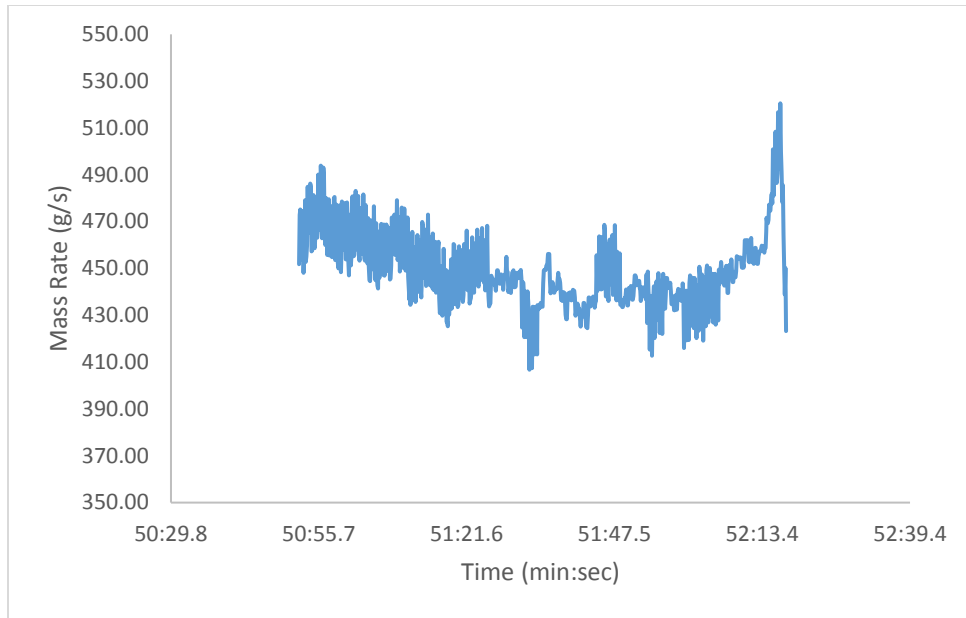


Figure A-34 a Experiment # 35 Granular flow rate vs. time

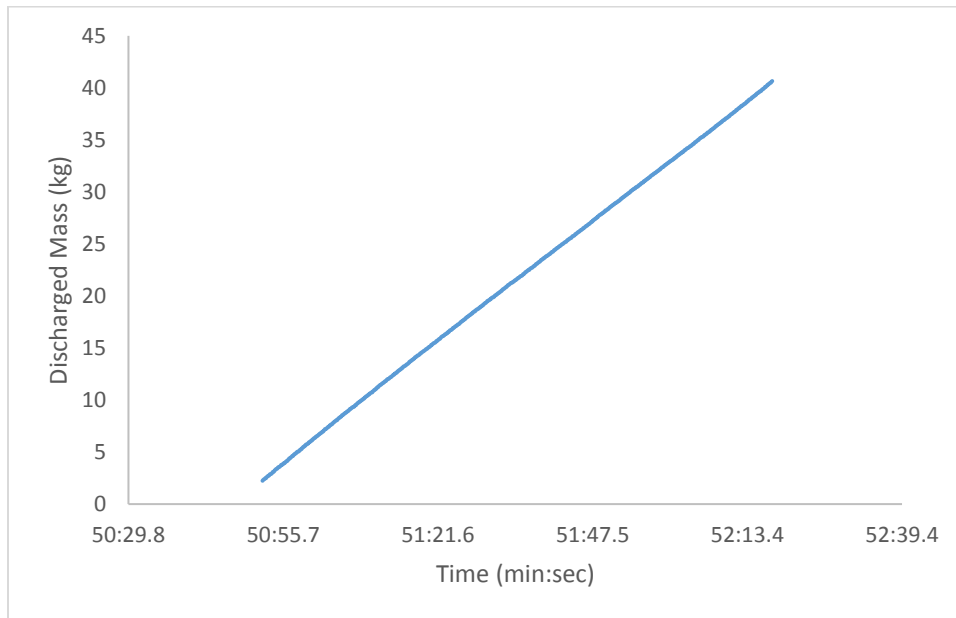


Figure A-34 b Experiment # 35 Cumulative discharge mass vs. time

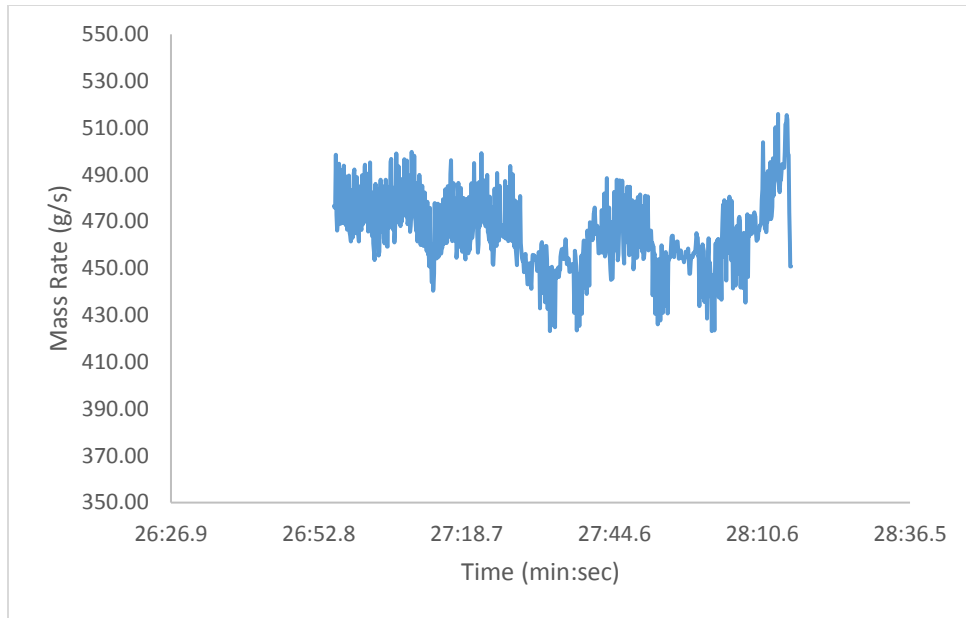


Figure A-35 a Experiment # 36 Granular flow rate vs. time

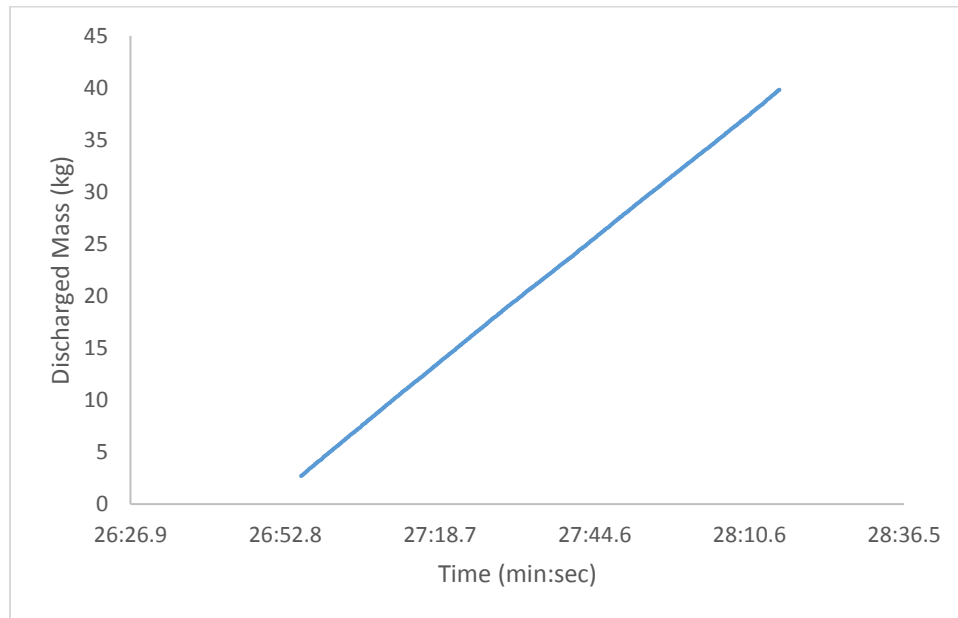


Figure A-35 b Experiment # 36 Cumulative discharge mass vs. time

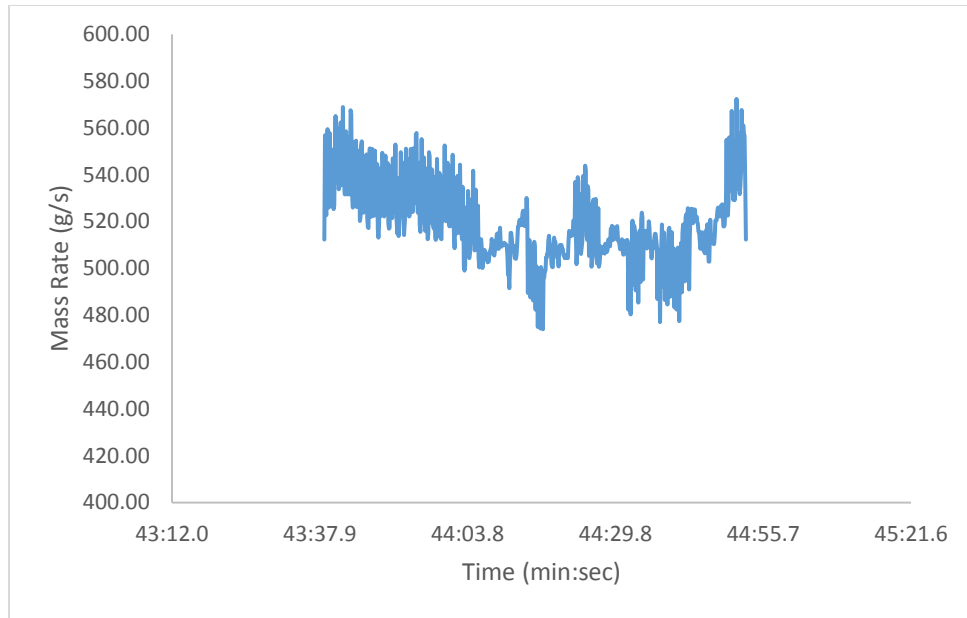


Figure A-36 a Experiment # 37 Granular flow rate vs. time

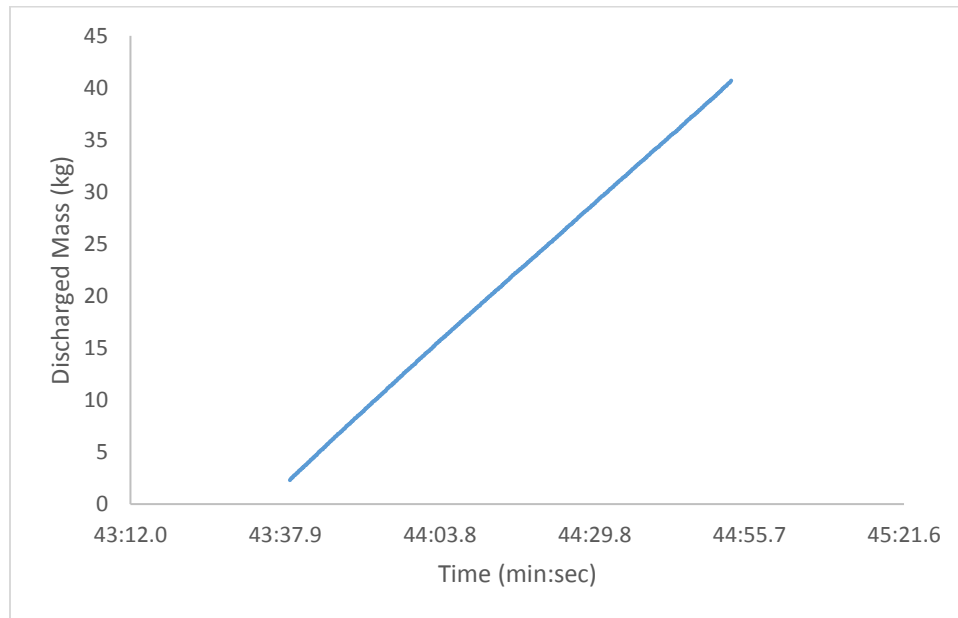


Figure A-36 b Experiment # 37 Cumulative discharge mass vs. time

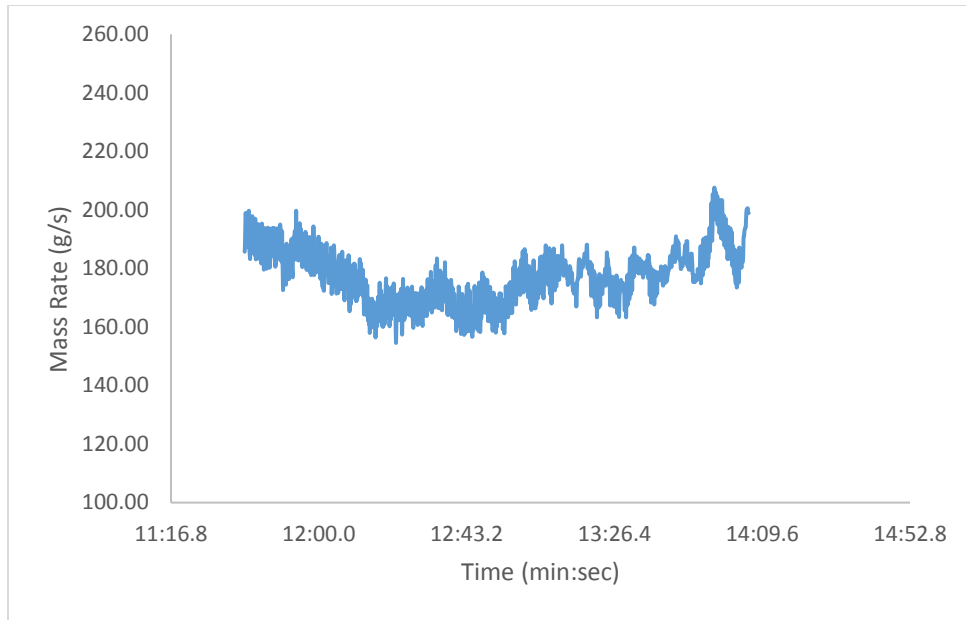


Figure A-37 a Experiment # 39 Granular flow rate vs. time

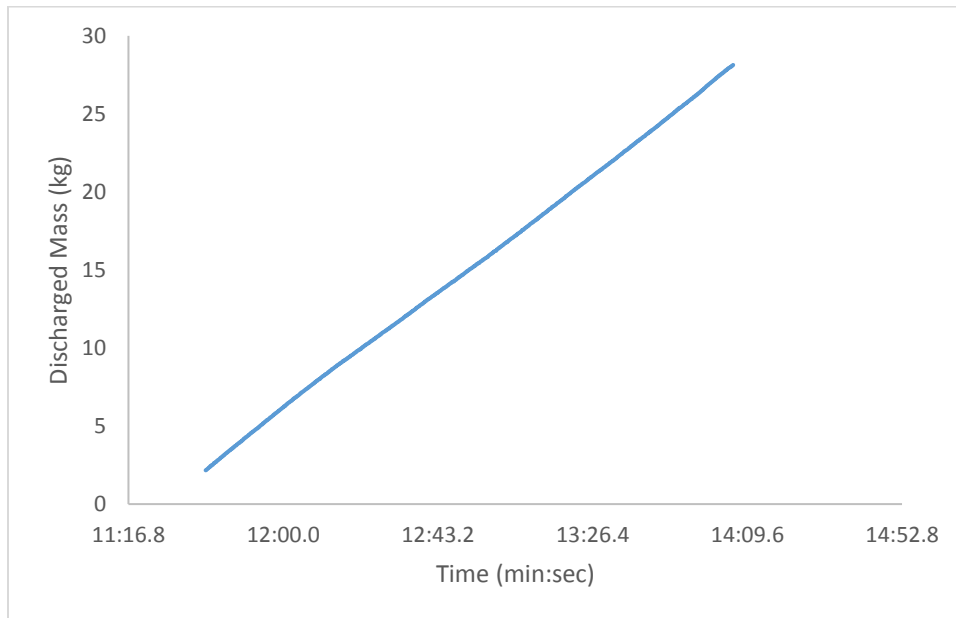


Figure A-37 b Experiment # 39 Cumulative discharge mass vs. time

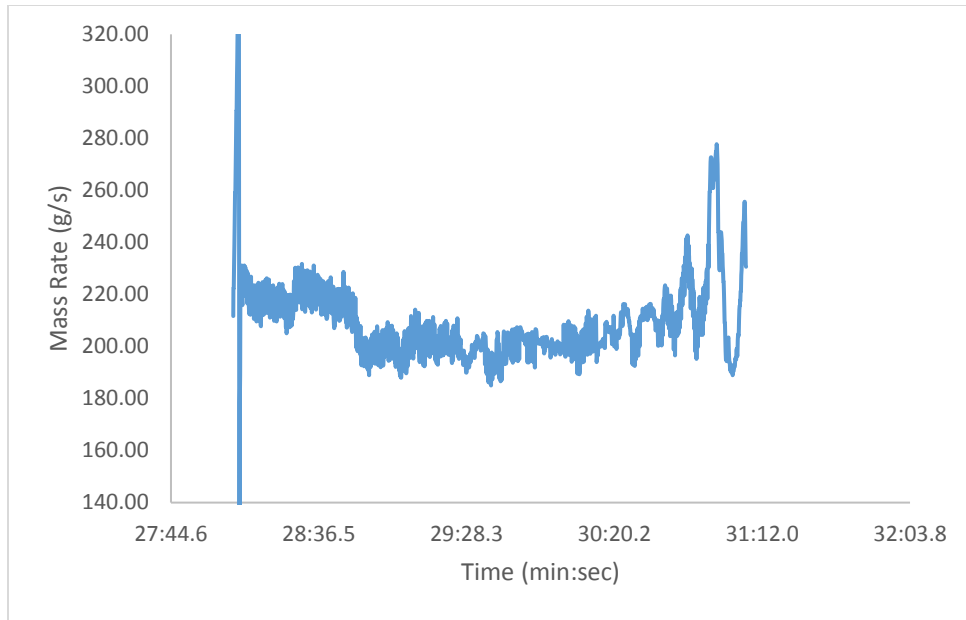


Figure A-38 a Experiment # 40 Granular flow rate vs. time

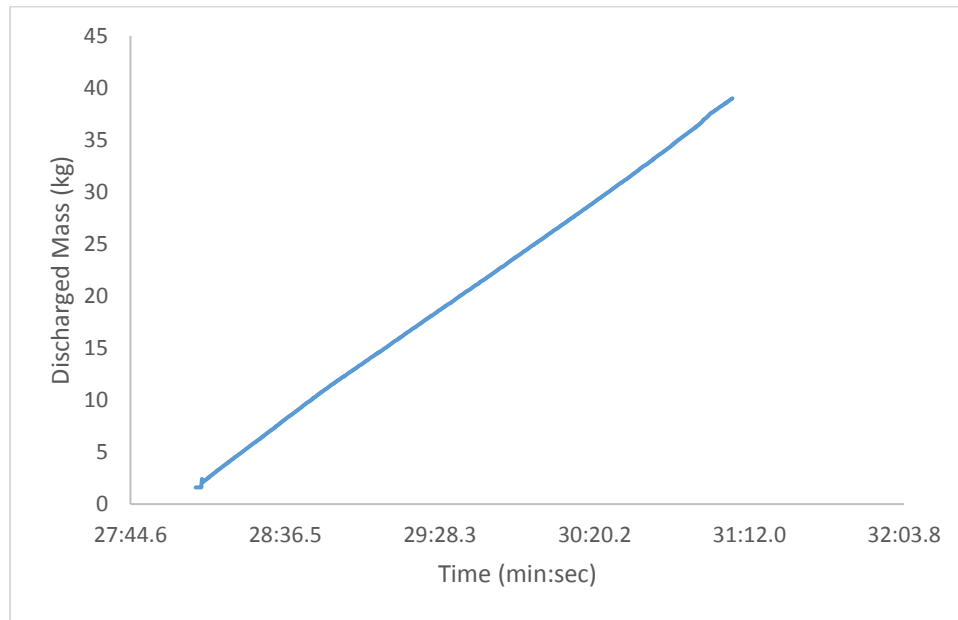


Figure A-38 b Experiment # 40 Cumulative discharge mass vs. time

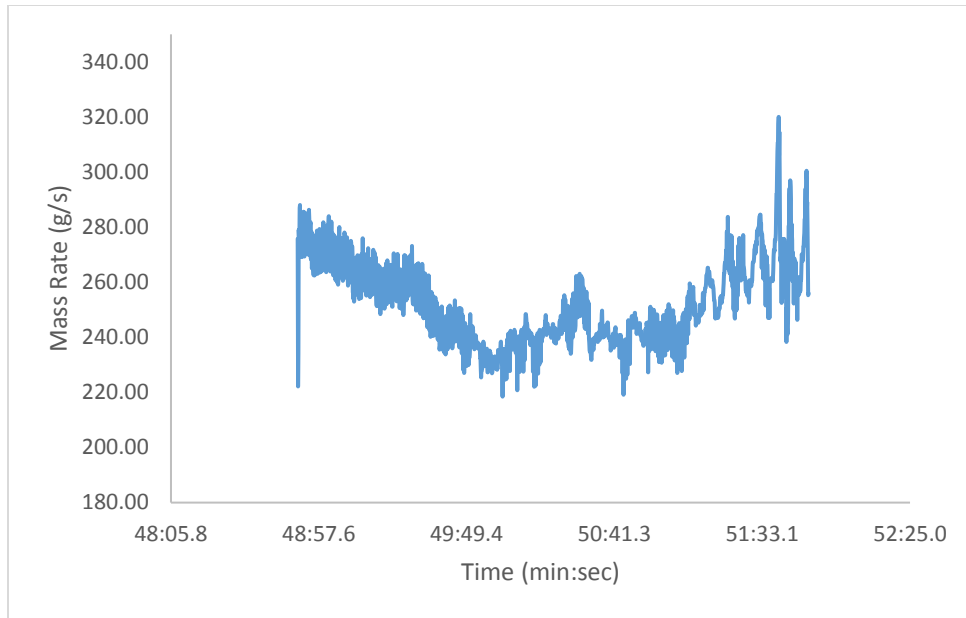


Figure A-39 a Experiment # 41 Granular flow rate vs. time

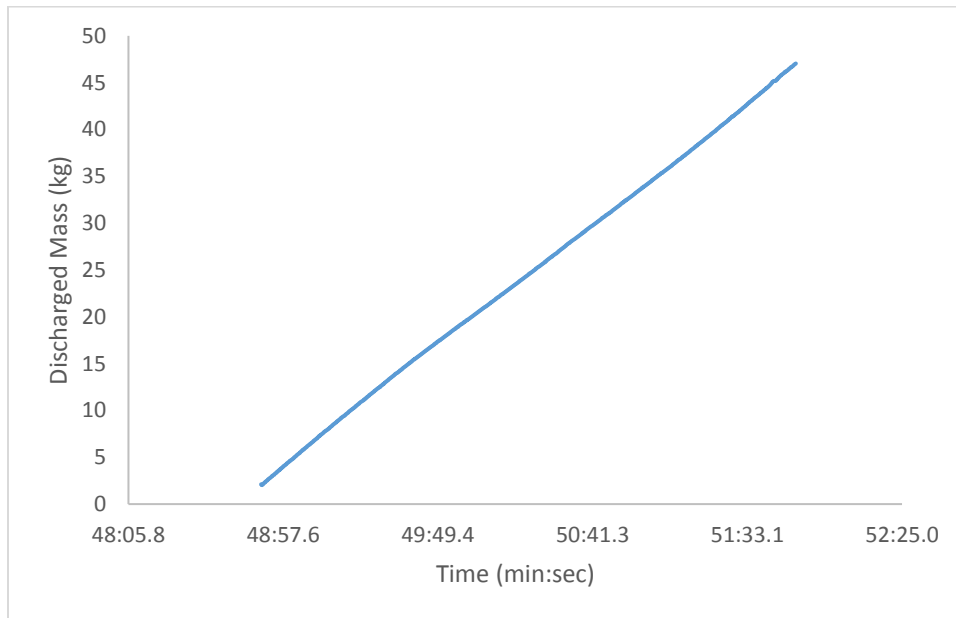


Figure A-39 b Experiment # 41 Cumulative discharge mass vs. time

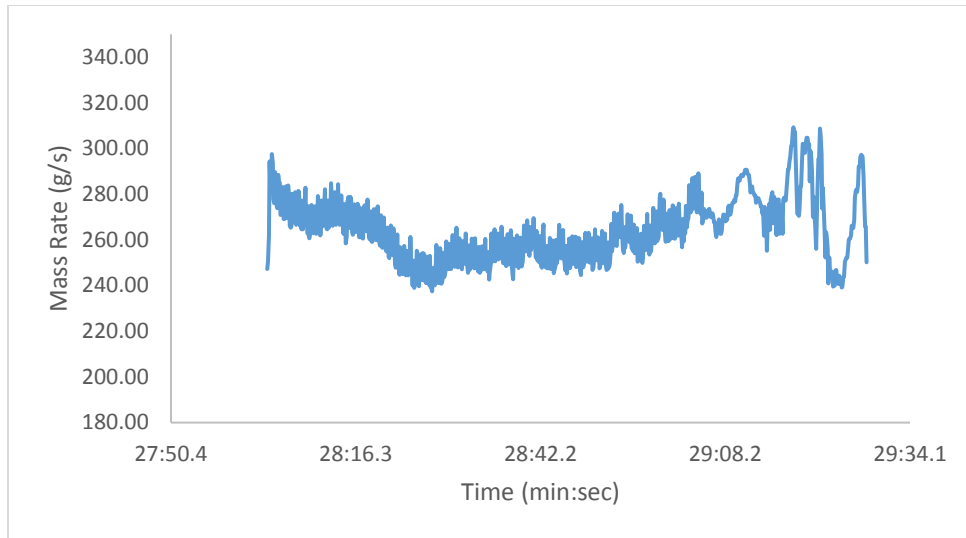


Figure A-40 a Experiment # 42 Granular flow rate vs. time

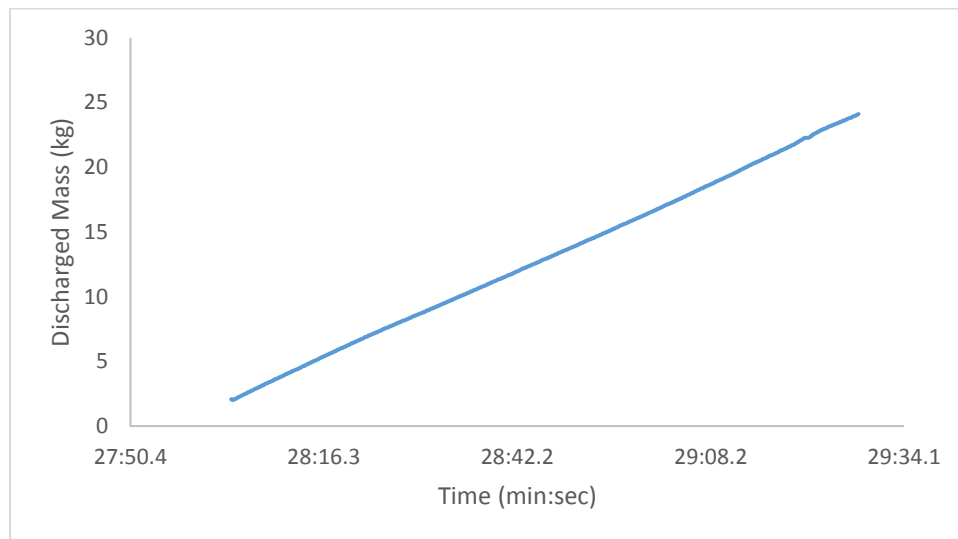


Figure A-40 b Experiment # 42 Cumulative discharge mass vs. time

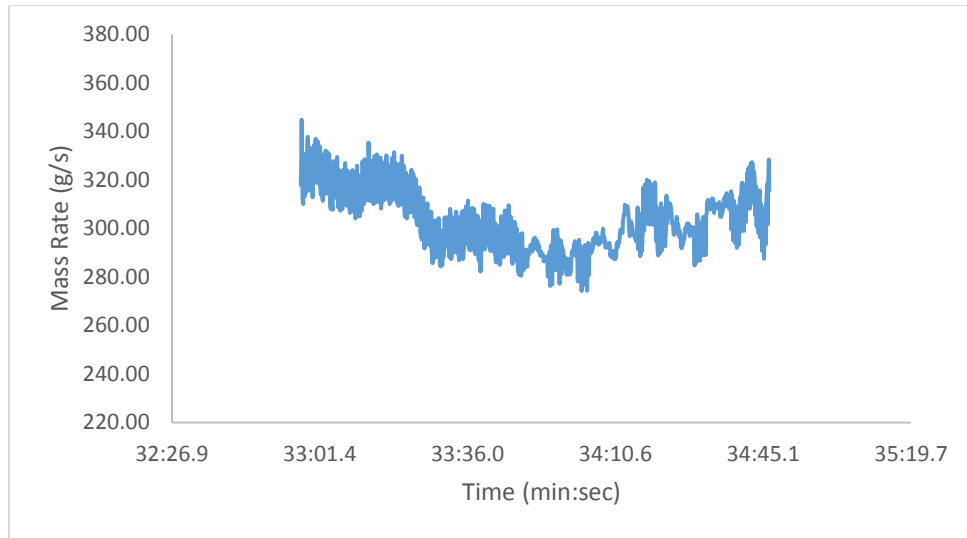


Figure A-41 a Experiment # 43 Granular flow rate vs. time

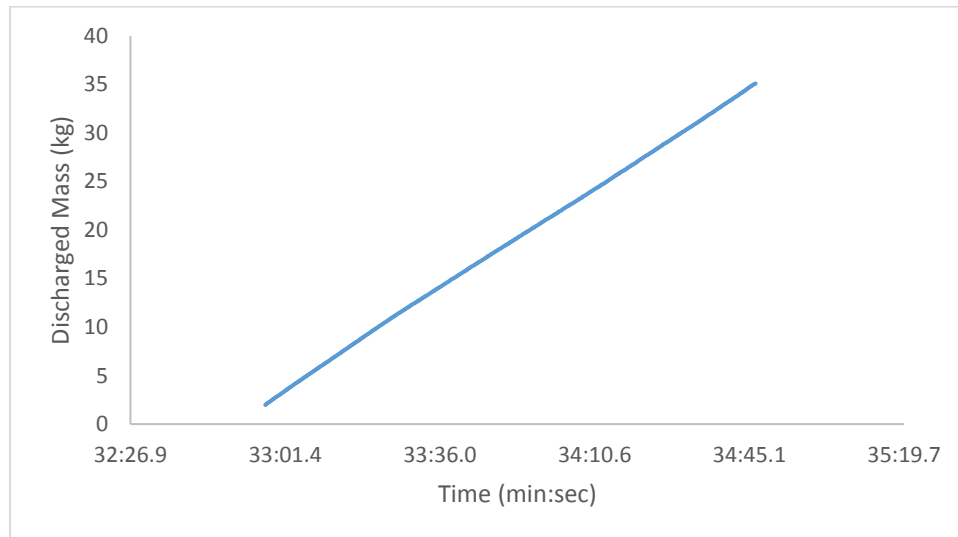


Figure A-41 b Experiment # 43 Cumulative discharge mass vs. time

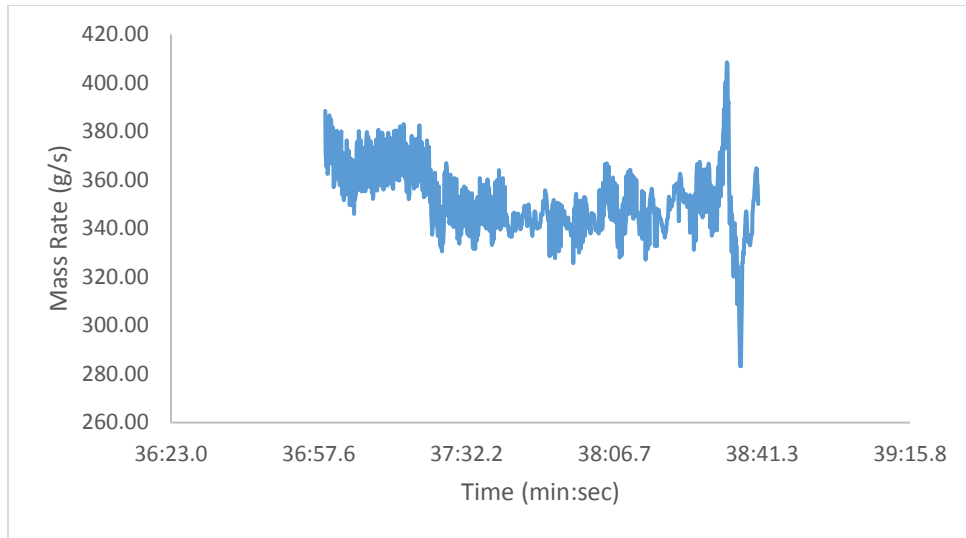


Figure A-42 a Experiment # 44 Granular flow rate vs. time

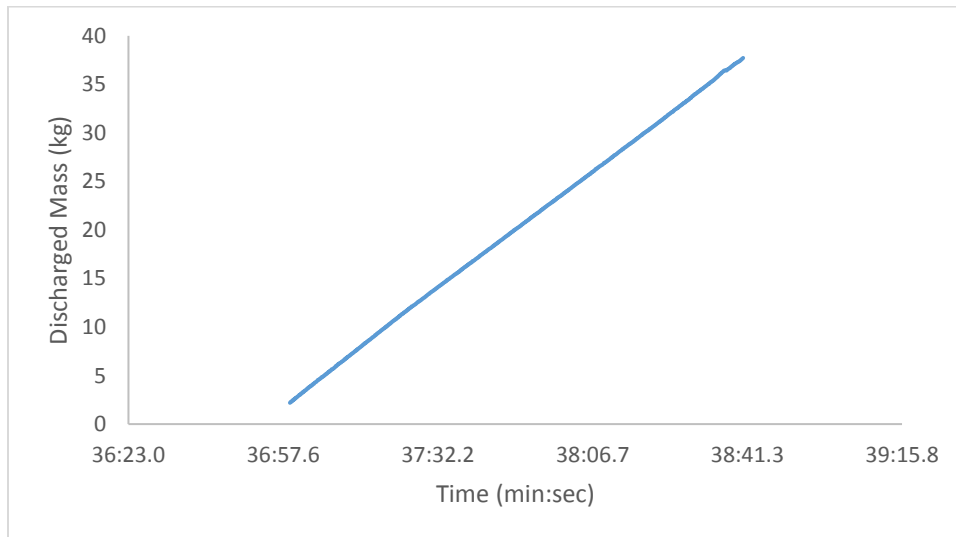


Figure A-42 b Experiment # 44 Cumulative discharge mass vs. time

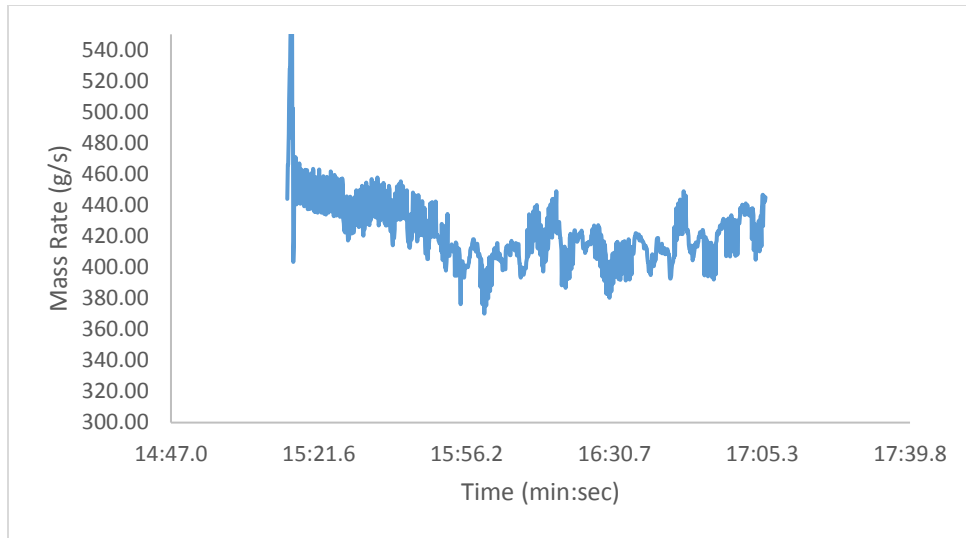


Figure A-43 a Experiment # 45 Granular flow rate vs. time

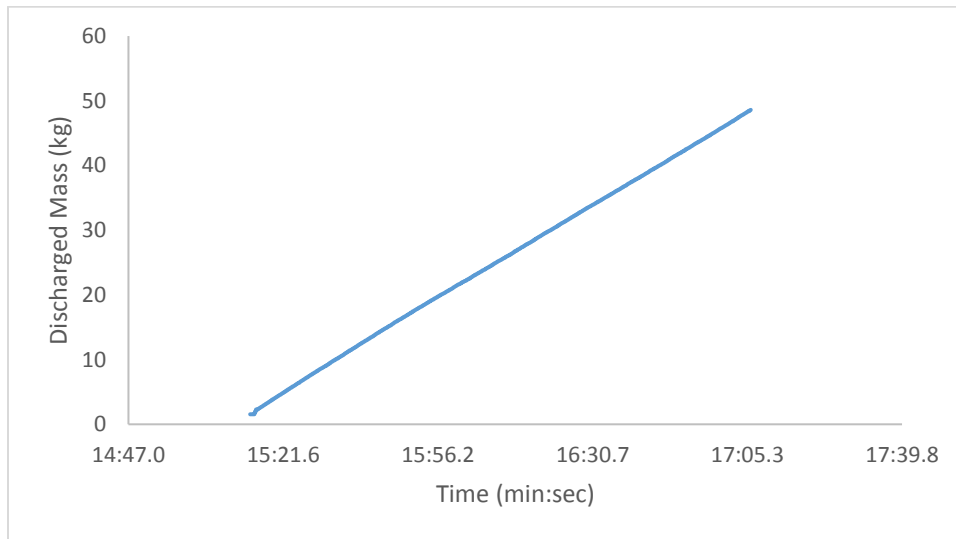


Figure A-43 b Experiment # 45 Cumulative discharge mass vs. time

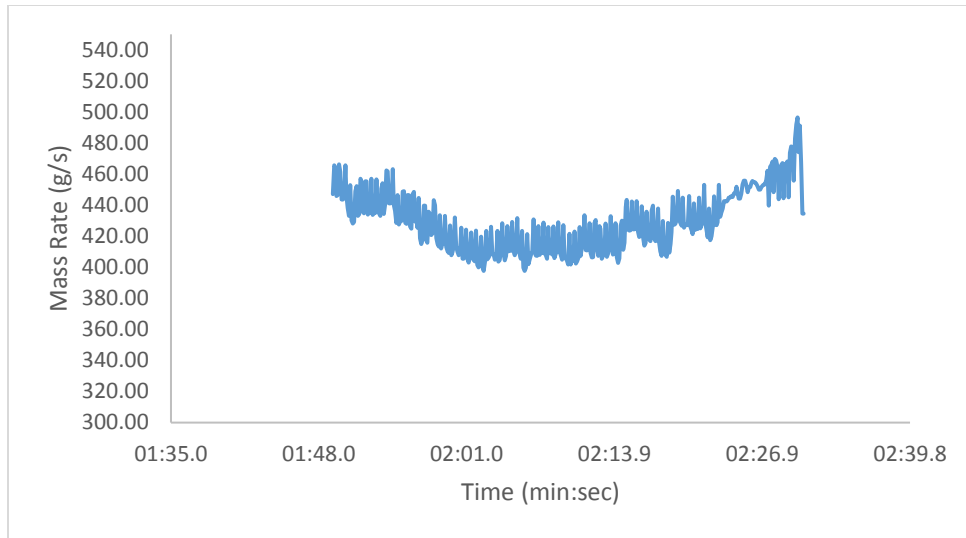


Figure A-44 a Experiment # 46 Granular flow rate vs. time

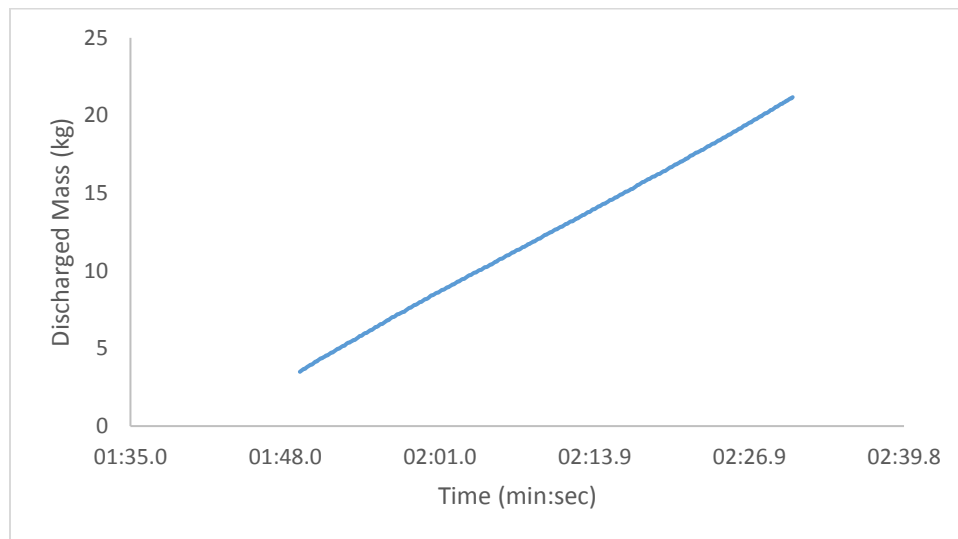


Figure A-44 b Experiment # 46 Cumulative discharge mass vs. time

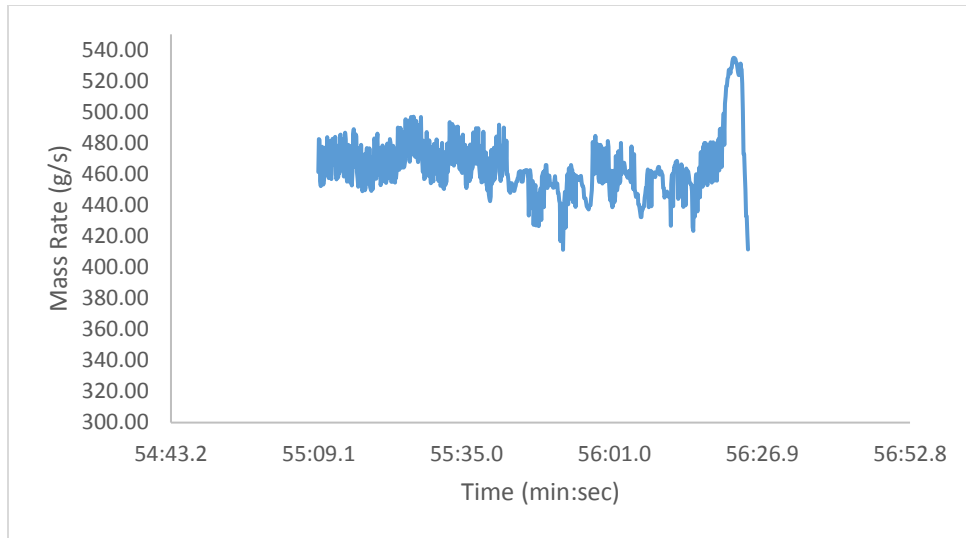


Figure A-45 a Experiment # 47 Granular flow rate vs. time

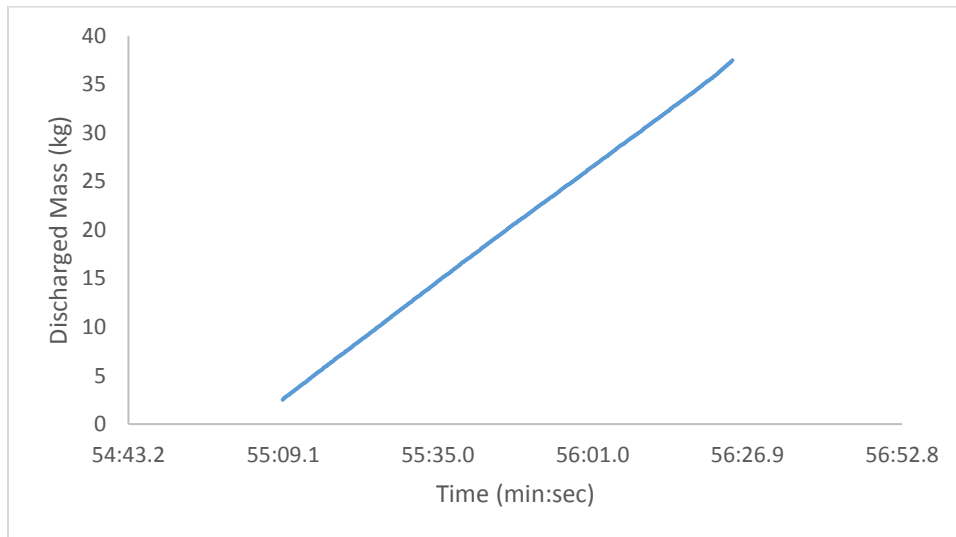


Figure A-45 b Experiment # 47 Cumulative discharge mass vs. time

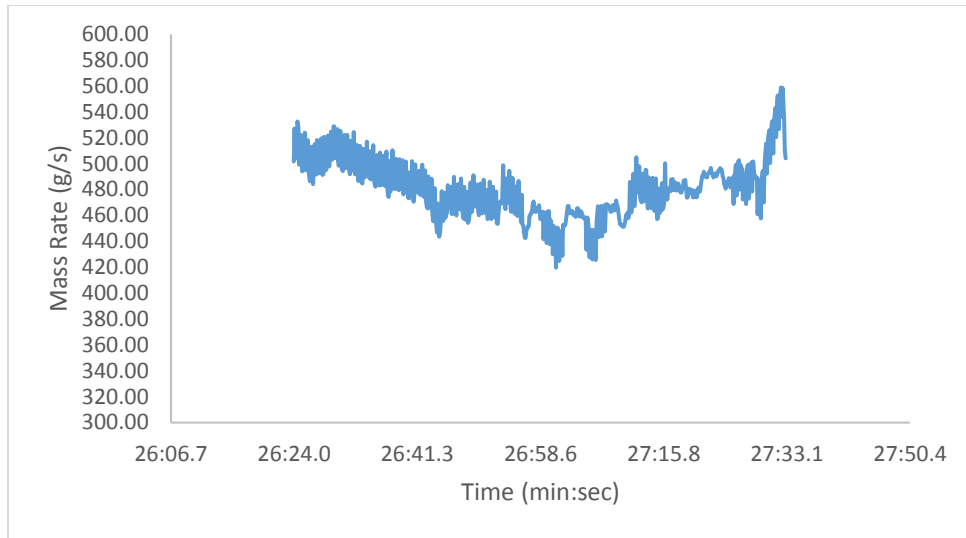


Figure A-46 a Experiment # 48 Granular flow rate vs. time

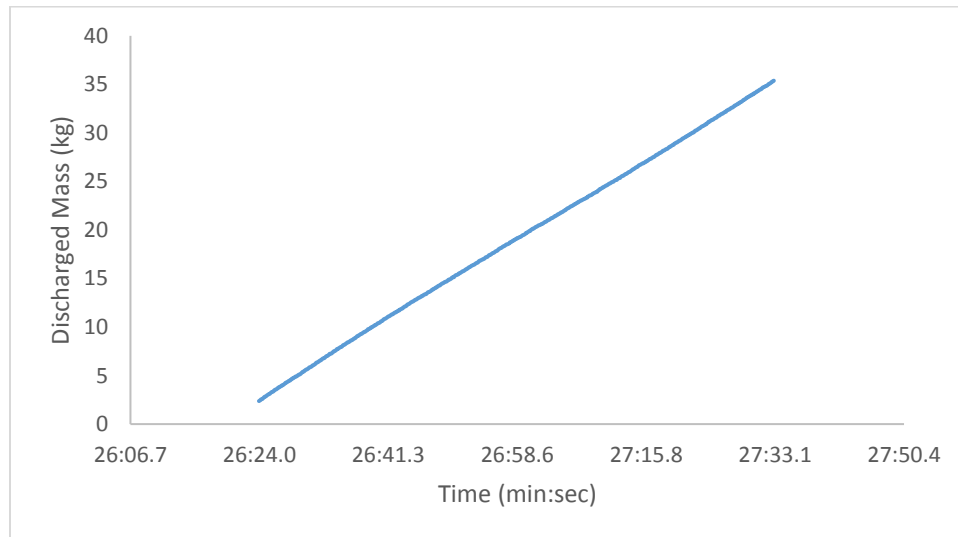


Figure A-46 b Experiment # 48 Cumulative discharge mass vs. time

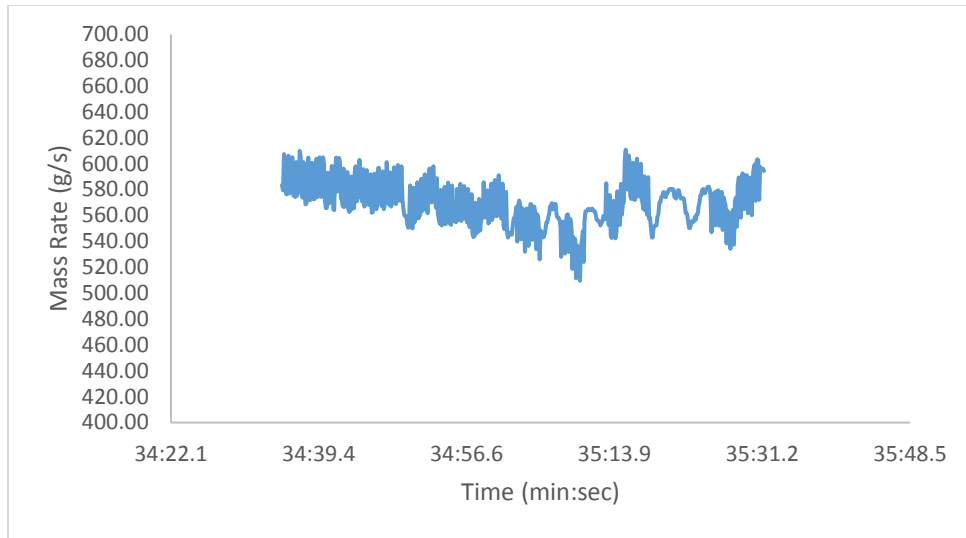


Figure A-47 a Experiment # 49 Granular flow rate vs. time

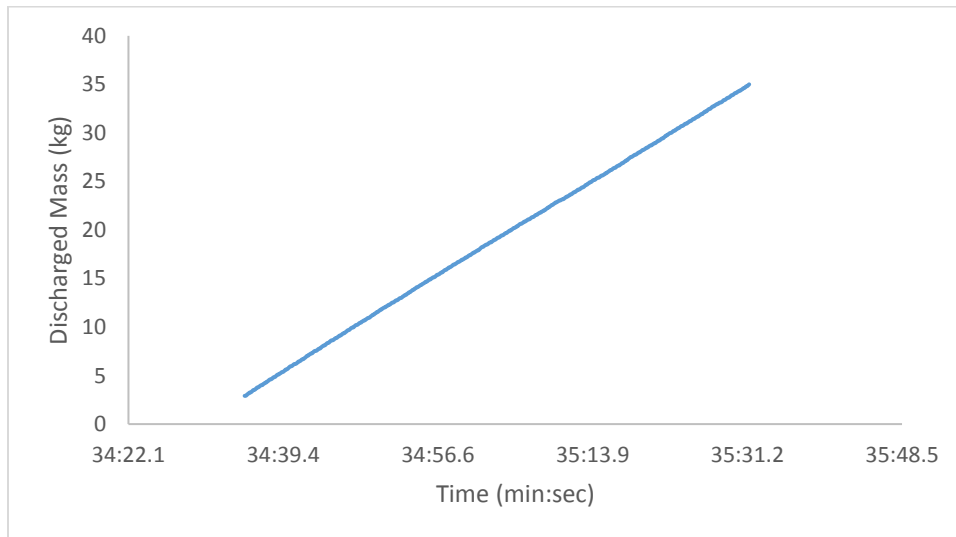


Figure A-47 b Experiment # 49 Cumulative discharge mass vs. time

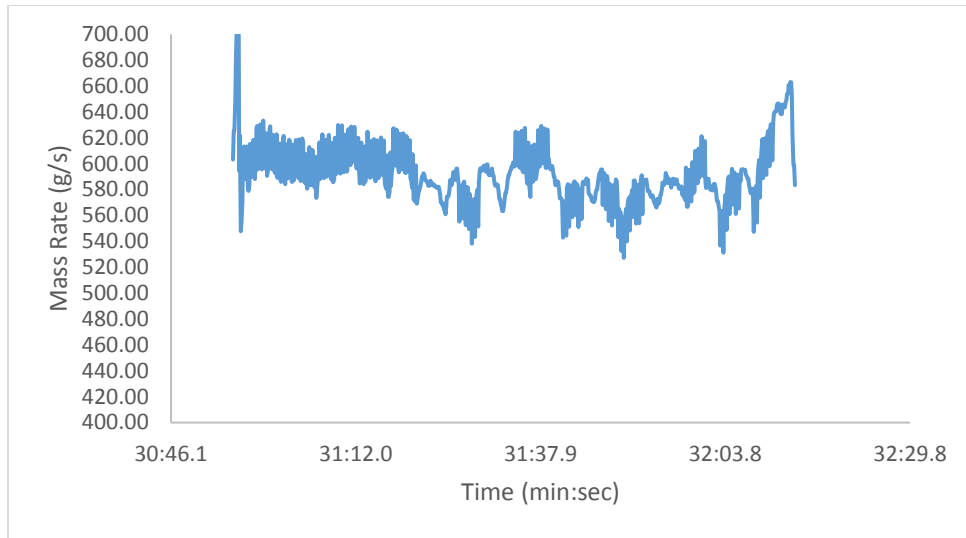


Figure A-48 a Experiment # 50 Granular flow rate vs. time

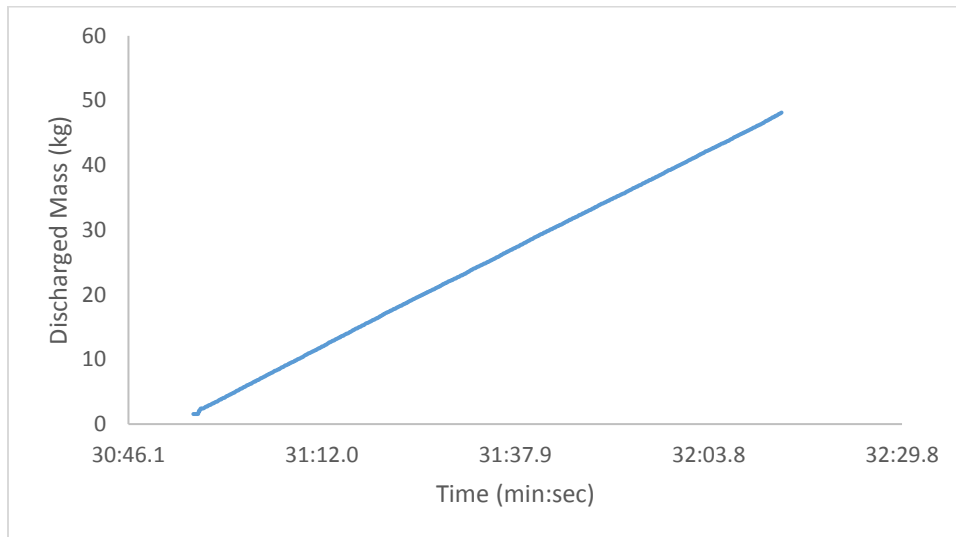


Figure A-48 b Experiment # 50 Cumulative discharge mass vs. time

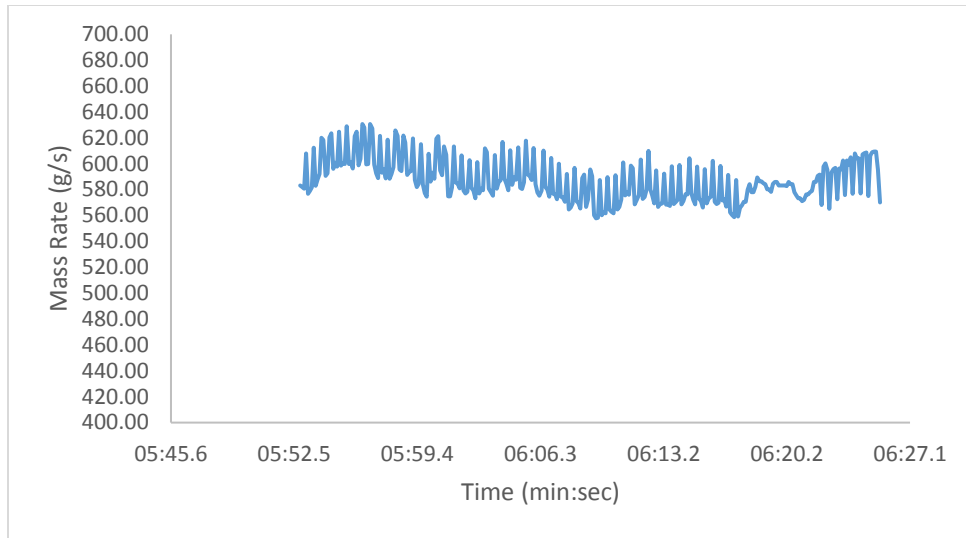


Figure A-49 a Experiment # 51 Granular flow rate vs. time

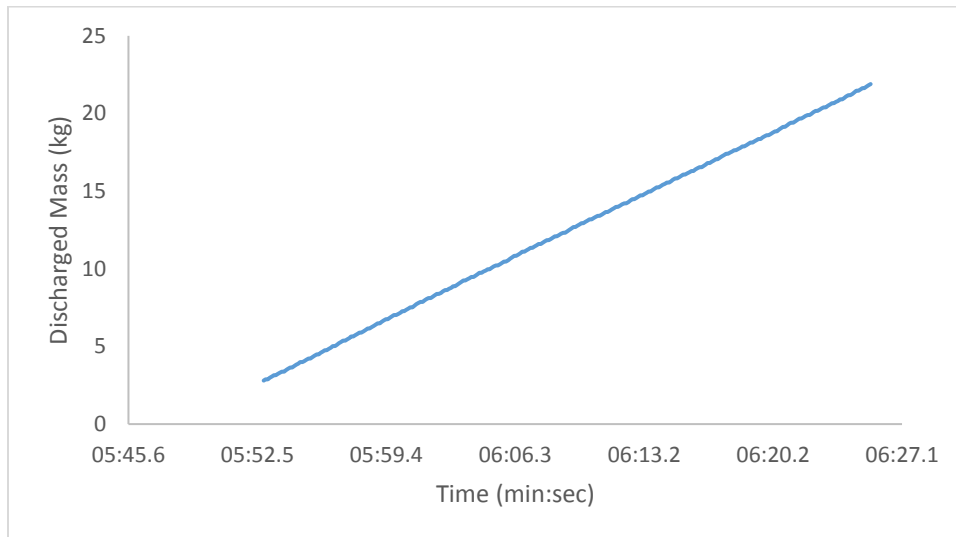


Figure A-49 b Experiment # 51 Cumulative discharge mass vs. time

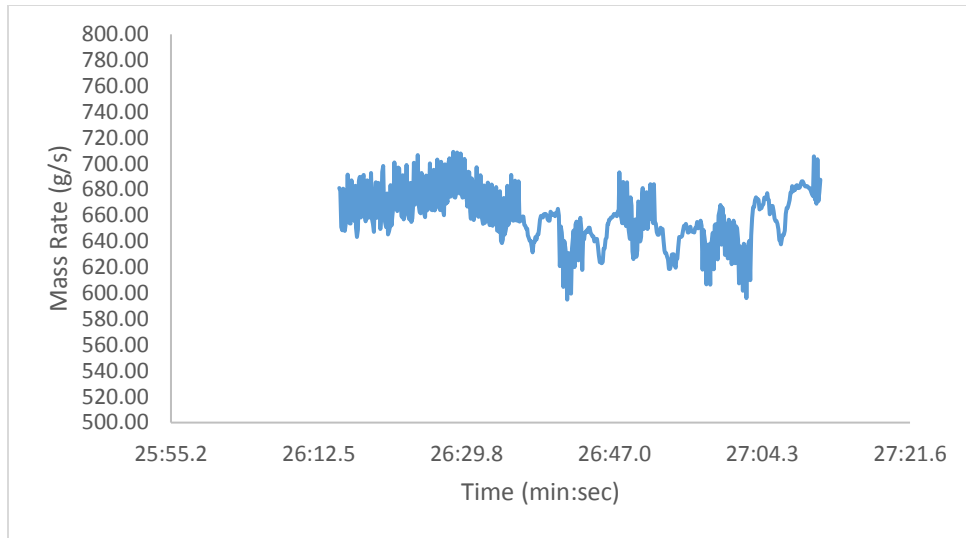


Figure A-50 a Experiment # 52 Granular flow rate vs. time

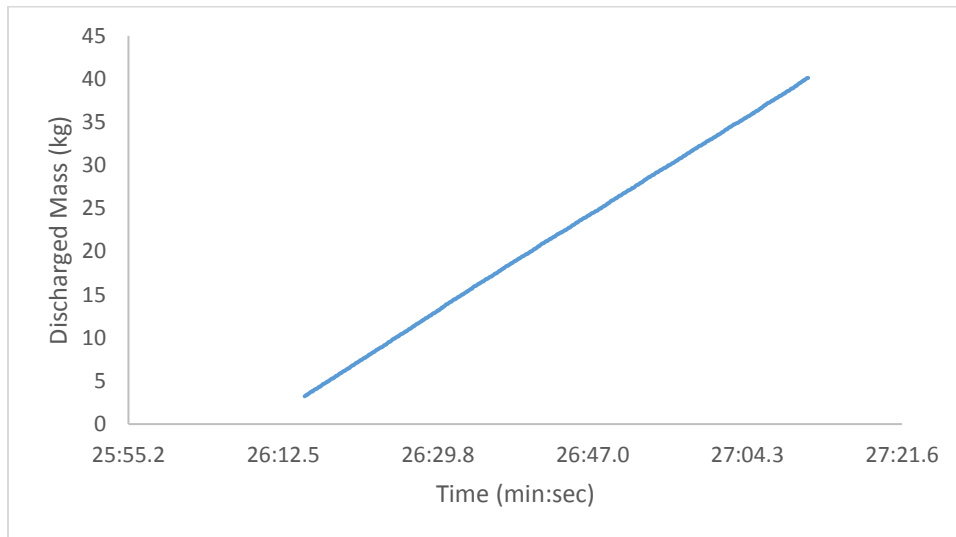


Figure A-50 b Experiment # 52 Cumulative discharge mass vs. time

## **Appendix B Apparatus Shop Drawings**

This appendix presents shop drawings of experiment apparatus. All dimensions are in inches.

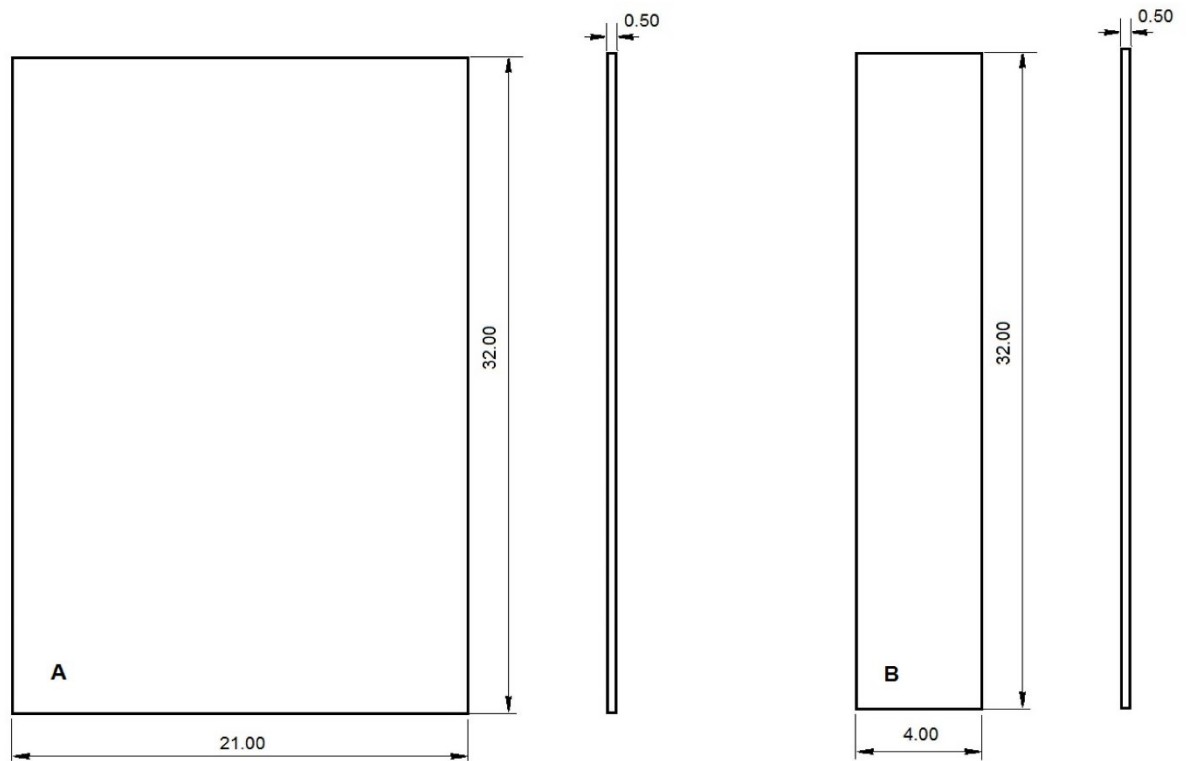


Figure B-1 Apparatus walls – all are made of transparent polycarbonate- dimensions are in inches

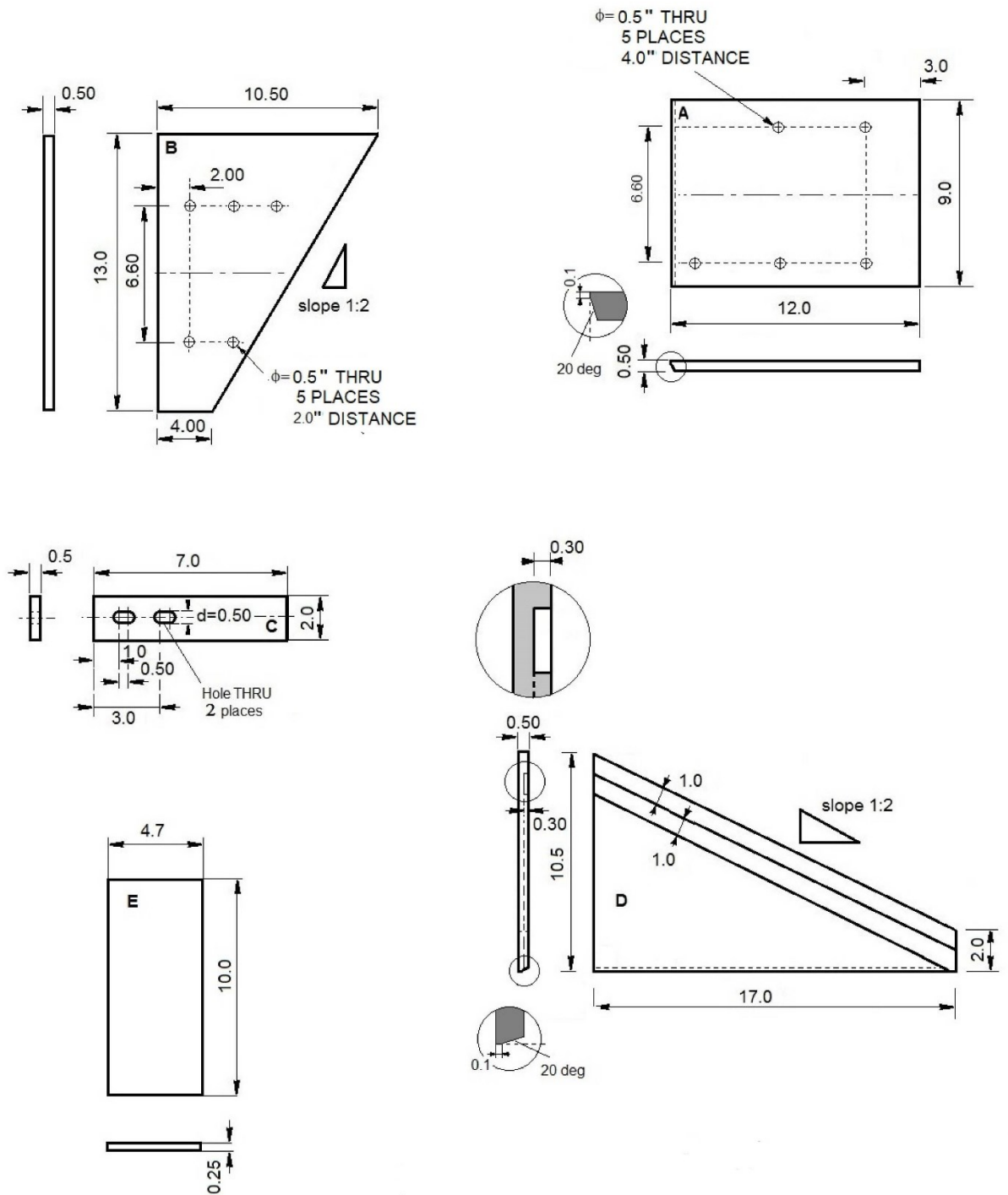


Figure B-2 Parts of apparatus bottom side consisting of movable triangle for slot width adjustment – These elements are made of Aluminum 6061 – dimensions are all in inches